Edge tunneling and transport in non-abelian fractional quantum Hall systems

by

Bas Jorn Overbosch

M.Sc. Physics
University of Amsterdam, 2000

Submitted to the Department of Physics
in partial fulfillment of the requirements for the degree of

Doctor of Philosophy in Physics

at the

MASSACHUSETTS INSTITUTE OF TECHNOLOGY

September 2008

Author .....
Department of Physics
August 1, 2008

Certified by .....
Xiao-Gang Wen
Cecil and Ida Green Professor of Physics
Thesis Supervisor

Accepted by .....
Thomas J. Greytak
Professor, Associate Department Head for Education

Edge tunneling and transport in non-abelian fractional quantum Hall systems

by
Bas Jorn Overbosch

Submitted to the Department of Physics
on August 1, 2008, in partial fulfillment of the
requirements for the degree of
Doctor of Philosophy in Physics

Abstract

Several aspects of tunneling at the edge of a fractional quantum Hall (FQH) state are studied. Most examples are given for the non-abelian filling fraction $\nu = \frac{5}{2}$ Moore-Read Pfaffian state.

For tunneling between opposite edges of an abelian fractional quantum Hall state at a quantum point contact, the perturbative calculation of tunneling current, conductance, and current noise, as a function of finite bias and temperature, is reviewed. We extend this formalism to include non-abelian FQH states as well. The crucial ingredient is conformal block decomposition. We argue the validity of perturbation theory to arbitrary order.

A double point contact interferometer is considered for the $\nu = \frac{5}{2}$ FQH state, for which a vanishing interference pattern in the tunneling current was predicted when a non-abelian quasiparticle is trapped inside the interferometer. We confirm this result in a dynamical edge calculation. We show how interference can be restored through a higher order tunneling process, which exchanges a charge neutral quasiparticle between the central island and one of the edges.

On the edge of the $\nu = \frac{5}{2}$ Pfaffian and anti-Pfaffian FQH states interactions can cause a transition to another phase. The relevant operator that condenses in this process consists of tunneling of electrons between the different edge branches. Under the phase transition a pair of counterpropagating Majorana modes acquires a gap. The transition is an edge only phase transition, as the bulk state is unchanged. Such a transition can change the observed quasiparticle charge and exponent as measured in transport. The Majora-gapping transition shows similarities to a transition due to edge reconstruction.

A setup is proposed that can probe slow edge velocities that may be present in certain abelian and non-abelian FQH state. At a long tunneling contact the coherent interference of tunneling quasiparticles causes a resonance in the tunneling current. From a high-precision observation of such a resonance not only the slow edge velocity can be determined, but also quasiparticle charge as well as neutral and charged tunneling exponents. Temperature is found to set an effective decoherence length scale.

Thesis Supervisor: Xiao-Gang Wen
Title: Cecil and Ida Green Professor of Physics

Acknowledgments

Wow, time flies by in an unpredictable manner.
MIT has been my home away from home for seven years. I have experienced ups and downs throughout that period; I recall two Nobel prizes at the Physics department, six national championships for Boston based sports teams, several fourth of July fireworks, but also a September eleven. It will be interesting to see how much of the American and MIT spirit I will try to uphold in the years to follow. Let me thank several people now, without whom getting my PhD would have been impossible, or at least a lot less fun.

I would like to start with my advisor Xiao-Gang Wen. Xiao-Gang is truly unique and he likes to go where no-one has gone before in physics-land; sooner or later the rest of the community then realizes that they want to follow him. I have learned a lot of condensed matter physics from Xiao-Gang, and appreciate the freedom he has given me throughout the years.

My professional home was of course the condensed matter theory (or CMT) corridor, for most of the time in building 12, more recently in building 4. The buildings unfortunately suffered from the standard MIT approach to maintenance (hint: none), but the folks were nice. Several people have come and gone at CMT, and in particular I want to thank Margaret O'Meara who was always there for us in case we needed something.

I have had several office-mates, Vincent Liu, Michael Levin, Brian Swingle and Maissam Barkeshli. I have enjoyed their companionship and I have made them endure lots of hours of me talking on the phone. I hope you guys have not picked up too many of my Dutch swear-words whenever LaTeX or Mathematica did not agree with me. Not part of the office, but part of the Wen group were Ying Ran and Tiago Ribeiro with whom I talked about both physics and non-physics.

Then there are the 'brothahs': our group of CMT students who hung out, ate lunch, and discussed life-as-a-physicist on a daily basis: über-brother David Chan, Cody Nave, Peter Bermel and Michael Levin. And of course I need to included our CMX-cousin Sami Amasha as well. You guys have been my family of friends here at MIT, and will be my friends for life. The most interesting discussions we have had are not quite appropriate to write down here, but I can assure the reader they were that much fun.

Building 13 not only become a place to hide from fire-alarms, or to say hi to Sami, but also to see all my theoretical efforts put into practice. This is were Iuliana Radu rules over the dilution fridge and the $\nu = \frac{5}{2}$ state within (with the help of Jeff, Colin and dean Marc of course). Iuliana's experiment indirectly had a big impact on my PhD thesis: it introduced me to the non-abelian anyon aspect of quantum Hall systems. If not for the whole $\nu = \frac{5}{2}$ hype this thesis would look somewhat different, definitely.

With Chris, Matt, Chris, Wouter, Neville, Andreas (& Iuliana of course!), Ghislain, Ashley, Tom and Millie, I have learned amongst other things to celebrate Thanksgiving, watch Superbowls, play no-limit Texas hold'em, and have Westgate barbecues.

One of the loves in my life, starting from a young age, is swimming: Swim Free or Fly Hard! Although I could not join the MIT swim team as a graduate student, the MIT Masters swim club proved to be quite more than just a surrogate. Masters kept me sane in times when MIT would otherwise have driven me crazy. There are way too many names of fellow simmers from seven years of practices, swim meets, and board meetings, to list here,

but I do want to mention our coach Bill Paine and Patti Christie for all their efforts and devotion to our group of swimmers.

As is custom in physics literature, I would now like to acknowledge my sources of 'funding'. Getting where I am today would have been impossible without the full support of my parents Evert and Henriëtte. And this is not just financial support (because the MIT stipend just does not cover living in a culture with different habits of e.g. housing and food, and occasional transatlantic trips to prevent homesickness), but all other kinds of endless support and love as well. You have always been there for me and my sister Femke since the days we were born.

Finally there is the one person who has had the most patience throughout all these years: my wife Elske. Deciding that I would pursue a graduate degree in the US was a decision we did not make lightly, but I guess even then we did not fully realize what we were getting ourselves into. When the Atlantic distance proved to be too far you began your own adventure into the unknown with Eleni & Petros in Chicago. When a total of five years had passed we finally decided to give up the long distance relationship and to get married. On my part that was probably the best decision I ever made. Getting a PhD is one thing, but being with the one you love is a whole different ballpark! You have stood by me throughout and especially these last months; although we are now moving back to The Netherlands we are in fact moving forward in *our* life.

Contents

Chapter 1

Introduction to the problem

1.1 Transport with point contacts in the quantum Hall effect

We begin this thesis with a description of an experimental setup to measure transport in quantum Hall systems. Most the statements made in this thesis about edge tunneling and transport in quantum Hall systems, or interference in such systems, will at some point refer to a potential measurement of some quantity, e.g. the quasiparticle exponent g, using a setup with a quantum point contact (QPC). Therefore it seems very appropriate to start with a description of the basic 'tunneling current' measurement setup as 'warm-up'.

The setting is the quantum Hall effect, which consists of a two-dimensional electron gas (also called 2DEG) in a perpendicular magnetic field. For certain ranges of (strong) magnetic field and at low enough temperatures the 2DEG forms an incompressible liquid state: this is the quantum Hall state.

At low energies the only excitations the quantum Hall state possesses are chiral edge excitations. Chiral means that these excitations can only propagate in one direction, which is set by the (Lorentz-force) direction of the drift velocity of the electrons at the edge. As such the edge excitations form a chiral Luttinger liquid, another word for a one-dimensional one-way channel without any backscattering: what comes in must come out in the same form. The conductance of these edge 'channels' is quantized.

The physics of the edge channels can be probed if a channel is split into two. The only way this can physically be realized is if another edge, on the other side of the incompressible liquid, is involved as well. This is the basic idea: the current in the 'incoming' edge channel is split into a 'transmitted' channel on the same edge and a 'reflected' channel on the opposite edge.

A sketch of a physical setup is given in Fig. 1-1. This setup has one source and two drains. A very similar setup with only one drain is shown in Fig. 1-3. The only simplification we make at this point is the assumption the the current is carried by a *single* channel with conductance $1/R_H$ where R_H is the quantized Hall resistance. This simple picture can straightforwardly be generalized to the case where the current is carried by multiple channels as long as only one of the channels (the innermost channel) is being scattered by the QPC and the other channels pass by undisturbed.

The incompressible quantum Hall liquid is usually drawn as a rectangular area, with the liquid inside and the rest of the world outside. In Fig. 1-1 DC bias current I_{sup} is supplied

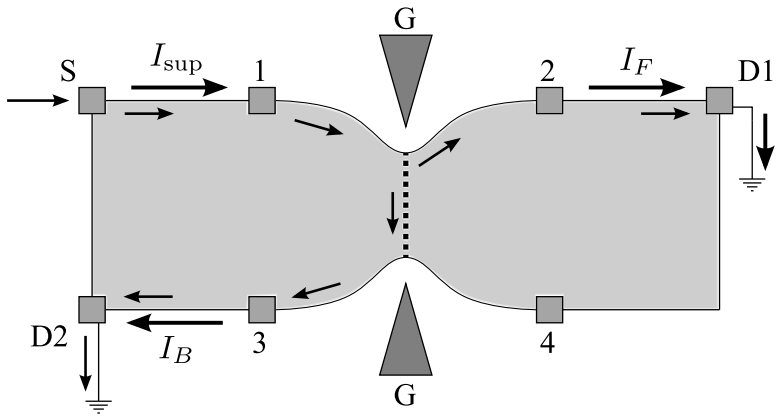

Figure 1-1: Schematic for transport measurement at a point contact in the quantum Hall effect with two drains. The supplied current I_{sup} is sourced at S. The current then propagates along the edge of the quantum Hall fluid, here we chose the top (bottom) edge to be right (left) moving (as set by the direction of the external perpendicular magnetic field). At the quantum point contact the current is split into two. The back-scattered current I_B 'tunnels' to the opposite edge and continues on along the bottom edge towards drain D2. The forward-scattered current I_F continues along the top edge toward drain D1. Arrows indicate direction of current propagation along edges. There are four voltage probes sketched that can be used to measure transport: $V_{21} = V_{34} = R_H I_B$, $V_{13} = V_{24} = R_H I_F$, $V_{14} = R_H I_{\text{sup}}$. The tunneling amplitude strength of the QPC is (partially) controlled by applying a negative voltage on a gate G that squeezes the edges of the quantum Hall liquid towards each other. Note that in this setup the voltage difference $V = V_{14}$ between the two edges does not depend on the tunneling amplitude. Even though this figure is drawn in the weak-tunneling regime, the mentioned current-voltage relations are in fact valid for all regimes of tunneling amplitude strength, see Fig. 1-2.

at source S; it is carried by the top edge channel, passes by voltage probe V_1 and at the QPC is split into two parts: back-scattered current I_B and forward-scattered current I_F, with conservation of current $I_B + I_F = I_{\text{sup}}$. The back-scattered current propagates along the bottom edge channel, passes by probe V_3 and exits at drain D2. The forward-scattered current passes by V_2 on the top edge and exits at drain D1. No net current flows on the edge segments between D1 and S and between D2 and V_4; total net current flowing from left to right through the *entire* quantum Hall liquid at any vertical slice is always I_F.

Since scattering is completely elastic the QPC introduces no additional resistance, and the resistance experienced by the source is always R_H. In other words, we have the relations

$$V = V_{14} = R_H I_{\text{sup}}, \tag{1.1}$$

$$V_{13} = V_{24} = R_H I_F, \tag{1.2}$$

$$V_{12} = V_{34} = R_H I_B. \tag{1.3}$$

Experimentally, it is usually a *differential* resistance $\frac{\partial V_{ij}}{\partial I_{\text{sup}}}$ that is being measured by adding a small AC modulated contribution to I_{sup}, which is then measured using a lock-in technique. This procedure is used to reduce noise in the measurement. Theoretically, it is

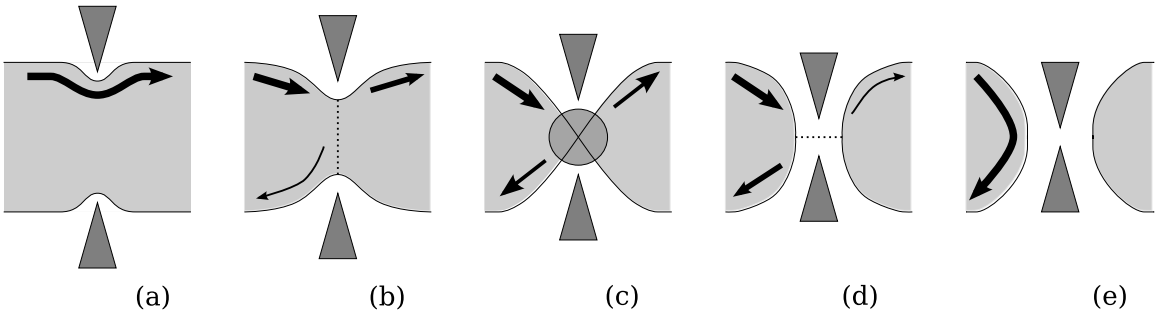

Figure 1-2: Five regimes of transport at a QPC for different tunneling amplitudes. In (a) the QPC is fully 'open' and the injected current continues along the top edge undisturbed; (b) is the weak back-scattering regime in which a tiny fraction of the current is tunneling to the other side. This is the regime primarily considered in this thesis, also called the weak-tunneling limit. It can be described in terms of tunneling quasiparticles; (c) is the generic regime representing arbitrary tunneling amplitude strength. The incoming current is scattered in forward and backward directions; the tunneling current in this generic state cannot be described in terms of isolated quasiparticles or electrons that tunnel and becomes a many-particle problem. In (d) the QPC is close to 'pinch-off', where most of the current is transported to the bottom edge and only a tiny fraction of the current is scattered in the forward channel, and can be described in terms of tunneling electrons. This is also called weak forward-scattering; (e): the QPC is completely pinched-off and all current is transmitted along the bottom edge.

usually the tunneling current I_B or the (differential) tunneling conductance $\frac{\partial I_B(V)}{\partial V}$ that is calculated. Experimental differential resistance and theoretical tunneling conductance are related to each other through

$$\frac{\partial V_{12}}{\partial I_{\rm sup}} = R_H^2 \frac{\partial I_B}{\partial V_{14}} = R_H^2 \left.\frac{\partial I_B(V)}{\partial V}\right|_{V=R_H I_{\rm sup}} . \tag{1.4}$$

Important fact is that the tunneling current $I_B(V)$ can be non-linear in V. Although the tunneling current is bounded by the supplied current, i.e., $0 \leq I_B(V) \leq \frac{V}{R_H}$, the differential tunneling conductance is not necessarily bounded by $1/R_H$. Non-linearity also means that *it makes no sense to define transmission and reflection coefficients* to characterize the tunneling amplitude strength (one could of course define voltage-dependent reflection and transmission coefficients, for instance at zero bias). Generically though, the non-linearity is not so extreme such that for one voltage all current is reflected and for another bias V all current is transmitted, and one can still classify the QPC as falling into several regimes, depending on which direction most of the current is being scattered in, as indicated in Fig. 1-2. In this thesis we are primarily interested in the regime of weak back-scattering, or 'weak-tunneling', where $I_B(V) \ll I_F(V)$ for all V.

An alternative setup for transport-measurement at a quantum point contact is shown in Fig. 1-3. The main difference with the setup in Fig. 1-1 is that there is only one drain. We introduced slightly different notation to not mixup the two distinct setups. Since the tunneling current is not drained it becomes part of the incoming current. This introduces

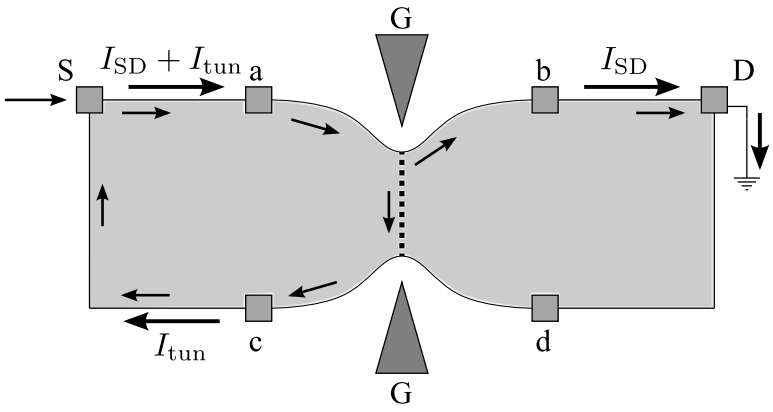

Figure 1-3: Schematic of setup that uses only one drain to measure transport at a QPC in the quantum Hall effect. The main difference with the two-drain setup, Fig. 1-1, is that the voltage difference $V = V_{ad}$ between the top and bottom edges *does* depend on the tunneling amplitude strength. Current $I_{\rm SD}$ is sourced between source S and drain D. At the point contact part of the current, $I_{\rm tun}$, tunnels to the opposite edge. We have $V_{ac} = V_{bd} = R_H I_{\rm SD}$, and $V_{ab} = V_{cd} = R_H I_{\rm tun}$. The voltage $V = V_{ad}$ is the (unique) solution to the equation $V_{ad} = R_H I_{\rm tun}(V_{ad}) + R_H I_{\rm SD}$. In this setup the fully pinched-off regime cannot be reached since net current $I_{\rm SD}$ always makes it through the QPC.

the difficulty that the tunneling current depends on the voltage difference between top and bottom incoming edges V_{ad}, but this voltage in turn depends on the tunneling current.

The relations between current and voltages in this single-drain setup are as follows

$$V_{ac} = V_{bd} = R_H I_{\rm SD}, \tag{1.5}$$

$$V_{ab} = V_{cd} = R_H I_{\rm tun}, \tag{1.6}$$

$$V_{ad} = R_H I_{\rm tun}(V_{ad}) + R_H I_{\rm SD}. \tag{1.7}$$

There is always at least one self-consistent solution for V_{ad} of this last equation. If $\frac{\partial I_{\rm tun}(V)}{\partial V} < \frac{1}{R_H}$ for all V then this solution would be unique, but in general there could be multiple solutions.

In the limit of weak tunneling the experimental differential resistance becomes proportional to the theoretical tunneling conductance. For the so-called diagonal differential resistance R_D the relation is

$$R_D = \frac{\partial V_{ad}}{\partial I_{\rm SD}} = \frac{R_H}{1 - R_H \frac{\partial I_{\rm tun}(V_{ad})}{\partial V_{ad}}} \approx R_H + R_H^2 \left.\frac{\partial I_{\rm tun}(V)}{\partial V}\right|_{V = R_H I_{\rm SD}}. \tag{1.8}$$

This weak-tunneling approximation can only be valid if the following two relations are satisfied:

$$\frac{\partial I_{\rm tun}(V)}{\partial V} \ll \frac{1}{R_H} \quad \text{and} \quad \frac{I_{\rm tun}}{V_H} \ll \frac{1}{R_H}, \qquad \text{where } V_H = R_H I_{\rm SD}. \tag{1.9}$$

1.2 What is the problem?

The main reasons we study edge tunneling and transport in non-abelian quantum Hall systems *from the theory side* can, roughly, be put in three categories. We would like to:

1. Understand the phase(s) of matter of the generic fractional quantum Hall system.

2. Bridge the gap with experiment.

3. Consider the topological quantum computation perspective.

Let us go over these three points, and the relations between them, in some more detail.

1.2.1 Understanding the phases of matter of the generic FQH system

On the one hand, it would seem that the theory of the integer and fractional quantum Hall (IQH and FQH) effects is well-developed. Quantum Hall physics was mainstream in the 1980's and 1990's, and the 1998 Nobel prize that was awarded for the FQH effect puts, at first sight, a natural end on an era.

So the question is, what is new in the fractional quantum Hall effect since, say, the year 2000? The answer is: non-abelian fractional quantum Hall states. Although several non-abelian FQH states were studied in the 1990's, the theory of non-abelian FQH states today *cannot* be called well-developed at all.

Surely, lots of non-abelian candidate states exist in theory, but a description of how they would show themselves in an experimental situation is lacking. The two main topics that we address in this thesis are the stability of the edge, or rather the potential instabilities of the edge, in chapter 5, and the non-abelian effects in edge transport, in chapters 3 and 4. In the past, edge 'reconstruction' instabilities and exact transport calculations were performed for some abelian systems, and it would seem that these concepts apply to and explain all abelian systems. However, these concepts are not sufficient to explain what happens in non-abelian systems. To understand non-abelian systems, the existing concepts need to be non-trivially generalized to include non-abelian systems as well. In this thesis we make a start of this generalization process; we consider certain specific non-abelian candidate states for which we need to the extend the existing 'abelian' concepts to describe e.g. weak-tunneling interferometry and edge phase transitions. Ultimately the goal is that several of these extensions can grow into the complete theory of all quantum Hall systems, both abelian and non-abelian, and not just for the edges but for the bulk as well.

In a sense abelian fractional quantum Hall states are a special, and very simple, case of the most generic non-abelian quantum Hall system. Why has the more generic case, the non-abelian FQH system, not been studied a lot in the past? Part of the answer is that although *mathematically* the non-abelian system is generic and the abelian states are a special case, most of the *experimentally* observed fractional quantum Hall states have been successfully identified with *abelian* states with no positive identification on any non-abelian state *yet*. And this is the other thing that is new since 2000: there may very well be an experimentally accessible non-abelian state; more on this in Sec. 1.3.

1.2.2 Bridging the gap with experiment

Although the theory side of the *abelian* fractional quantum Hall effect is well-developed, this is only partially true for the experimental side. Very succesful experiments were the measurements of the shot-noise in $\nu = \frac{1}{3}$ state (de Picciotto, Reznikov, Heiblum, Umansky, Bunin, and Mahalu, 1997; Saminadayar, Glattli, Jin, and Etienne, 1997), confirming a fractional charge $e/3$, and of tunneling of electrons into/out of the quantum Hall liquid that obeyed a power-law like curve over several decades. However, the theoretically predicted non-linear I-V-curve for tunneling at a constriction, for instance, has not been observed in experiment yet (non-linear behavior has been observed, but it does not give a good fit to the exact theoretical curve).

The discrepancy between theory and experiment comes primarily from the difficulty of the experiment: these were and are state-of-the-art experiments at the boundaries of what is currently physically possible (e.g. dilution fridge temperatures of about 10 millikelvin, high mobility samples, nano-scale gated structures). Hence there are big error-bars on all of the experimental results. The implications of noisy measurements are usually not considered in theory papers. One could argue that error analysis is just part of statistical analysis of the data. However, the implications of noisy measurements are not that trivial to be waived away like that. The theoretical curves that are predicted are not mere exponentials or power-laws for which error analysis is straightforward. For instance, for some complicated curve with fitting parameter g it may not be obvious at all how to reduce the error bars on (a fit of) g.

A second reason for a gap between experiment and theory is that theory tends to idealize the experimental situation *a lot*. Considering a more realistic setup typically does not introduce new physical concepts, it primarily makes the calculation more complicated. But this could be a necessary 'evil' to compare theory and experiment.

Third, sometimes a translation is necessary in order to bring the theoretical prediction into a form that is suitable for comparison with experiment; unfortunately more than often theorists will plot curves as a function of the one parameter that does *not* correspond to a knob an experimentalist can turn. Additional issue for abelian fractional quantum Hall effect is that a lot of these papers have been written over fifteen years ago, original authors may have moved on to other fields, and therefore knowledge about it tends to be 'rusty'.

In other words, there is a gap between theoretical predictions and experimental reality. Efforts to bridge this gap from the theory side should focus on how to extract the physically relevant information (such as quasiparticle charges and exponents) from noisy measurements in a 'language' spoken by experiment. Some of this noise is inherent to the cutting-edge-challenging nature of experiment, sometimes theory is too ideal and needs to be adjusted to provide a more realistic version.

Although closing the gap between theory and experiment is not the primary goal in this thesis, it is certainly an important aspect. Experimental boundaries of what is achievable have been pushed further out in the last ten to fifteen years, and it is important to ask and answer the question as to what can realistically be measured in current and future experiments. Explicit efforts in this thesis can be found in chapter 6 where the positive implications of a non-ideal finite-size quantum point contact are considered; but also in much simpler/smaller things, like a plot of the tunneling conductance instead of the tunneling

current.

1.2.3 Considering the topological quantum computation perspective

The third reason to study non-abelian quantum Hall systems comes from the, at-first-sight distant, corner of quantum information. Nevertheless it is quantum information, or topological quantum computation to be precise, that as a matter of fact stimulated the renewed interest in quantum Hall systems.

In quantum computation the emphasis is put on manipulating the information that is stored in quantum states, which is quite a different view than that of physics as a science trying to explain the natural world we observe around us. However, once questions about quanta of information are cast into problems on ground states of quantum systems, the overlap between quantum information and condensed matter physics becomes surprisingly large all of a sudden: the relevant questions on low-energy behavior of quantum systems turn out to be very similar.

As such, topological quantum computation offers a different, but complementary, view to some of the problems of non-abelian fractional quantum Hall systems. Switching to this alternative prespective can be refreshing at times. A good example of this line of thought would be the 'urge' to manipulate anyons: to show that anyons exist as controllable quasiparticles that can be braided and measured in interference experiments. Interference of abelian anyons in quantum Hall systems is introduced in chapter 2 and interference of non-abelian anyons is a main topic in chapter 4.

1.3 Why the $\nu = \frac{5}{2}$ state?

The fractional quantum Hall state at filling fraction $\nu = \frac{5}{2}$ is possibly a non-abelian state. Its existence, as in a quantized plateau in the Hall resistance, was first observed by Willett, Eisenstein, Störmer, Tsui, Gossard, and English (1987) (see also Pan, Yeh, Xia, Störmer, Tsui, Adams, Pfeiffer, Baldwin, and West, 2001). A candidate wavefunction was proposed by Moore and Read (1991), and due to the pairing nature of the trial wavefunction in terms of a Pfaffian factor the Moore-Read wavefunction is also called the 'Pfaffian' state. The quasiparticles in the Pfaffian trial wavefunction are non-abelian anyons, and several of their properties were studied by Nayak and Wilczek (1996). Numerical simulations with exact diagonalization by Morf (1998), and later Rezayi and Haldane (2000), showed that on closed systems (i.e., without an edge, such as a sphere or a torus, also called compact) with a small number of electrons the Pfaffian state has a decent overlap with the 'physical' state corresponding to 2D electrons with 3D Coulomb interaction. In other words, there is a reason to believe that the physically observed state at filling fraction $\nu = \frac{5}{2}$ falls in the universality class of the Pfaffian state which is a non-abelian state: the $\nu = \frac{5}{2}$ state could very well be non-abelian.

However, this educated guess of a possible non-abelian state was not enough to stimulate further interest in the $\nu = \frac{5}{2}$ state, especially since the observed plateau is already very fragile (i.e., a plateau is observed at very low temperatures only, and it has a small width as function of magnetic field) in an ungated structure, let alone a gated structure. Besides, there was no proposal of how to detect a signature of non-abelian effects

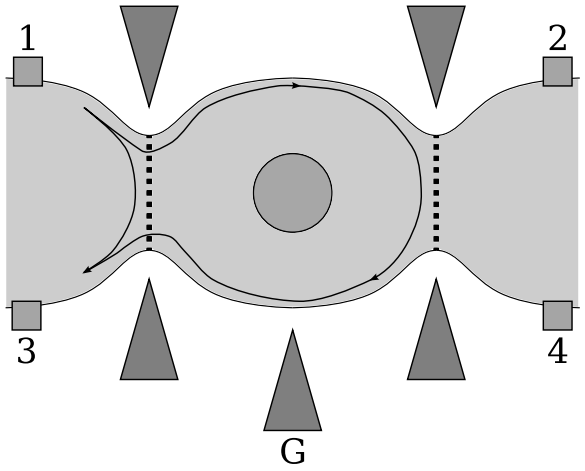

Figure 1-4: If there are two point contacts then a tunneling quasiparticle can 'choose' between two distinct paths to tunnel from the top edge to the bottom edge. The difference of the two paths is a closed path that fully encircles the inside of the interferometer. Interference oscillations can be observed in a measurement of the tunneling current, e.g. V_{12}, as a function of Aharonov-Bohm phase. One way the Aharonov-Bohm phase can be tuned is by changing the area of the interferometer, by applying a gate G which locally pushes the edge of quantum Hall liquid inwards. For the $\nu = \frac{5}{2}$ Pfaffian state there is an even-odd effect if non-abelian quasiparticles are trapped inside the interferometer, e.g. on a central island: for an even number of quasiparticles interference oscillations can be observed, for an odd number interference is predicted to vanish completely.

The turning point in a sense was the proposal (in 2005) of a relatively simple setup for the $\nu = \frac{5}{2}$ that predicted a very clear signature of a non-abelian effect, made by Bonderson, Kitaev, and Shtengel (2006a); Stern and Halperin (2006). Their setup, see Fig. 1-4, uses an interferometer made out of two quantum point contacts, a setup similar to the one with only one QPC as described in section 1.1. Tunneling quasiparticles now have two paths to tunnel from one edge to the other edge and these two different paths can interfere. If non-abelian quasiparticles are trapped inside the interferometer paths there should be a clear non-abelian signature based on the parity of the number of trapped quasiparticles: for an even number interference between the two paths should be observable, and for an odd number of quasiparticles the interference should vanish entirely. Note that this proposal did not introduce any new concepts but combined several existing ingredients, two point contact interferometers in fractional quantum Hall setting (Chamon, Freed, Kivelson, Sondhi, and Wen, 1997), interference measurement outcomes for non-abelian anyons (Overbosch and Bais, 2001; Bonderson, Shtengel, and Slingerland, 2008), braid properties of the Pfaffian non-abelian quasiparticles (Moore and Read, 1991; Nayak and Wilczek, 1996), storing qubits in a $\nu = \frac{5}{2}$ state (Freedman, Nayak, and Walker, 2006), into a setup with a *very simple* 'even-odd' signature of a non-abelian effect, and they provided arguments that suggested the interferometer setup could be physically realized in a $\nu = \frac{5}{2}$ system. Final aspect was the possibility for funding of such an experiment in terms of an application for topological quantum computation, a field started by a paper by Kitaev (2003, first appeared in 1997).

With several experiments underway since 2006 the non-abelian fractional quantum Hall arena was (re-)opened.

1.3.1 Encountered hurdles in the $\nu = \frac{5}{2}$ state

Present day (summer 2008) reality is that no non-abelian signature has been observed in the $\nu = \frac{5}{2}$ state (yet). This is not entirely surprising given the fact that interference due to tunneling fractional quasiparticles has not been unambiguously observed in *any* fractional quantum Hall state. There have been interferometer setups with two point contacts that observe some form of interference (see e.g. Camino, Zhou, and Goldman, 2007), but it has not been cleared up what exactly interferes in those setups (and these might very well be charging/quantum dot related oscillations).

It is also still unclear whether the physical state at filling fraction $\nu = \frac{5}{2}$ is the Pfaffian state or not, in other words whether the actual state is in the same universality class as the wavefunction proposed by Moore and Read. To answer this question does not necessarily require an interferometer though. Transport experiments on a *single* QPC should in principle be able to determine the fractional charge e^* and tunneling exponent g of the tunneling quasiparticle. The reason is that the tunneling current I in relation to finite bias V is non-linear, with functional dependence on both e^* and g; we provide a detailed discussion on such conductance and noise measurements in chapter 2. The quasiparticles in the Pfaffian trial wavefunction have charge $e^* = e/4$ and exponent $g = 1/4$; the quarter charge is truly fixed without wiggle-room, the value of the exponent g could be renormalized by interactions however, such that the experimentally observed g could be lower than the predicted value.

Trying to measure the quasiparticle charge and exponent with a setup with a single QPC may seem simpler than an interferometer constructed from two QPCs but is challenging enough by itself. The non-linear I-V-curve had not been matched to theoretically predicted cures for *any* fractional state. The celebrated shot-noise measurements that revealed $e^* = e/3$ for the $\nu = \frac{1}{3}$ Laughlin state is basically a measurement of the linear regime. The underlying cause is that a quantum point contact does more than just induce tunneling between isolated points on opposite sides of the quantum Hall liquid. A QPC is an external electrostatic potential which repels electrons; it does not only move the boundaries of the quantum Hall liquid but it also influences the local electron density. If the electron density changes too much the quantum Hall state itself becomes locally unstable and the local state under the QPC can become different from the bulk state. All assumptions about tunneling and interference are primarily based on the fact that the same quantum Hall state exists everywhere: on both sides of and underneath each quantum point contact. The good news is that very recently measurements on a single QPC in the $\nu = \frac{5}{2}$ state have been performed (Dolev, Heiblum, Umansky, Stern, and Mahalu, 2008; Radu, Miller, Marcus, Kastner, Pfeiffer, and West, 2008), including a 'local' experiment by an MIT group.

Theoretically things became more interesting as well for the $\nu = \frac{5}{2}$ state, through the discovery of another candidate state dubbed the anti-Pfaffian (Lee, Ryu, Nayak, and Fisher, 2007; Levin, Halperin, and Rosenow, 2007). The anti-Pfaffian is the particle-hole conjugated state of the Pfaffian wavefunction. The filling fraction $\nu = 2 + \frac{1}{2}$ lies at a symmetric point inside the Landau-level (the particle-hole symmetric point of the second Landau level), but

the Pfaffian state breaks this symmetry. The conjugate anti-Pfaffian state was shown to be in a different universality class, with predicted charge still $e^* = e/4$ but with exponent $g = 1/2$ (Lee *et al.*, 2007; Levin *et al.*, 2007). In other words these states should be distinguishable in a transport measurement on a single QPC (see for instance the figures in sections 2.4 and 2.6).

The single QPC experiments (Dolev *et al.*, 2008; Radu *et al.*, 2008) where consistent with a fractional charge $e^* = e/4$ and a quasiparticle exponent $g \approx 0.4$. This favors the anti-Pfaffian state, since this value is consistent with a value of $g = 1/2$ that is renormalized downwards due to interactions. However, there is another type of interaction that needs to be considered: edge reconstruction. Edge reconstruction is a phase transition on the edge which can lead to different exponents g and even change the quasiparticle exponent e^* (paradoxically). Under edge reconstruction pairs of counterpropagating edge modes can appear, for instance through a change of the confining potential and/or local interactions. Under the opposite process pairs of counterpropagating edge branches can become gapped. This is the mains subject of chapter 5. Important to note is that under edge reconstruction and/or gapping of modes the value of the exponent g can *increase*.

It may thus seem that a measurement on a single QPC cannot even identify the actual state amongst the differen $\nu = \frac{5}{2}$ candidate states, because the only theoretical distinction, the value quasiparticle exponent g, can both be increased and decreased by interactions. The current truth is that it is too early to make any such claim. Edge reconstruction for non-abelian states is not well understood yet. Recent numerical simulations for $\nu = \frac{5}{2}$ (Wan, Hu, Rezayi, and Yang, 2008) show traces of edge reconstruction as well, and may help shine light on the open issues here. Furthermore, experiments have not actively explored the possibility of inducing such a phase transition on the edge.

A challenge that lies ahead for *interference* setups is that of decoherence due to slow neutral velocities. If multiple edge branches are concerned (like for the non-abelian $\nu = \frac{5}{2}$ candidate states) there typically is a separation into a fast charged mode and a neutral mode. The neutral mode have a much slower velocity than the fast mode that could lead to decoherence on a scale smaller than the interferometer. The result would be no interference. Numerical simulations on systems with a few electrons have identified a neutral edge velocity that is much smaller than the charged one.

The neutral mode has never been observed yet in experiment, and is an interesting and physical question by itself, valid for any multiple-branch quantum Hall state (including well-known abelian state such as the $\nu = \frac{2}{3}$ state). In chapter 6 we propose a setup that can probe slow edge velocities; the setup uses a single but very long quantum point contact and coherent tunneling.

Although no open issues about the $\nu = \frac{5}{2}$ state have been settled, there is also some good news. Both the Pfaffian and the anti-Pfaffian are non-abelian states, and experiments have not ruled out either of them yet. Both states would display a similar even-odd effect, and the $\nu = \frac{5}{2}$ state is still a *very* strong candidate state to observe the first-ever signature of non-abelian statistics.

1.4 Organization

The organization of this dissertation is as follows. Chapter 1 is meant as warm-up, and to get the reader acquainted with the backgrounds of the problem that will be studied: edge tunneling and transport in non-abelian fractional quantum Hall systems. Calculating transport in perturbation theory for abelian fractional quantum Hall states is reviewed in chapter 2; interference in a double point contact interferometer setup is also described here. Chapter 3 deals with the extension of the abelian transport theory to be applicable to non-abelian FQH systems as well: the conformal block decomposition. Throughout this thesis the $\nu = \frac{5}{2}$ Pfaffian state will be used as concrete example for a non-abelian FQH system. Chapters 4, 5 and 6 treat specialized topics based on research papers.

In chapter 4 we consider the vanishing interference in a $\nu = \frac{5}{2}$ interferometer setup with a non-abelian quasiparticle inside the interferometer; we identify a higher order process that restores some interference, and we determine the temperature and voltage (scaling) dependence of the quasiparticle tunneling current.

Tunneling between different branches on the *same* edge is studied in chapter 5 for the cases of the Pfaffian and anti-Pfaffian descriptions for the $\nu = \frac{5}{2}$ state. A phase transition on the edge (not in the bulk) is found that involves the gapping of two Majorana modes. Such a phase transition can change the values of quasiparticle charge and exponent that are measured in transport.

Chapter 6 describes a proposal for a setup to detect slow edge velocities. The proposed mechanism is resonant tunneling due to coherent interference at a long point contact. Slow edge velocities are suspected to play a role in the $\nu = \frac{5}{2}$ state, but can be present in various other states as well, such as the abelian $\nu = \frac{2}{3}$ state.

We reflect on some of aspects in the earlier chapters and conclude in chapter 7.

Note that in this thesis we *do not* review the quantum Hall effect or conformal field theory. A basic understanding of the quantum Hall effect is a prerequisite; an introduction to the quantum Hall effect can be found in most standard condensed matter textbooks. To fully appreciate the results in this thesis, some familiarity with conformal field theory is required; the main results should nevertheless be comprehensible with such prior knowledge.

1.5 Notation and scales in the fractional quantum Hall effect

There exist several reference textbooks dedicated to the (fractional) quantum Hall effect (Prange and Girvin, 1987; Das Sarma and Pinczuk, 1997; Ezawa, 2000; Yoshioka, 2002), but none stands out in particular. For the chiral Luttinger liquid theory of the fractional quantum Hall edge Wen (1992, 1995, 2004) is the main reference.

Throughout this thesis we will mainly work in units in which most physical constants be ignored, i.e., $c = 1$, $k_B = 1$, $\hbar = 1$. In two-dimensions, the complex notation $z = x + iy$ is used to write coordinates x and y. Lengths are expressed in terms of the magnetic length l_B, i.e., the cyclotron (Larmor) radius,

$$l_B = \sqrt{\frac{\hbar}{eB}} \simeq \frac{25.6}{\sqrt{B}}\,\mathrm{nm} \overset{B=4\mathrm{T}}{=} 12.8\,\mathrm{nm}. \tag{1.10}$$

Here we substituted some actual numbers, with perpendicular magnetic field B in Tesla, with typical strength $B = 4\mathrm{T}$ (in Radu *et al.*, 2008, the $\nu = \frac{5}{2}$ plateau appears for $B \approx 4.3\,\mathrm{T}$). With n_e the electron density in the 2DEG the filling fraction is given by

$$\nu = 2\pi l_B^2 n_e. \tag{1.11}$$

One has to realize that the 2DEG is situated inside a GaAs/AlGaAs semiconductor heterostructure, and electrons do not behave as free electrons in vacuum , but instead have an effective mass $m^* \simeq 0.067\, m_e$, a g-factor $g^* \simeq -0.44$ and experience a dielectric constant $\varepsilon \simeq 12.9\,\varepsilon_0$. Typical energy scales, in kelvin, for the Coulomb energy, cyclotron energy, and Zeeman energy are then (from Ezawa, 2000)

$$\frac{e^2}{4\pi\varepsilon l_B} \simeq 50.8\sqrt{B}\,\mathrm{K} \overset{B=4\mathrm{T}}{=} 100\,\mathrm{K}, \tag{1.12}$$

$$\hbar\omega_c = \frac{\hbar e B}{m^*} \simeq 20.0 B\,\mathrm{K} \overset{B=4\mathrm{T}}{=} 80\,\mathrm{K}, \tag{1.13}$$

$$|g^*\mu_B B| \simeq 0.296 B\,\mathrm{K} \overset{B=4\mathrm{T}}{=} 1.2\,\mathrm{K}. \tag{1.14}$$

Activation gaps can range from a few hundred millikelvin to several kelvin for the less fragile FQH states.

We do not distinguish between quasiparticles and quasiholes, and refer to these generically as quasiparticles.

1.5.1 What is an abelian FQH state, what a non-abelian?

The distinction between abelian and non-abelian, fundamentally, has to do with a difference in quasiparticle statistics. For an application in quantum Hall effect, in a setting where fractional statistics of anyons itself is not the main focus, one could also advocate either one of the following point of views:

- The edges of an abelian FQH state can be described in terms of bosonic degrees of freedom and a K matrix; everything else, like a Majorana edge mode is non-abelian.
- the bulk-quasiparticles of an abelian FQH state form a one-dimensional irreducible representation of the braid group; for a non-abelian state they form a higher-than-one dimensional irreducible representation.
- the conformal field theory of the edge of an abelian FQH state is described by a central charge $c = 1$ CFT, otherwise the state is non-abelian

In chapter 3 we provide yet another alternative point of view that emphasizes the basis of the internal state of non-abelian anyons.

1.6 Guide to literature

Throughout this thesis we provide numerous references to the literature, often quite specialized to the subject. Here we list a few references for the reader interested in either a broader view or a more pedagogical treatment of the basics.

An overview of the state of the field of the fractional quantum Hall edge *before* $\nu = \frac{5}{2}$ is given in the review by Chang (2003).

For the theory-side of the $\nu = \frac{5}{2}$ FQH state, Milovanović and Read (1996) is both easy-to-read and very detailed; it explains very well how the edge excitations of the Moore-Read state can be understood in terms of a Majorana mode. Other, perhaps more original, references are Greiter, Wen, and Wilczek (1991); Moore and Read (1991); Wen (1993); Fradkin, Nayak, Tsvelik, and Wilczek (1998). In Nayak and Wilczek (1996); Georgiev (2003); Georgiev and Geller (2006); Georgiev (2006) some of the subtleties in dealing with $\nu = \frac{5}{2}$ and conformal field theory are worked out in detail.

A good starting point for topological quantum computation and non-abelian anyons is the review by Nayak, Simon, Stern, Freedman, and Das Sarma (2007), perhaps more advanced is Kitaev (2003, 2006). More connections to topological order, quantum hall states, fractional statistics, Chern-Simons theory, can be found in e.g. Witten (1989); Wen (1995); Fröhlich, Pedrini, Schweigert, and Walcher (2001); Oshikawa and Senthil (2006); Oshikawa, Kim, Shtengel, Nayak, and Tewari (2007).

Chamon *et al.* (1997) summarizes the important aspects of calculating transport in fractional quantum Hall states and is the reference for double point contact interferometry. A more detailed discussion about noise and introduction to Keldysh ordering can be found in Chamon, Freed, and Wen (1995, 1996).

Chapter 2

Tunneling between edges in perturbation theory

In this section the leading order perturbative calculation for tunneling current, noise, and interference in current and noise will be discussed. Most of this is based on previous work, especially (Chamon *et al.*, 1997), see also (Wen, 1991a, 1995), except for the interference in the noise and the unequal arm-lengths of the two interferometer paths. Since the details in the original work have several typos, and for the sake of completeness, a very detailed treatment is given here. The conformal block decomposition required for non-abelian states is not yet discussed, so strictly speaking these results hold for abelian states only.

For the Laughlin states, with filling fraction $\nu = \frac{1}{m}$, $m = 3, 5, 7, \ldots$, there exists a non-perturbative solution for the tunneling current (Fendley, Ludwig, and Saleur, 1995); this is an exact numerical solution valid for arbitrary tunneling amplitude strengths, not just weak-tunneling. It is unclear at this point though if this solution, based on a thermodynamic Bethe ansatz, can be applied to other FQH states as well, whereas perturbation theory can be used for any FQH states.

2.1 Tunneling current in linear response

Tunneling of quasiparticles between opposite edges of the same QH fluid is considered. Tunneling takes place at given sites (the QPCs). The basic idea is to calculate the expectation value of the tunneling current operator in linear response,

$$I_{\text{tun}} = \langle j_{\text{tun}}(t) \rangle = \langle 0 |\, S^\dagger(t, -\infty)\, j_{\text{tun}}(t)\, S(t, -\infty)\, |0\rangle, \tag{2.1}$$

where $S(t, -\infty)$ is the time evolution operator. The full Hamiltonian H is written as the sum of an unperturbed free Hamiltonian H_{free} and a perturbation H_{tun}, $H = H_{\text{free}} + H_{\text{tun}}$. The tunneling current to lowest non-zero order is the familiar linear response result in terms of a commutator of the operator and the perturbation,

$$\langle j_{\text{tun}}(t) \rangle = -i \int_{-\infty}^{t} dt' \, \langle 0 | [j_{\text{tun}}(t), H_{\text{tun}}(t')] | 0 \rangle. \tag{2.2}$$

The expectation value is taken with respect to the groundstate of the free Hamiltonian; we will consider this expectation value both at zero and at finite temperature.

The tunneling Hamiltonian destroys quasiparticles on one edge and creates them on the opposite edge, with some coupling Γ,

$$H_{\text{tun}} = \sum_{i=1}^{N} \Gamma_i e^{-i\omega_{J_i} t} \psi_i^\dagger(t, x_{L_i}) \psi_i(t, x_{R_i}) + \text{H.c.} \tag{2.3}$$

The voltage bias V between the two edges is explicitly included in the tunneling Hamiltonian through a phase factor in terms of the Josephson frequency $\omega_{J_i} = e_i^* V/\hbar$, which amounts to integrating over the vector potential between the two tunneling sites (Wen, 2004, p. 135). In principle there can be multiple tunneling sites and multiple types of quasiparticles tunneling. We restrict ourselves to only one type of quasiparticle that is allowed to tunnel (having multiple types is conceptually the same and can straightforwardly be included), and N then indicates the number of tunneling sites, with coordinates x_{L_i/R_i} on the left- and right-moving edges. The quasiparticle charge is e^*.

The tunneling current operator j_{tun} is closely related and looks very similar to the tunneling Hamiltonian (but notice the additional sign under complex conjugation)

$$j_{\text{tun}}(t) = ie^* \sum_{i=1}^{N} \Gamma_i e^{-i\omega_J t} \psi^\dagger(t, x_{Li}) \psi(t, x_{Ri}) + \text{H.c.}, \tag{2.4}$$

and follows from considering the time evolution of total charge on the left and right edges.

Setting $N = 1$ for simplicity, plugging tunneling Hamiltonian and current operator into Eq. (2.2) gives eight terms, two from the commutator and two for each Hermitean conjugation. Half of these eight terms are zero because they create a net charge, which has zero expectation value. Shifting time by t, the remaining four terms are of the form of a fouriertransform along the half-line $t' < 0$. Two of the four are a time-ordered expectation value, the other two are anti-time-ordered. Using knowledge that switching time-ordering amounts to switching the sign of of time, we can combine the four terms as follows

$$\begin{aligned}
&e^*|\Gamma|^2 \int_{-\infty}^{0} dt' \Big[e^{i\omega_J t'} (\mathcal{T}\text{-order}) - e^{-i\omega_J t'} (\mathcal{T}\text{-order}) \\
&\qquad\qquad - e^{i\omega_J t'} (\text{anti-}\mathcal{T}\text{-order}) + e^{-i\omega_J t'} (\text{anti-}\mathcal{T}\text{-order}) \Big] \\
=&e^*|\Gamma|^2 \left[\int_{-\infty}^{\infty} dt' e^{i\omega_J t'} (\mathcal{T}\text{-order}) - \int_{-\infty}^{\infty} dt' e^{-i\omega_J t'} (\mathcal{T}\text{-order}) \right] \\
=&e^*|\Gamma|^2 \int_{-\infty}^{\infty} dt' e^{i\omega_J t'} (\mathcal{T}\text{-order}) - (\omega_J \leftrightarrow -\omega_J).
\end{aligned}$$

The tunneling current is now expressed in terms of the fouriertransform of a time-ordered correlation function, with only the odd part in ω_J contributing (in other words, flipping sign of bias voltage V flips the direction of the current).

Two-particle (time-ordered) correlation functions at zero temperature are given by

$$\langle\psi^\dagger(t_1,x_1)\psi(t_2,x_2)\rangle = \langle\psi(t_1,x_1)\psi^\dagger(t_2,x_2)\rangle = \frac{1}{\{\delta + i[t_1 - t_2 \pm (x_1 - x_2)]\}^g}, \tag{2.5}$$

where the $\pm$ sign indicates left- or right-mover, and the exponent g is determined by the quasiparticle type. Notice that the infinitesimal δ in the correlation function prevents the function from crossing the branch-cut for any value of t and x. Therefore one can unambiguously replace an anti-time-ordered function by the complex-conjugated time-ordered fucation, which clearly amounts to swapping the sign of $t_i - t_j$ and $x_i - x_j$.

For N larger than 1 the expression for the tunneling current becomes more involved, because the dependence on distance x on both edges enters the expression. Defining

$$x_{ij} \equiv \frac{x_{L_{ij}} + x_{R_{ij}}}{2}, \qquad \delta x_{ij} \equiv \frac{x_{L_{ij}} - x_{R_{ij}}}{2}, \tag{2.6}$$

the general expression for the tunneling current becomes

$$\boxed{\begin{aligned} I_{\rm tun} =& e^* \sum_{i,j=1}^{N} \frac{\Gamma_i\Gamma_j^* e^{i\omega_J \delta x_{ij}} + \Gamma_i^*\Gamma_j e^{-i\omega_J \delta x_{ij}}}{2} \left[\int_{-\infty}^{\infty} e^{i\omega_J t} P_g(t, x_{ij}) - (\omega_J \leftrightarrow -\omega_J)\right] \\ =& e^* \sum_{i,j=1}^{N} \frac{\Gamma_i\Gamma_j^* e^{i\omega_J \delta x_{ij}} + \Gamma_i^*\Gamma_j e^{-i\omega_J \delta x_{ij}}}{2} \left[\tilde{P}_g(\omega_J, x_{ij}) - (\omega_J \leftrightarrow -\omega_J)\right]. \end{aligned}} \tag{2.7}$$

The right-most factor is still odd in ω_J but the phase-factor in front is not when $\delta x_{ij} \neq 0$. The possibility of a non-zero δx_{ij} was not considered in the original work by Chamon *et al.* (1997). Here we see that the effects of including $\delta x_{ij} \neq 0$ are relatively small; depending on the circumstances the extra phase-factors may be fully observed into the Γ_i, or the ω_J dependence may cause an observable shift in phase that is linear in bias.

P_g and $\tilde{P}_g$ are the two-particle correlation function and its fouriertransform for quasiparticle tunneling operators; P_g is the product of the two-particle correlation functions on the left and right edges. At zero temperature they are

$$P_g(t,x) = P_g(t,-x) = \frac{1}{[\delta + i(t-x)]^g\ [\delta + i(t+x)]^g}, \tag{2.8}$$

$$\tilde{P}_g(\omega,x) = \tilde{P}_g(\omega,-x) \equiv \tilde{P}_g(\omega,0) H_g(\omega,x), \tag{2.9}$$

$$\tilde{P}_g(\omega,0) = \lim_{\delta\to 0}\int_{-\infty}^{\infty} e^{i\omega t}\frac{1}{(\delta+it)^{2g}} = \lim_{\delta\to 0}\frac{2\pi}{\Gamma[2g]}\theta(\omega)\omega^{2g-1}e^{-\omega\delta} = \frac{2\pi}{\Gamma[2g]}\theta(\omega)\,\omega^{2g-1}. \tag{2.10}$$

At finite temperature they are

$$P_g(T,t,x) = P_g(T,t,-x) \equiv \frac{(\pi T)^{2g}}{[i\sinh\pi T(t-x)]^g\ [i\sinh\pi T(t+x)]^g}, \tag{2.11}$$

$$\tilde{P}_g(T,\omega,x) = \tilde{P}_g(T,\omega,-x) = \tilde{P}_g(T,\omega,0)H_g(T,\omega,x), \tag{2.12}$$

$$\tilde{P}_g(T,\omega,0) = \int_{-\infty}^{\infty} dt e^{i\omega t} \frac{(\pi T)^{2g}}{[i\sinh \pi T t]^{2g}} = (2\pi T)^{2g-1} B[g+i\bar{\omega}, g-i\bar{\omega}] e^{\pi\bar{\omega}}. \tag{2.13}$$

The notation $\bar{\omega} \equiv \omega/(2\pi T)$ was introduced to reduce the number of 2π factors. The function $H_g(\omega, x)$ (and likewise $H_g(T,\omega,x)$) is even in x and $H_g(\omega, x=0) = 1$; explicit expressions are given in section 2.3.

2.2 Origin of power-law correlation functions

Where does the power-law form of the correlation functions come from? In this thesis we will not go too deep into understanding this question. More important at this point is that exact (even analytical) expressions exist for these correlation functions and fouriertransforms at zero and finite temperature. The χLL theory for the edge (Wen, 1995) tells us they have this form. One can trust this outcome based on the results from free boson field theory and/or conformal field theory. Another approach is to consider a set of (chiral) harmonic oscillators ϕ, with a linear dispersion relation. The quasiparticle correlation functions can be written as exponentials of ϕ-field correlation functions.

Consider the small q behavior of the following expression,

$$\sum_{n=1}^{\infty} \frac{e^{inq}}{n} = -\log(1-e^{iq}) = -\log q + \frac{i\pi}{2} + \mathcal{O}(q). \tag{2.14}$$

This diverges when $q \to 0$; introduce a cut-off (infinitesimal, small-distance) δ, then the form of a power-law correlation function appears

$$e^{\alpha \sum_{n=1}^{\infty} \frac{e^{inq}}{n}} = \frac{1}{(\delta + it)^{\alpha}}, \qquad q \to -t + i\delta. \tag{2.15}$$

To connect this to physical system of harmonic oscillators, express correlation function in basis of momentum eigenstates, which then looks as follows

$$\langle \phi(t)\phi(0)\rangle \sim \sum_k \frac{e^{-ivkt}}{k}, \qquad k = \frac{2\pi n}{L}, \qquad q \to -\frac{2\pi}{L} vt + i\delta. \tag{2.16}$$

For the power-law form (without the cut-off δ) to be valid times should be large enough such that the cut-off at $t = 0$ does not enter, but should be smaller than the system size L/v.

At finite temperature one could repeat such a calculation for the expectation value of harmonic oscillator operators at finite temperature. Alternatively (Shankar, 1990), from a conformal field theory point of view, this amounts to making imaginary time periodic, with period $\beta = 1/T$. This can be interpreted as a conformal map from z to w,

$$z = e^{2\pi T(i\tau \pm x/v)} \equiv e^{w}. \tag{2.17}$$

The finite temperature correlation function then simply follows from the CFT transformation rules for primary fields under a map $z \to w$, and going back to real time. The cut-off δ can be reinserted to assure proper ordering of imaginary time.

2.3 Mathematical intermezzo: analytic expressions for fourier-transforms of correlation functions

The result

$$\int_{-\infty}^{\infty} dt e^{i\omega t} \frac{(\pi T)^{2g}}{[i \sinh \pi T t]^{2g}} = (2\pi T)^{2g-1} B[g + i\bar{\omega}, g - i\bar{\omega}] e^{\pi\bar{\omega}}, \tag{2.18}$$

is meant as the limit of taking δ to zero of

$$\int_{-\infty}^{\infty} dt e^{i\omega t} \frac{(\pi T)^{2g}}{[\sin \pi T(\delta + it)]^{2g}} = (2\pi T)^{2g-1} B[g + i\bar{\omega}, g - i\bar{\omega}] e^{\pi\bar{\omega}} e^{-\omega\delta}. \tag{2.19}$$

Equation (2.19) can be obtained starting from an explicit primitive in terms of a hypergeometric function,

$$\begin{aligned} \int dt e^{i\omega t} \frac{(\pi T)^{2g}}{[\sin \pi T(\delta + it)]^{2g}} &= (2\pi T)^{2g-1} e^{i\omega t} \frac{(iz)^{2g}}{g + i\bar{\omega}} \, {}_2F_1[2g, g + i\bar{\omega}, 1 + g + i\bar{\omega}; z^2] \\ &= (2\pi T)^{2g-1} (i)^{2g} e^{-2\pi i \delta T} \sum_{n=0}^{\infty} \frac{e^{2\pi T t(g + i\bar{\omega} + n)}}{n!(g + i\bar{\omega} + n)} \frac{\Gamma[2g + n]}{\Gamma[2g]}, \qquad z = e^{\pi T(t - i\delta)}. \end{aligned}$$

Taking the derivative with respect to t again indeed verifies the expression for the primitive, with the help of the identities

$$\sin \pi T(\delta + it) = \frac{1 - z^2}{2zi}, \qquad \sum_{n=0}^{\infty} \frac{z^{2n}}{n!} \frac{\Gamma[2g + n]}{\Gamma[2g]} = (1 - z^2)^{-2g}. \tag{2.20}$$

Evaluating the limits for the primitive, Eq. (2.20), the limit $t \to -\infty$ gives zero. Evaluating the limit $t \to \infty$ requires a transformation identity for hypergeometric functions, basically an analytic continuation, where instead of z the argument is $1/z$ (Abramowitz and Stegun, 1964, Eq. (15.3.7), p. 559). The resulting expression contains several gamma functions, which can be straightforwardly simplified to give Eq. (2.19).

The hypergeometric function is the standard primitive given by Mathematica, but alternative expressions in terms of incomplete beta functions exist as well,

$$e^{i\omega t} \frac{z^{2g}}{g + i\bar{\omega}} \, {}_2F_1[2g, g + i\bar{\omega}, 1 + g + i\bar{\omega}; z^2] = e^{-\omega\delta} B[z^2; g + i\bar{\omega}, 1 - 2g], \tag{2.21}$$

$$\int dt e^{i\omega t} \frac{(\pi T)^{2g}}{[\sin \pi T(\delta + it)]^{2g}} = (2\pi T)^{2g-1} e^{-\omega\delta} (i)^{2g} B[z^2; g + i\bar{\omega}, 1 - 2g], \tag{2.22}$$

$$\int dt e^{i\omega t}\frac{(\pi T)^{2g}}{[\sin \pi T(\delta+it)]^{2g}} = -(2\pi T)^{2g-1}e^{-\omega\delta}(-i)^{2g}B[z^{-2};g-i\bar{\omega},1-2g]. \tag{2.23}$$

These primitives can be deduced from integral representation of the incomplete beta function and a substitution $z = e^{\pm\pi T(t-i\delta)}$, with reference point at $t = \mp\infty$. The difference between the two distinct primitives should be a constant, and we have

$$(i)^{2g}B[z^2;g+i\bar{\omega},1-2g]+(-i)^{2g}B[z^{-2};g-i\bar{\omega},1-2g] = B[g+i\bar{\omega},g-i\bar{\omega}]e^{\pi\bar{\omega}}, \tag{2.24}$$

valid for $\mathrm{Re}(z) > 0$, i.e., $\delta < 1/(2T)$, which follows from analytic continuation identities. Recall that a series expansions for hypergeometric function or beta function is only valid for argument $|z| \leq 1$ since the series diverges when argument $|z| > 1$.

The beta function is very well behaved, and decays exponentially for any $g > 0$, and in the limit of large $\bar{\omega}$ the zero temperature limit is easily recovered,

$$\lim_{s\to\infty} B[g+is,g-is] = \frac{2\pi}{\Gamma[2g]}e^{-\pi|s|}|s|^{sg-1}. \tag{2.25}$$

For integer and half-integer values of g the beta function simplifies to a hyperbolic trigonometric function, $B[1+is,1-is] = \pi s/\sinh \pi s$, $B[\frac{1}{2}+is,\frac{1}{2}-is] = \pi/\cosh \pi s$.

The function H_g can be defined by using inverse fouriertransforms, which gives a product (convolution) of beta functions, which then need to be fouriertransformed with respect to x. There are various ways to express $H_g(T,\omega,x)$ with no real preference for one over the other,

$$\begin{aligned}
H_g(T,\omega,x) =& \frac{1}{B[g,g]}\int_{-\infty}^{\infty}\frac{d\bar{u}}{4\pi}e^{-i\bar{u}\bar{x}}B\left[\frac{g}{2}-i\frac{\bar{\omega}+\bar{u}}{2},\frac{g}{2}-i\frac{\bar{\omega}-\bar{u}}{2}\right]B\left[\frac{g}{2}+i\frac{\bar{\omega}+\bar{u}}{2},\frac{g}{2}+i\frac{\bar{\omega}-\bar{u}}{2}\right]\\
=& \frac{1}{B[g,g]}\int_0^{\infty}da\frac{a^{g-1}}{(1+a)^{g-i\bar{\omega}}}\frac{1}{(e^{-\bar{x}}+ae^{\bar{x}})^{g+i\bar{\omega}}} &(2.26)\\
=& 2\pi\frac{\Gamma[2g]}{\Gamma[g]}\frac{e^{\bar{x}g}}{\sinh \pi\bar{\omega}}\mathrm{Im}\left\{-\frac{e^{i\bar{\omega}\bar{x}}}{\Gamma[g-i\bar{\omega}]\Gamma[1+i\bar{\omega}]}{}_2F_1[g,g+i\bar{\omega},1+i\bar{\omega},e^{2\bar{x}}]\right\} &(2.27)\\
=& \frac{1}{B[g\pm i\bar{\omega}]}\int_{-\infty}^{\infty}\frac{d\bar{u}}{4\pi}e^{-i\bar{u}\bar{x}}B\left[\frac{g}{2}+i\frac{\bar{\omega}+\bar{u}}{2},\frac{g}{2}-i\frac{\bar{\omega}+\bar{u}}{2}\right]B\left[\frac{g}{2}\pm i\frac{\bar{\omega}-\bar{u}}{2}\right]\\
=& \frac{1}{B[g+i\bar{\omega},g-i\bar{\omega}]}\int_0^{\infty}ds\frac{e^{i\bar{\omega}\bar{x}}s^{g-1+i\bar{\omega}}}{(1+s)^g(e^{-\bar{x}}+e^{\bar{x}}s)^g} &(2.28)\\
=& 2\pi\frac{\Gamma[2g]}{\Gamma[g]}\frac{e^{-\bar{x}g}}{\sinh \pi\bar{\omega}}\mathrm{Im}\left\{\frac{e^{i\bar{\omega}\bar{x}}}{\Gamma[g+i\bar{\omega}]\Gamma[1-i\bar{\omega}]}{}_2F_1[g,g-i\bar{\omega},1-i\bar{\omega},e^{-2\bar{x}}]\right\} &(2.29)\\
=& \frac{1}{B[g+i\bar{\omega},g-i\bar{\omega}]}\int_{-\infty}^{\infty}dte^{i\bar{\omega}t}\frac{2^{-g}}{(\cosh \bar{x}+\cosh t)^g} &(2.30)
\end{aligned}$$

Here $B[a\pm ib] \equiv B[a+ib,a-ib]$. From this last expression, Eq. (2.30), it is at least clear that $H_g(T,\omega,x)$ is real and an even function in both ω and x. Although it is not that obvious that $|H_g(T,\omega,x)| \leq 1$ with equality holding only when $x = 0$.

A series expansion in small x or ω becomes very hard very fast. To fourth order in x

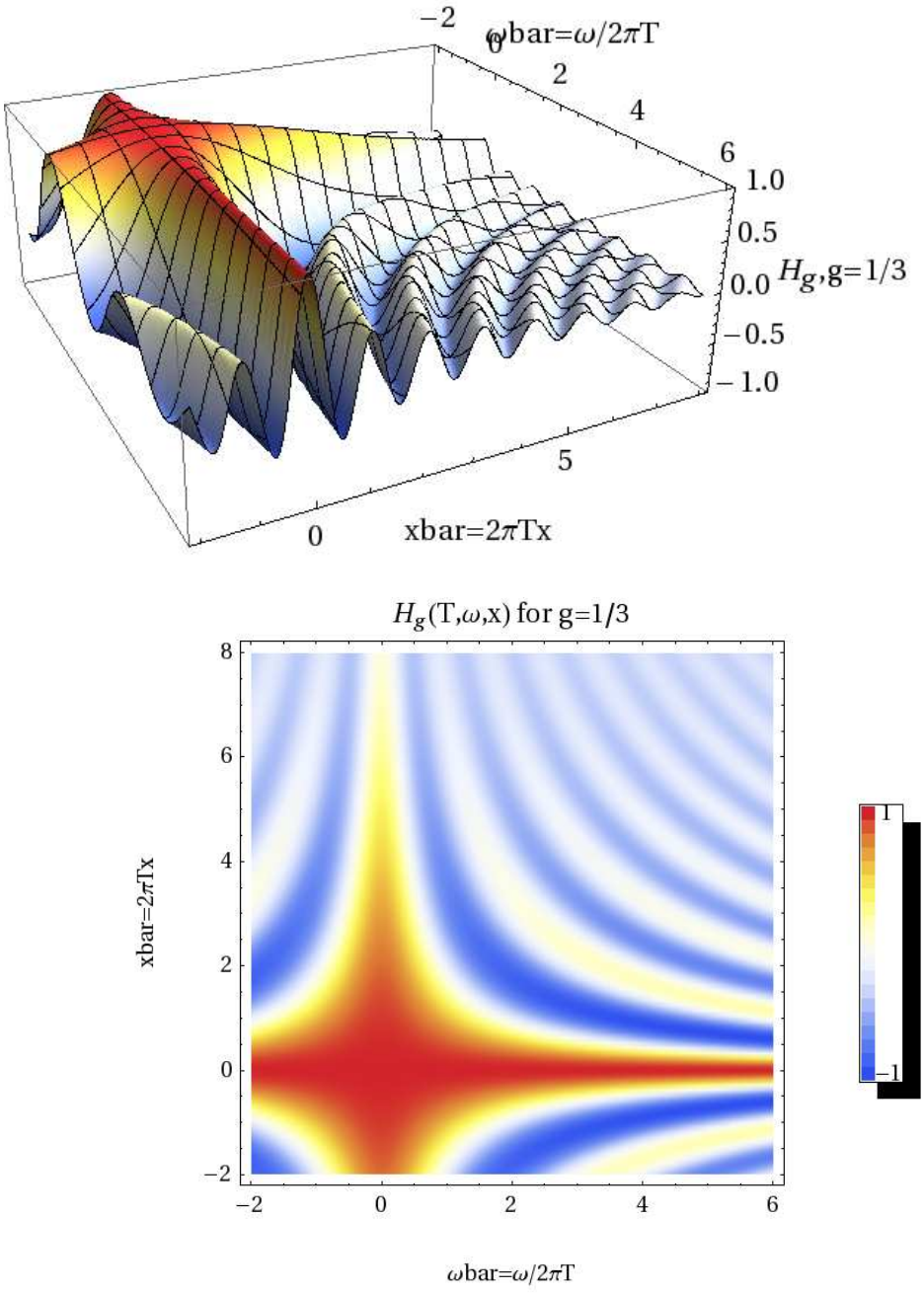

Figure 2-1: Plot of the function $H_g(T, \omega, x)$, Eq. (2.30), for $g = \frac{1}{3}$, as a 3D-plot and a density-plot. Axes are $\bar{\omega} = \omega/2\pi T$ and $\bar{x} = 2\pi T x$.

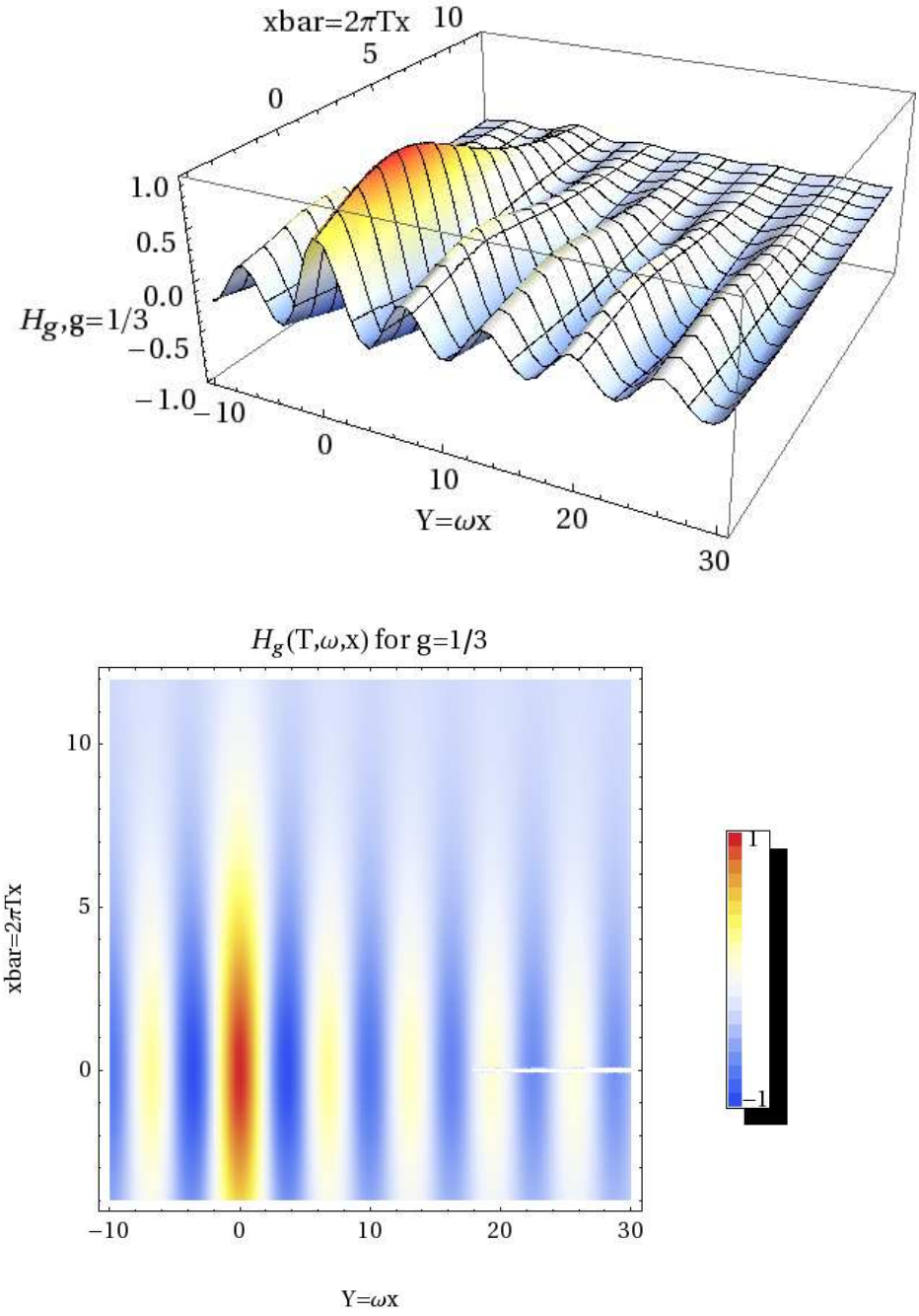

Figure 2-2: Plot of the function $H_g(T, \omega, x)$ for $g = \frac{1}{3}$, as a 3D-plot and a density-plot. Same plot as previous page, except that axes are now $Y = \omega x$ and $\bar{x} = 2\pi T x$.

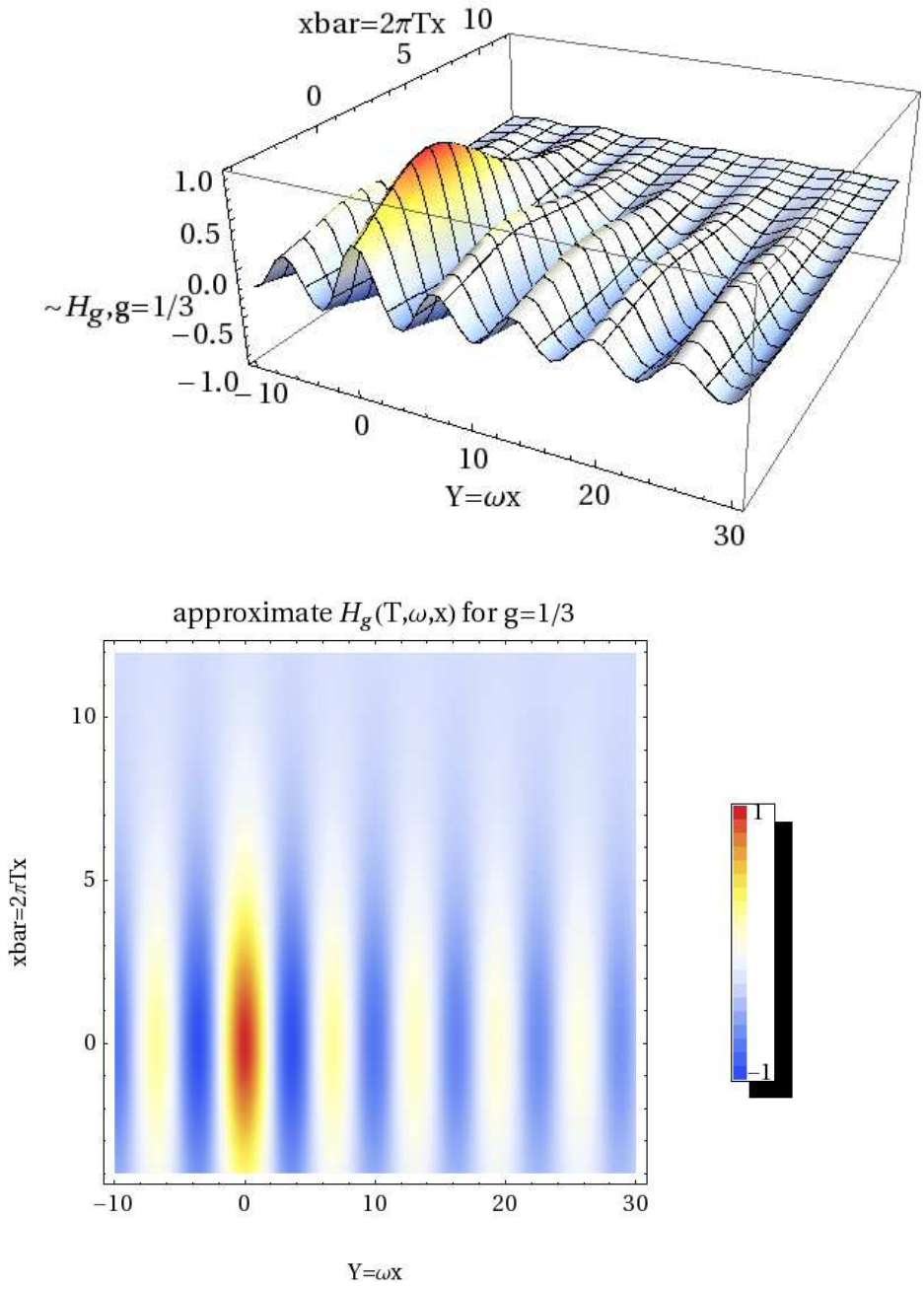

Figure 2-3: Plot of the *approximation* to the function $H_g(T, \omega, x)$, Eq. (2.33), for $g = \frac{1}{3}$, as a 3D-plot and a density-plot. Axes are $Y = \omega x$ and $\bar{x} = 2\pi T x$. The approximation captures the oscillations as a function as ωx and the exponential decay as a function of $2\pi T x$.

this is

$$H_g(Y_1=\omega x, Y_2=2\pi T x) = 1 - \frac{Y_1^2+g^2Y_2^2}{2(1+2g)} + \frac{3Y_1^4+2g(2+3g)Y_1^2Y_2^2+g^3(4+3g)Y_2^4}{24(3+2g)(1+2g)} + \mathcal{O}(x^6). \quad (2.31)$$

An analytical result for derivative of $H_g(T,\omega,x)$ with respect to ω is a very large and ugly expression. Numerical evaluation is reasonable though. The hypergeometric function written as an explicit sum is a series that converges fast, so only a few terms need to be included. The derivative with respect to ω introduces additional digamma functions. So as long as any numerical framework can evaluate gamma and digamma functions with complex arguments both $H_g(T,\omega,x)$ and $\frac{\partial}{\partial\omega}H_g(T,\omega,x)$ can be numerically evaluated to arbitrary precision (without any additional integration).

At zero temperature

$$H_g(\omega,x) = {}_0F_1\left[g+\frac{1}{2}, -\frac{1}{4}(\omega x)^2\right] = \sum_{n=0}^{\infty}\frac{\left(-\frac{1}{4}(\omega x)^2\right)^n}{(g+\frac{1}{2})_n n!} = \sqrt{\pi}\frac{\Gamma[2g]J_{g-1/2}[\omega x]}{\Gamma[g](2\omega x)^{g-1/2}}. \quad (2.32)$$

Qualitatively the function $H_g(T,\omega,x)$ can be approximated by the zero-temperature result times a decaying factor $\cosh g(2\pi T)x$,

$$H_g(T,\omega,x) \approx \frac{H_g(\omega,x)}{\cosh g\bar{x}} = \frac{\sum_{n=0}^{\infty}\frac{\left(-\frac{1}{4}(\omega x)^2\right)^n}{(g+\frac{1}{2})_n n!}}{\cosh g\bar{x}}. \quad (2.33)$$

This approximation is exact at $2\pi Tx \equiv \bar{x} = 0$, and captures the leading exponential decay at large $\bar{x}$. Leading correction at large $\bar{x}$ is a term linear in $\bar{x}$ (multiplying the overall exponential). For $g=1$ the relation is exactly $H_1(\omega,T,x) = \frac{\bar{x}}{\cosh\bar{x}}H_1(\omega,x)$.

See Figures 2-1, 2-2 and 2-3 for plots of $H_g(T,\omega,x)$ as a *scaling* function of different dimensionless ratios. We chose to set $g=\frac{1}{3}$ in these plots, which is a representative value for a whole range of exponents g, including $g=\frac{1}{4}$ and $g=\frac{1}{2}$. The approximation, Eq. (2.33), to the real $H_g(T,\omega,x)$ is useful for faster plotting, or for rough calculations, but no substitute for any real calculations.

2.4 Tunneling conductance at a single point contact

For a single tunneling site (i.e., a single QPC) the tunneling current in linear response at zero and finite temperature is

$$I_{\rm tun}(\omega=e^*V) = e^*|\Gamma|^2\frac{2\pi}{\Gamma[2g]}\mathrm{sgn}(\omega)|\omega|^{2g-1}, \quad (2.34)$$

$$I_{\rm tun}(T,\omega=e^*V) = 2e^*|\Gamma|^2(2\pi T)^{2g-1}\sinh(\pi\bar{\omega})B[g+i\bar{\omega}, g-i\bar{\omega}] \quad (2.35)$$

$$\equiv e^*|\Gamma|^2(2\pi T)^{2g-1}F_g(\bar{\omega}). \quad (2.36)$$

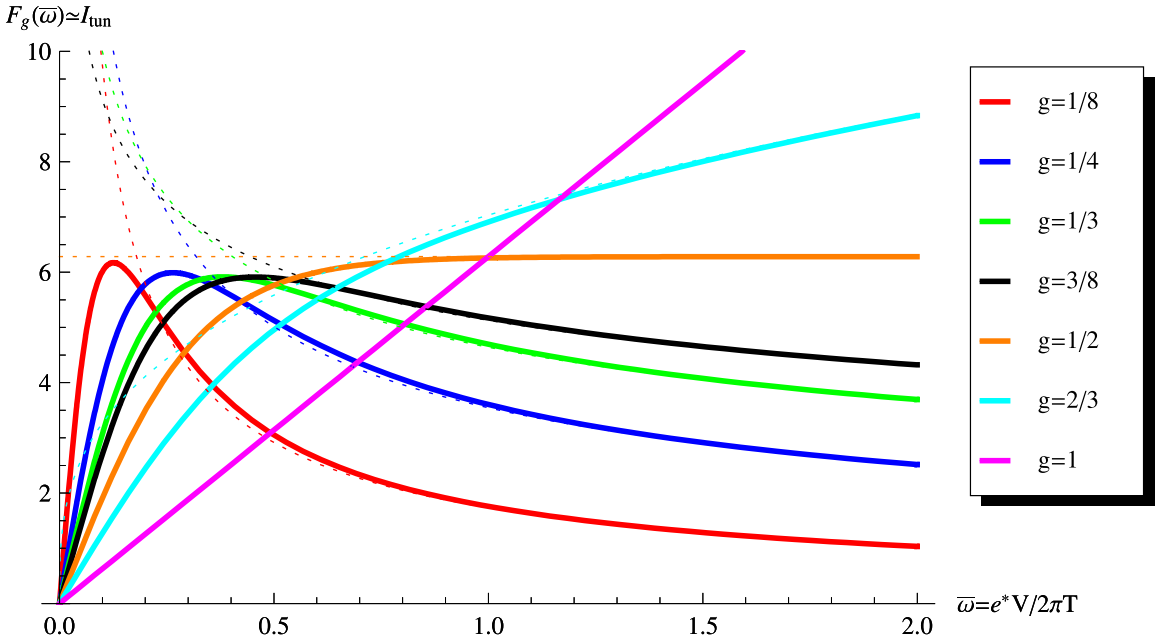

Figure 2-4: Plots of the scaling function $F_g(\bar{\omega})$, see Eq. (2.36), as function of the dimensionless ratio V/T for various values of quasiparticle exponent g. This is basically a plot of the *tunneling current* as a function of bias voltage V at fixed temperature with all constant prefactors set to one. Dotted lines indicate the zero temperature power-law behavior V^{2g-1}, which generally holds for $e^*V > 2\pi T$. For $g = 1$ (electrons) the current is linear in V (Ohm's law holds), but for any other g the I-V-curve is non-linear. For $g < \frac{1}{2}$ there is a maximum in the current at finite $\bar{\omega}$.

This defines a dimensionless scaling function $F_g(z)$. Recall that $\bar{\omega} \equiv \omega/(2\pi T)$. Figure 2-4 shows $F_g(\bar{\omega})$ for various tunneling exponents g.

Experimentally, it is usually not the tunneling current itself that is being measured, but rather the differential tunneling conductance $G_{\rm tun} = \frac{\partial}{\partial V} I_{\rm tun}$. In linear response the tunneling conductance then becomes

$$G_{\rm tun}(\omega = e^*V) = (e^*)^2 |\Gamma|^2 (2g-1) \frac{2\pi}{\Gamma[2g]} \mathrm{sgn}(\omega) |\omega|^{2g-2}, \tag{2.37}$$

$$\begin{aligned} G_{\rm tun}(T, \omega = e^*V) =& 2(e^*)^2 |\Gamma|^2 \, (2\pi T)^{2g-2} \, B[g + i\bar{\omega}, g - i\bar{\omega}] \times \\ & \Big(\pi \cosh \pi\bar{\omega} - 2 \sinh \pi\bar{\omega} \, \mathrm{Im}\big(\Psi[g + i\bar{\omega}]\big) \Big) \end{aligned} \tag{2.38}$$

$$\equiv (e^*)^2 |\Gamma|^2 \, (2\pi T)^{2g-2} f_g(\bar{\omega}), \tag{2.39}$$

where $f_g(z) = \frac{\partial}{\partial z} F_g(z)$ and $\Psi[z] = \Gamma[z]'/\Gamma[z]$ is the digamma function. Tunneling conductance for several values of g is plotted in Fig. 2-5.

The scaling function $f_g(z)$ is even in z and has a maximum at zero bias ($z = 0$) for values $0 < g < 1$. It goes through zero at $z \approx g$ for $0 < g < 1/2$, see also Fig. 2-6. At large values of z it behaves as z^{2g-2} as is obviously required by the zero temperature result.

If the tunneling conductance can be measured for different bias V and temperature T

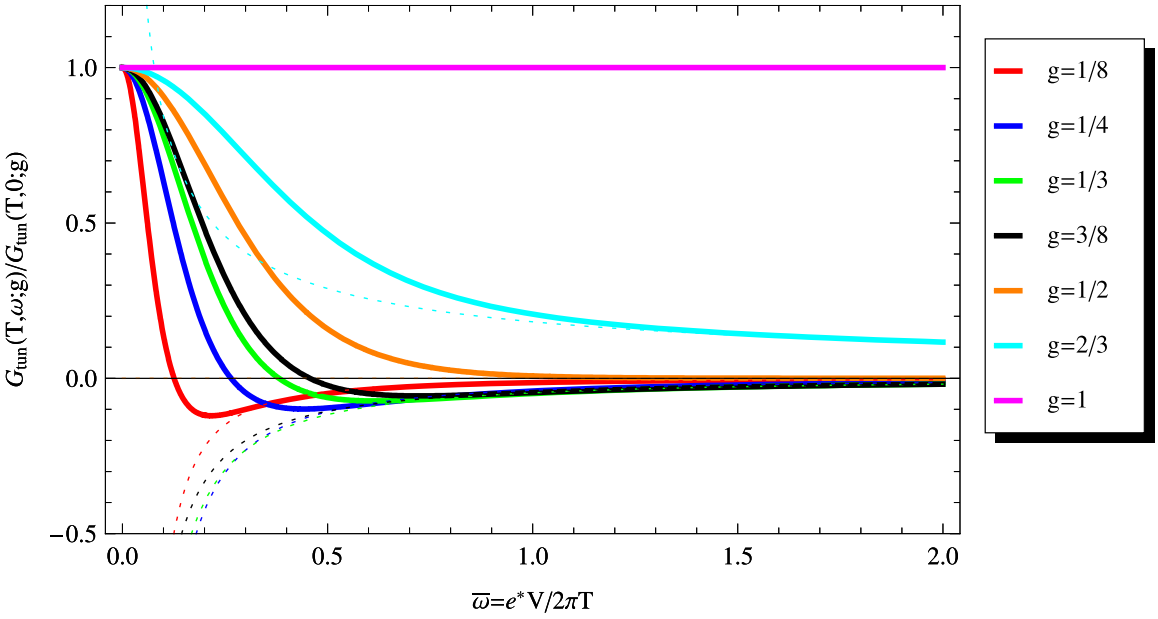

Figure 2-5: Plot of tunneling conductance $G_{\rm tun}(T,\omega;g)$, Eq. (2.39), as a function of dimensionless ratio V/T for a single QPC in linear response, plotted for several values of g. In other words this is the tunneling conductance as a function of bias voltage V at fixed temperature T. The curves are normalized to one at $\bar{\omega}=0$ (note that this is a different normalization than used in Fig. 2-4). Dotted lines indicate the zero temperature power-law behavior V^{2g-2}, which is good when $\bar{\omega}>1$. For Ohmic electrons, i.e., $g=1$, the conductance is constant as a function of bias, but for generic $g<1$ the curve is non-linear with a peak at zero bias. For $g<\frac{1}{2}$ there is a 'side-dip' negative minimum, which is much weaker than the zero bias peak; the amplitude of the side-dip is at most about 10 percent of the amplitude at zero bias. The main distinction between possible $\nu=\frac{5}{2}$ Pfaffian and anti-Pfaffian exponents $g=\frac{1}{4}$ (blue curve) and $g=\frac{1}{2}$ (orange curve) are the occurence of a minimum for $g=\frac{1}{4}$, and of course a difference in width of the zero bias peak. Measure for the width of the zero bias peak is the second derivative of the shown curves, which is $\pi^2-6\text{PolyGamma}[1,g]$. The location of the point where the tunneling conductance goes through zero is shown in Fig. 2-6.

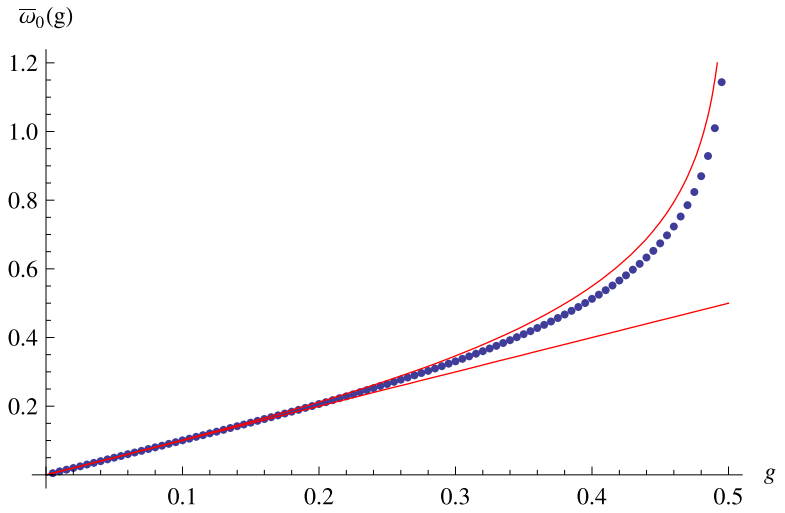

Figure 2-6: Plot of the locations of the *zeros* of the tunneling conductance, i.e., $\bar{\omega}_0(g)$ is defined through $G_{\rm tun}(\bar{\omega}_0; g) = 0$. The tunneling conductance has a zero for $0 < g < \frac{1}{2}$, which approaches infinity as $g \to \frac{1}{2}$. Blue dots are numerical solutions, red lines are the straight line $\bar{\omega}_0 = g$ and $\bar{\omega}_0 = \frac{1}{2}\,\mathrm{arctanh}\,2g$. For small values of g the linear approximation is quite good, the arctangent is a good approximation throughout the whole range $0 < g < \frac{1}{2}$.

and the linear response regime is valid (i.e., weak tunneling), *then* both e^* and g can be fitted from Eq. (2.39): g is determined from the scaling of the zero bias peak with T, and e^* is subsequently determined from the width of the peak (or location of the zero or the minimum if present). The unknown tunneling amplitude $|\Gamma|^2$ would also be determined from such a fit. Note that g and e^* cannot really be determined independently, so any experimental uncertainty translates to a range of probable values for g and e^*, as in the 'airfoil' plot in Radu *et al.* (2008).

2.5 Two point contacts: interference

For the case of two quantum point contacts that are separated by distances $x \pm \delta x$ on left and right edges, the linear response expression for the tunneling current follows from the expressions in section 2.1, especially Eq. (2.7) with $N = 2$,

$$I_{\rm tun}^{N=2}(T, \omega = e^*V) = e^*|\Gamma_{\rm eff}|^2(2\pi T)^{2g-1} 2\sinh(\pi\bar{\omega})B[g + i\bar{\omega}, g - i\bar{\omega}] \tag{2.40}$$

$$= e^*|\Gamma_{\rm eff}|^2(2\pi T)^{2g-1} F_g(\bar{\omega}). \tag{2.41}$$

This has the form of the tunneling current for a single point contact, but with an effective coupling

$$|\Gamma_{\rm eff}|^2 = |\Gamma_1|^2 + |\Gamma_2|^2 + 2\mathrm{Re}(\Gamma_1\Gamma_2^* e^{i\theta_{\rm AB}} e^{i\omega\delta x}) H_g(T, \omega, x) \tag{2.42}$$

$$= |\Gamma_1|^2 + |\Gamma_2|^2 + 2|\Gamma_1\Gamma_2| \cos(\varphi_0 + \theta_{\rm AB} + \omega\delta x) H_g(T, \omega, x). \tag{2.43}$$

The effective coupling has the 'standard' two-path interference form $|\Gamma_1|^2+|\Gamma_2|^2+2|\Gamma_1\Gamma_2|\cos\varphi_0$ of a term with squared amplitude of path 1, a term with squared amplitude of path 2 and interference term with amplitudes of path 1 and 2 times a relative phase, albeit that there is some additional modulation through the factor $H_g(T,\omega,x)$. The effect of the interference is largest when $|\Gamma_1| = |\Gamma_2|$. We have explicitly included the Aharonov-Bohm phase $\theta_{\rm AB}$ that the quasiparticle picks up upon encircling the interferometer (i.e., the phase difference between the two different paths due to the magnetic field).

The effective coupling is not a constant however, it depends on temperature, bias voltage, and distances x and δx. Only when left and right arm-lengths are equal, $\delta x = 0$, and in the limit of small x, that is $\omega x \ll 1$ and $2\pi T x \ll 1$, does the effective coupling become approximately constant, and the tunneling conductance in linear response is

$$G^{N=2}_{\rm tun}(T,\omega,x\approx 0,\delta x=0) = (e^*)^2\big|\Gamma_{\rm eff}\big|^2_{x=0=\delta x}\,(2\pi T)^{2g-2} f_g(\bar\omega), \tag{2.44}$$

$$\big|\Gamma_{\rm eff}\big|^2_{x=0=\delta x} = |\Gamma_1|^2+|\Gamma_2|^2+2{\rm Re}(\Gamma_1\Gamma_2^* e^{i\theta_{\rm AB}}). \tag{2.45}$$

Note that $H_g(T,\omega,x)$ is even in x, but the phase-factor $e^{i\omega\delta x}$ is neither even nor odd.

For generic values of x and δx the tunneling conductance for two point contacts is

$$G^{N=2}_{\rm tun} = (e^*)^2(2\pi T)^{2g-2}\bigg(\Big[|\Gamma_1|^2+|\Gamma_2|^2\Big]f_g(\bar\omega) + 2|\Gamma_1\Gamma_2|\bigg\{-\delta\bar x\sin\big(\varphi_0+\theta_{\rm AB}+\bar\omega\,\delta\bar x\big)\times$$
$$H_g(\bar\omega,\bar x)F_g(\bar\omega) + \cos\big(\varphi_0+\theta_{\rm AB}+\bar\omega\,\delta\bar x\big)\left[H_g(\bar\omega,\bar x)f_g(\bar\omega)+\frac{\partial H_g(\bar\omega,\bar x)}{\partial\bar\omega}F_g(\bar\omega)\right]\bigg\}\bigg), \tag{2.46}$$

where the 'barred' variables are the dimensionless quantities $\bar\omega \equiv \omega/(2\pi T)$, $\bar x \equiv x 2\pi T$, $\delta\bar x \equiv \delta x\, 2\pi T$.

2.6 Noise spectrum and interference

Another possible probe of the quantum Hall state through edge transport, beside tunneling conductance, is the noise spectrum. Measurement of shot noise in the $\nu = \frac{1}{3}$ state showed that the charge of tunneling quasiparticles was a fractional charge $e^* = e/3$ as predicted by the Laughlin wavefunction.

The noise spectrum $S(\omega)$ of the tunneling current is defined through

$$S(\omega) = \int_{-\infty}^{\infty} dt\, e^{-i\omega t}\langle 0|\big\{j_{\rm tun}(t), j_{\rm tun}(0)\big\}|0\rangle, \tag{2.47}$$

where it is the anti-commutator instead of the commutator that enters the expression, and integration extends to $t\to\pm\infty$. The noise spectrum can be evaluated in perturbation theory similar to the tunneling current (including expressing expectation values that are anti-time-ordered into ones that are time-ordered). Note that there are two frequencies now: ω_J related to the bias voltage, and ω the frequency of the measured spectrum. The expression for the tunneling current noise spectrum to lowest order in coupling constants

Γ_i for a set of N point contacts is

$$S(\omega,\omega_J) = (e^*)^2 \sum_{i,j=1}^{N} \times \left[\frac{\Gamma_i\Gamma_j^* e^{i(\omega_J+\omega)\delta x_{ij}} + \Gamma_i^*\Gamma_j e^{-i(\omega_J+\omega)\delta x_{ij}}}{2}\left(\tilde{P}_g(\omega_J+\omega,x_{ij}) + \tilde{P}_g(-\omega_J-\omega,x_{ij})\right) + \frac{\Gamma_i\Gamma_j^* e^{i(\omega_J-\omega)\delta x_{ij}} + \Gamma_i^*\Gamma_j e^{-i(\omega_J-\omega)\delta x_{ij}}}{2}\left(\tilde{P}_g(\omega_J-\omega,x_{ij}) + \tilde{P}_g(-\omega_J+\omega,x_{ij})\right)\right]. \tag{2.48}$$

Comparing this expression with that of the tunneling current, Eq. (2.7), the main difference is that the noise is an even function of frequency in $\tilde{P}_g(\omega)$ whereas the tunneling current is odd in frequency, which can be traced back to commutator versus anti-commutator. Of course there is also an extra e^* prefactor and two different frequencies. For small measurement frequencies ω, $\omega \ll \omega_J$, the two terms become equal and the expression for the tunneling current noise reduces to

$$\boxed{S_{\rm tun}(\omega_J) = 2(e^*)^2 \sum_{i,j=1}^{N} \frac{\Gamma_i\Gamma_j^* e^{i\omega_J\delta x_{ij}} + \Gamma_i^*\Gamma_j e^{-i\omega_J\delta x_{ij}}}{2}\left(\tilde{P}_g(\omega_J,x_{ij}) + \tilde{P}_g(-\omega_J,x_{ij})\right).} \tag{2.49}$$

Assuming noise measurement takes place at a very small frequency ω (but non-zero to avoid the $1/f$ noise due to other sources of noise in an experimental setup), we set ω equal to zero. Since ω effectively disappears from the problem, there is no further need to distinguish between notations ω_J and ω, since both then refer to the only frequency in the problem, $e^*V/\hbar$.

From Eq. (2.49) the tunneling current noise for a single QPC and for a double point contact interferometer can straightforwardly be given, especially since the even/odd part of $\tilde{P}_g(\omega)$ is simply the even/odd part of an exponential (finite temperature) or step function (at zero temperature). For a single tunneling site, $N = 1$, the noise, to leading order in $|\Gamma|^2$, at zero and finite temperature is

$$S_{\rm tun}(T=0,\omega=e^*V) = 2(e^*)^2|\Gamma|^2\frac{2\pi}{\Gamma[2g]}|\omega|^{2g-1}, \tag{2.50}$$

$$S_{\rm tun}(T,\omega=e^*V) = 4(e^*)^2|\Gamma|^2(2\pi T)^{2g-1}\cosh(\pi\bar{\omega})B[g+i\bar{\omega},g-i\bar{\omega}]. \tag{2.51}$$

The tunneling current noise is plotted for several values of g in Fig. 2-7.

For the case of two quantum point contacts, $N = 2$, the expression for the zero-frequency noise is

$$S_{\rm tun}(T=0,\omega=e^*V) = 2(e^*)^2|\Gamma_{\rm eff}|^2\frac{2\pi}{\Gamma[2g]}|\omega|^{2g-1}, \tag{2.52}$$

$$S_{\rm tun}^{N=2}(T,\omega=e^*V) = 2(e^*)^2|\Gamma_{\rm eff}|^2(2\pi T)^{2g-1}2\cosh(\pi\bar{\omega})B[g+i\bar{\omega},g-i\bar{\omega}], \tag{2.53}$$

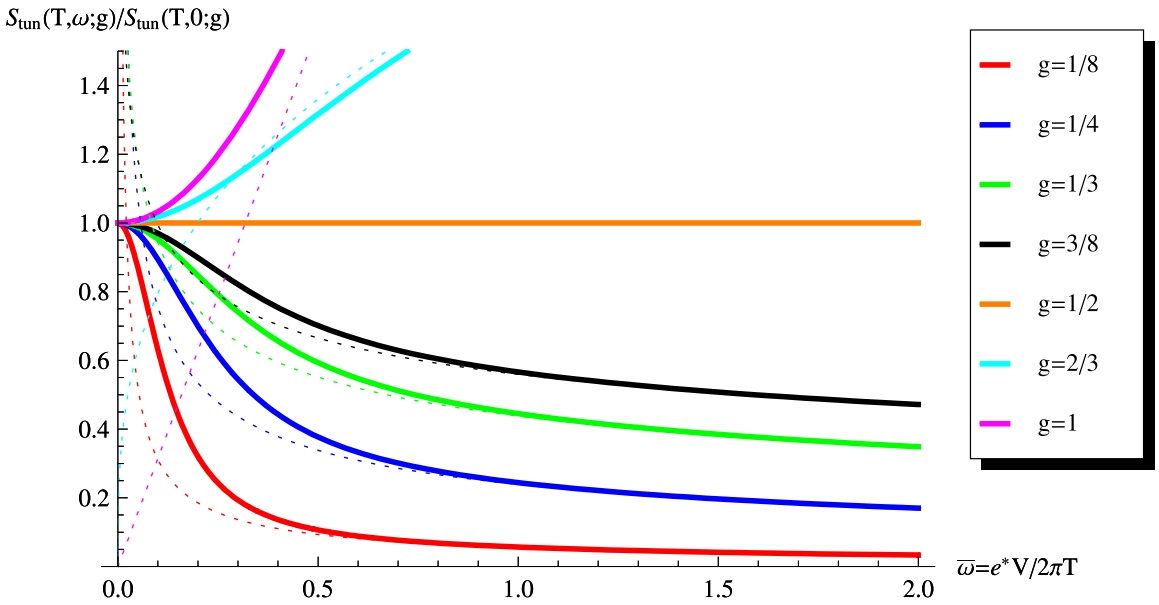

Figure 2-7: Plot of the tunneling current noise $S_{\rm tun}$ as a function of applied bias voltage V for various values of g. The curves are normalized to one at $V = 0$ and represent the dimensionless scaling function of the noise as a function of the dimensionless ratio V/T. The dotted lines are the corresponding zero temperature curves which behave as a power-law V^{2g-1}; for $e^*V > 2\pi T$ the zero temperature result clearly holds. Note that the curves for $g = \frac{1}{4}$ and $g = \frac{1}{2}$ are quite distinguishable; $g = \frac{1}{2}$ is a special value since here the noise is *independent* of voltage for any temperature. The value of the second derivative at zero bias of the normalized noise (i.e. the plotted function) is given by $\pi^2 - 2\text{PolyGamma}[1, g]$. Since near $g = \frac{1}{2}$ the width of the zero-bias peak scales roughly linear with g a measurement of the width of the peak cannot measure g and e^* independently.

where $\Gamma_{\rm eff}$ is the same effective tunneling amplitude, Eq. (2.42), as for the tunneling current.

Comparing with the expressions for the tunneling current, we see the following relations between tunneling noise and tunneling current at zero and finite temperatures

$$S_{\rm tun}(V) = 2e^* I_{\rm tun}(V), \text{ for } T = 0, \tag{2.54}$$

$$S_{\rm tun}(T,V) = 2e^* I_{\rm tun}(T,V) \coth \frac{e^*V}{2T}, \text{ for } T \neq 0. \tag{2.55}$$

Note that this relation between tunneling current and noise for weak tunneling, at order $|\Gamma|^2$, is valid for *any* N and is *independent* of the quasiparticle exponent g and amplitude Γ.

A measurement of the noise does not provide any new information compared to a measurement of the tunneling current (or conductance). An accurate measurement of either of these two will fit the parameters e^* and g, and the information obtained from the interference (e.g. x and δx) is in principle identical for the two measurements. However, current state-of-the-art measurements of conductance and noise are not accurate enough to determine the parameters e^* and g with high precision. It is here that performing both measurements might turn out to be fruitful, because a *combined* measurement of both the current (conductance) and the noise is statistically more restrictive on parameters e^* and g than either measurement by itself. An estimate of the measurement error bars on noise and current measurements should help predict whether a combined measurement of these complementary quantities is indeed worthwhile in any practical setup.

Chapter 3

Non-abelian anyons and conformal block decomposition

In this chapter we describe the conformal block decomposition that is required to evaluate expectation functions for non-abelian fractional quantum Hall states, which appear in the perturbative calculations of e.g. the tunneling current.

3.1 Non-abelian anyons and internal state

In worlds with three or more spatial dimensions, the statistics of particles can be either bosonic or fermionic. This stems from the fact that a double exchange of two indistinguishable particles is always smoothly connected to the identity map, hence the only allowed particle exchanges are those that square to one, i.e., $+1$ for bosons and -1 for fermions. In two spatial dimensions there is no such requirement, and as such under an exchange of two identical particles the wavefunction is in principle allowed to pick up any phase, and such particles were dubbed 'anyons' (Leinaas and Myrheim, 1977; Wilczek, 1982; Arovas, Schrieffer, and Wilczek, 1984). Anyons could exist in our world as quasiparticles in an engineered quasi-two-dimensional world.

Non-abelian anyons are usually introduced as a generalization of regular 'abelian' anyons, where upon interchange of two anyons the wavefunction does not just pick up a phase but a (unitary) matrix (Moore and Read, 1991; Wen, 1991b; Blok and Wen, 1992). The term '(non)-abelian' refers to the commutative property of particle statistics; for non-abelian statistics the order in which exchanges take place matters, as matrices do not commute in general. In this thesis we would like to take a slightly different approach by putting more focus on the internal space that these matrices act on, rather than the braid relations themselves. Note that neither of these approaches is incorrect, they are complementary. With conformal block decomposition, and topological quantum computation for that matter, in mind, putting emphasis on the topologically protected internal space seems justified and favorable.

The internal space is a multi-particle property. There are seemingly different ways to specify the locations of quasiparticles. These do not necessarily describe different physical states though. Remember that for bosons and fermions states that are related by particle

permutations (with appropriate signs) are in fact equal. Taking such exchanges into effect one finds *there are physically distinct states for the same configurations (of locations) of quasiparticles*.

A way to see this is to consider non-abelian anyons as carrying an irreducible representation (irrep) of the braid group (the generalization of the permutation group for particle exchange in two dimensions). In other words the quasiparticle type is labeled by an irrep. When two quasiparticles are brought close together, or 'fused', their product should also form a representation of the braid group. Just like a combination of two spin-half particles can be considered as a spin singlet plus a triplet, $\frac{1}{2} \otimes \frac{1}{2} = 0 \oplus 1$, the product-representation can be decomposed into a sum of irreps. In terms of so-called fusion rules, the product representation of quasiparticle types ϕ_i and ϕ_j is written as a sum over possible outcomes, or 'fusion channels', ϕ_k,

$$\phi_i \times \phi_j = \sum_k N_{ij}^k \phi_k, \tag{3.1}$$

where the N_{ij}^k are positive integers. For abelian states there is only a single ϕ_{k_0} that appears in the fusion channel of ϕ_i and ϕ_j, i.e., $N_{ij}^k = \delta_{k,k_0(i,j)}$. For a non-abelian state there is at least one combination of i and j for which there exists more than one fusion channel. One could also say that a non-abelian state carries a higher dimensional (i.e., two-dimensional or higher) representation of the braid group.

Now it becomes obvious why a a configuration of quasiparticles (i.e., a list of quasiparticle types and their locations) is not sufficient to fully specify the physical state: there can be multiple fusion channels associated with each configuration, and as long as each fusion channel is physically allowed these constitute distinct physical states. For quantum Hall states the physical requirement is that the fusion product of *all* quasiparticles is the identity channel. It is also clear that the internal space is a multi-particle property, as the size of the internal space grows with the number of quasiparticles.

3.1.1 Example: the Moore-Read Pfaffian wavefunction

Let us look at an example here, where there are distinct physical states for the same configuration of quasiparticles. In units where the magnetic length is set equal to one, the trial 'Pfaffian' wavefunction written down by Moore and Read (1991) for a filling fraction $\nu = \frac{1}{2}$ mod 2 FQH state is

$$\Psi_{\rm Pf}(\{z_i\},\{\eta_j\}) = {\rm Pf}\big(M_{jk}\big) \prod_{j<k} (z_j - z_k)^2 \prod_j e^{-\frac{1}{4}|z_j|^2}, \tag{3.2}$$

$$\begin{aligned}
&\text{for no quasiparticles: } M_{jk} = \frac{1}{z_j - z_k},\\
&\text{for 2 qps: } M_{jk} = \frac{(z_j-\eta_1)(z_k-\eta_2)+(z_k-\eta_1)(z_j-\eta_2)}{z_j-z_k},\\
&\text{for } 2n \text{ qps: } M_{jk} = \frac{(z_j-\eta_{\alpha_1})\cdots(z_j-\eta_{\alpha_n})(z_k-\eta_{\alpha_{n+1}})\cdots(z_k-\eta_{\alpha_{2n}})+(z_j \leftrightarrow z_k)}{z_j-z_k}.
\end{aligned} \tag{3.3}$$

The Pfaffian $\mathrm{Pf}(M_{jk})$ of a matrix M_{jk} is the antisymmetrized sum of the product $M_{12}M_{34}\ldots$, e.g.,

$$\mathrm{Pf}\left(\frac{1}{z_i - z_j}\right)\Big|_{1\leq i,j\leq 4} = \frac{1}{z_1 - z_2}\frac{1}{z_3 - z_4} - \frac{1}{z_3 - z_2}\frac{1}{z_2 - z_4} + \frac{1}{z_1 - z_4}\frac{1}{z_2 - z_3}. \tag{3.4}$$

Note that for more than two quasiparticles there is a choice of how to order the quasiparticles η_{α_i}, for which a different choice of ordering leads to a different trial wavefunction. Apparently there are $(2n)!/[2(n!)^2]$ different ways to split $2n$ quasiparticles into two groups. It was realized however (Nayak and Wilczek, 1996) that not all of the orderings are independent of each other. To be concrete, for four quasiparticles and two electrons, define

$$(12;34) \equiv (z_1 - \eta_1)(z_1 - \eta_2)(z_2 - \eta_3)(z_2 - \eta_4) + (z_1 \leftrightarrow z_2). \tag{3.5}$$

There are three different ways to make two groups of two out of a total of four quasiparticles. But there is the following relation between these three different orderings

$$(12;34) - (13;24) = \frac{(\eta_1 - \eta_4)(\eta_2 - \eta_3)}{(\eta_1 - \eta_3)(\eta_2 - \eta_4)}\big[(12;34) - (14;23)\big]. \tag{3.6}$$

What Nayak and Wilczek (1996) showed was that this linear relation also holds for the Pfaffian trial wavefunction for *any* even number of electrons,

$$\mathrm{Pf}_{(12;34)} - \mathrm{Pf}_{(13;24)} = \frac{(\eta_1 - \eta_4)(\eta_2 - \eta_3)}{(\eta_1 - \eta_3)(\eta_2 - \eta_4)}\big[\mathrm{Pf}_{(12;34)} - \mathrm{Pf}_{(14;23)}\big]. \tag{3.7}$$

So for four quasiparticles there are only two independent ways to order the quasiparticles, the wavefunction related to the third ordering is a linear combination of the wavefunctions associated with the first two orderings.

Nayak and Wilczek (1996) generalized their results for four quasiparticles to $2n$ quasiparticles and showed that there are 2^{n-1} linearly independent orderings in that case. To show that these linearly independent trial wavefunctions do indeed constitute distinct physical wavefunctions, their overlap has to be calculated. This amounts to numerically integrating over the electron coordinates z_i. There it turns out that these wavefunctions are not truly orthogonal to each other. This is also not expected, since there is no relation between the number of quasiparticles and the number of electrons, and it would seem as if the extra 2^{n-1} degrees of freedom could grow arbitrarily large for a fixed number of electrons. Instead, the physical interpretation is that for a fixed number of quasiparticles the overlap between two such wavefunctions goes to zero in the thermodynamic limit in which the number of electrons goes to infinity. Detailed numerical work (Baraban and Simon, 2008) for finite size closed system on a sphere shows that the overlap decays exponentially with the number of electrons, such that even for a finite ratio of electrons to quasiparticles the states are effectively perpendicular and thus physically distinct.

3.1.2 Conformal blocks as prefered basis

Given that a non-abelian state with multiple quasiparticles in it has an internal space associated with it (internal in the sense that it is not specified by the locations of quasiparticles), one can ask the question what would be a useful basis of this internal Hilbert space. For the Moore-Read Pfaffian state, the explicit trial wavefunction based on ordering of the quasiparticle coordinates in two groups gives rise to an overcomplete set of linearly dependent states, so a different orthogonal basis would be preferable.

The obvious choice for an orthogonal basis is that of definite fusion channel. A definite fusion channel one specifies the fusion channels of consecutive pairwise fusions. E.g. ϕ_1 and ϕ_2 fuse into ϕ_a, ϕ_a fuses with ϕ_3 into ϕ_b, ϕ_b fuses with ϕ_4 into ϕ_c, etcetera, all the way until there is only one quasiparticle left, which should be the identity or vacuum quasiparticle. Basis vectors are then labeled by the set of possible outcomes for ϕ_a, ϕ_b, ϕ_c, etcetera. There is however no unique way to specify a basis of definite fusion channel, since both the ordering in which quasiparticles are fused and the path-ordering of how quasiparticles are brought together upon fusion influences the outcome. So there is no unique basis, and sometimes it might be useful to change from one basis of definite fusion channel to another one. Fortunately, the basistransformation between such bases is known and completely specified by the defining relations of the non-abelian state, as given by the fusion and braiding F and R *moves*.

In a sense it is not unexpected that there are multiple ways to choose a basis, and that the number of ways to choose some basis increases rapidly with the size of the internal space. The claim from topological quantum computation is that upon braiding quasiparticles one can change the state of the system, and hopefully one can approximate any linear combination of basisvectors with some sequence of braidings and/or fusions of quasiparticles. It also indicates that the internal state is a truly topological property that intrinsically only depends on the topology of the paths of the quasiparticles, and hence the internal space cannot have direct interactions with external fields, which is why it is also called a space that is topologically protected from decoherence due to noise from the environment. Intrinsically decoherence free space is probably a more accurate description.

A basis of definite fusion channels is usually refered to as a *conformal block* (Di Francesco, Mathieu, and Sénéchal, 1997). Strictly speaking a conformal block is a specific correlation function of (quasiparticle) field operators in conformal field theory. There are very deep relations between (non-)abelian anyon states and CFT. Already for the abelian Laughlin trial wavefunctions, it was realized that these can be expressed as a CFT correlation function of a product of field operators, one operator for each electron and each quasiparticle in the trial state. A similar relation was found, (see e.g. Moore and Read, 1991; Nayak and Wilczek, 1996), for the Moore-Read Pfaffian state in terms of correlation functions of a central charge $c = 1$ bosonic field plus a $c = \frac{1}{2}$ Ising field, with quasiparticles corresponding to he σ spin operator of the Ising field. The explicit basistransformation from the Pfaffian trial wavefunctions to that of conformal blocks of these σ operators was given as well. Note that for CFT correlation functions the requirement that the fusion product of all operators is the identity channel is automatically satisfied because the correlation function is zero otherwise.

The F and R moves (Kitaev, 2006; Rowell, Stong, and Wang, 2007) are pictured in

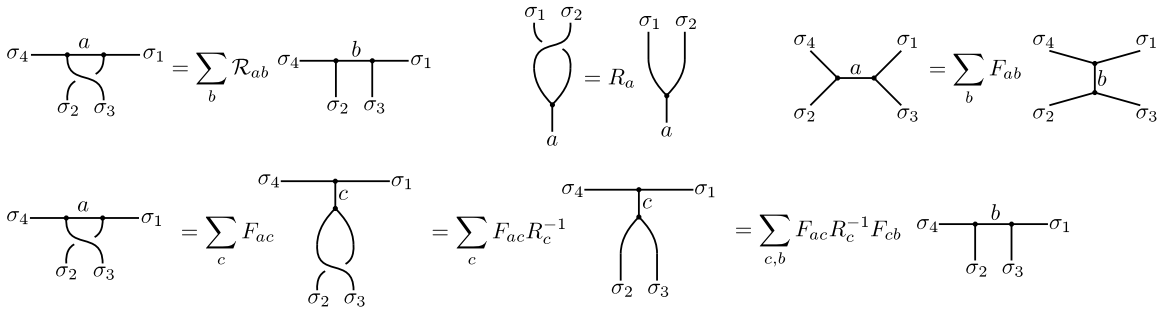

Figure 3-1: Top row: pictorial representation of definitions of braid matrix $\mathcal{R}$, braid move R and fusion matrix F. The bottom row shows the relation between $\mathcal{R}$ and F and R: $\mathcal{R}_{ab} = F_{ac} R_c^{-1} F_{cb}$. For the $\nu = \frac{5}{2}$ Pfaffian state the labels a, b and c take on values of $\mathbb{1}$ and ψ; the matrices F and R implicitly depend on the quasiparticle types of the external legs as well.

Fig. 3-1. All edges of these trivalent graphs (i.e. each vertex connects exactly three legs) carry a quasiparticle label. Convention is that external legs are kept fixed. The counterclockwise braiding operator $\mathcal{R}$ is introduced here as well, and it can be decomposed into two F-moves and an R-move,

$$\mathcal{R}_{ab=} \sum_{c,b} F_{ac} R_c^{-1} F_{cb}, \qquad (\text{for } \nu = \tfrac{5}{2}\text{: } a, b, c \in \{\mathbb{1}, \psi\}). \tag{3.8}$$

More on the $\mathcal{R}$ in the next section, where the braid matrix is explicitly calculated for the quasiparticles in the $\nu = \frac{5}{2}$ Pfaffian state as determined by the corresponding Ising conformal field theory, see Eq. (3.32).

3.2 Braiding and fusion matrices for Ising CFT from conformal blocks

We explicitly show some of the braiding and fusion relations for the four-point σ correlation function, based on the expressions for conformal block correlation functions. Note that for the Moore-Read Pfaffian wavefunction the quasiparticle coordinates were given by η_i; in this section we will instead use the, in CFT more conventional, notation z_i for these coordinates.

The relevant two-, three- and four-point functions for the Ising CFT (Di Francesco *et al.*, 1997) are

$$\langle \sigma(z)\sigma(w) \rangle = \frac{1}{(z-w)^{1/8}}, \tag{3.9}$$

$$\langle \psi(z)\psi(w) \rangle = \frac{1}{(z-w)^{1/2}}, \tag{3.10}$$

$$\langle \psi(z)\sigma(w)\sigma(v) \rangle = \frac{(w-v)^{3/8}}{\sqrt{2}(z-w)^{1/2}(z-v)^{1/2}}, \tag{3.11}$$

$$\langle\sigma(z_1)\sigma(z_2)\sigma(z_3)\sigma(z_4)\rangle \to \mathcal{F}_{\mathbb{1}/\psi} = \frac{1}{\sqrt{2}}\left(\frac{z_{13}z_{24}}{z_{12}z_{34}z_{14}z_{23}}\right)^{1/8}\sqrt{1 \pm \sqrt{\frac{z_{14}z_{23}}{z_{13}z_{24}}}} \tag{3.12}$$

$$= \frac{1}{\sqrt{2}}\left(\frac{1}{z_{12}z_{34}x}\right)^{1/8}\sqrt{1 \pm \sqrt{x}}. \tag{3.13}$$

where x is the cross-ratio $x = \frac{z_{14}z_{23}}{z_{13}z_{24}}$, and $z_{ij} \equiv z_i - z_j$. The four point function by itself is ill-defined without specifying the fusion channel, i.e., indicating the conformal block. The conformal blocks $\mathcal{F}_{\mathbb{1}/\psi}$ are well-defined.

The operator product expansion (OPE) for two σ operators in the Ising CFT is

$$\lim_{w\to z}\sigma(z)\sigma(w) = \frac{\mathbb{1}}{(z-w)^{1/8}} + \frac{(w-v)^{3/8}\psi(z)}{\sqrt{2}} + \dots \tag{3.14}$$

The dots represent higher order (non-singular) powers of $(z-w)$.

The conformal block $\mathcal{F}_{\mathbb{1}}$ is the state in which $\sigma(z_1)$ and $\sigma(z_2)$ are in the identity representation. By looking at the OPE for z_2 going to z_1 we confirm that indeed the fusion channel of $\sigma(z_1)$ and $\sigma(z_2)$ is the identity channel:

$$\lim_{z_2\to z_1}\mathcal{F}_{\mathbb{1}} = \frac{1}{\sqrt{2}}\left(\frac{z_{13}z_{14}}{z_{12}z_{34}z_{14}z_{13}}\right)^{1/8}\sqrt{1+\sqrt{\frac{z_{14}z_{13}}{z_{13}z_{14}}}} + \dots \tag{3.15}$$

$$= \frac{1}{\sqrt{2}}\left(\frac{1}{z_{12}z_{34}}\right)^{1/8}\sqrt{2} + \dots \tag{3.16}$$

$$= \langle\sigma(z_3)\sigma(z_4)\rangle(z_1-z_2)^{-1/8} + \dots \tag{3.17}$$

For the other conformal block, $\mathcal{F}_{\psi}$, the OPE is different. Since when $z_2 \to z_1$ we have that $x \to 1$ the leading order contribution vanishes and next order needs to be included,

$$\lim_{z_2\to z_1}\mathcal{F}_{\psi} = \frac{1}{\sqrt{2}}\left(\frac{z_{13}z_{14}}{z_{12}z_{34}z_{14}z_{13}}\right)^{1/8}\sqrt{1-\sqrt{1-\frac{z_{12}z_{34}}{z_{13}z_{14}}}} + \dots \tag{3.18}$$

$$= \frac{1}{\sqrt{2}}\left(\frac{1}{z_{12}z_{34}}\right)^{1/8}\frac{1}{\sqrt{2}}\left(\frac{z_{12}z_{34}}{z_{13}z_{14}}\right)^{1/2} + \dots \tag{3.19}$$

$$= \langle\psi(z_1)\sigma(z_3)\sigma(z_4)\rangle\frac{1}{\sqrt{2}}(z_1-z_2)^{3/8} + \dots, \tag{3.20}$$

which is of course consistent with the statement that $\sigma(z_1)$ and $\sigma(z_2)$ are in the ψ channel.

Fusion of $\sigma(z_2)$ and $\sigma(z_3)$ is the non-trivial calculation, since these two quasiparticles are not in a definite fusion channel. The associated OPE will be a superposition of all the

conformal blocks (two in this case), and constitutes the fusion matrix F,

$$\lim_{z_3\to z_2}\mathcal{F}_{\mathbb{1}/\psi} = \frac{1}{\sqrt{2}}\left(\frac{z_{12}z_{24}}{z_{12}z_{24}z_{14}z_{23}}\right)^{1/8}\sqrt{1\pm\sqrt{\frac{z_{14}z_{23}}{z_{12}z_{24}}}} \tag{3.21}$$

$$= \frac{1}{\sqrt{2}}\left(\frac{1}{z_{14}z_{23}}\right)^{1/8}\left[1\pm\frac{1}{2}\left(\frac{z_{23}z_{14}}{z_{12}z_{24}}\right)^{1/2}\right] \tag{3.22}$$

$$= \frac{1}{\sqrt{2}}\langle\sigma(z_1)\sigma(z_4)\rangle(z_2-z_3)^{-1/8} \tag{3.23}$$

$$\pm\frac{1}{\sqrt{2}}\langle\sigma(z_1)\psi(z_2)\sigma(z_4)\rangle\frac{1}{\sqrt{2}}(z_2-z_3)^{3/8} \tag{3.24}$$

The matrix elements of F can simply be read off from this result,

$$F = \frac{1}{\sqrt{2}}\begin{pmatrix}1 & 1\\ 1 & -1\end{pmatrix}. \tag{3.25}$$

The braid matrices R and $\mathcal{R}$ can be deduced from the expressions for the conformal blocks as well. Note that upon braiding the ordering (time-ordering, radial-ordering) of correlation functions is explicitly violated. The crossing of branch-cuts, and the associated multi-valuedness, is the mechanism through which the conformal block 'state' can be changed by braiding.

The non-trivial braid is a single braid of $\sigma(z_2)$ and $\sigma(z_3)$. Direction of the braid is important, here we choose a counter-clockwise braid. Under this braid operation, $x \to \frac{x}{x-1}$, and $\frac{1}{z_{12}z_{34}x} \to \frac{-(1-x)^2}{z_{12}z_{34}x}$. We assume that in starting position all the z_i are on the real axis with $z_1 > z_2 > z_3 > z_4$ which implies that x is real and $0 < x < 1$. In the complex plane, x performs a counter-clockwise motion around the origin, and $1/x$ a clockwise motion. We will also need the identity

$$\sqrt{2}\sqrt{1\pm\sqrt{1-y}} = \sqrt{1+\sqrt{y}}\pm\sqrt{1-\sqrt{y}}. \tag{3.26}$$

The action of a counter-clockwise braid $\mathcal{R}$ on the conformal blocks $\mathcal{F}_{\mathbb{1}}$ and $\mathcal{F}_{\psi}$, Eq. (3.13),

is

$$\mathcal{F}_{\mathbb{1}/\psi} \xrightarrow{z_2 \circlearrowleft z_3} \frac{1}{\sqrt{2}} \left(\frac{-(1-x)^2}{z_{12} z_{34} x} \right)^{1/8} \frac{1}{\sqrt{2}} \left[\sqrt{1+\sqrt{\frac{1}{1-x}}} \pm \sqrt{1-\sqrt{\frac{1}{1-x}}} \right] \tag{3.27}$$

$$= \frac{e^{-i\pi/8}}{\sqrt{2}} \left(\frac{1}{z_{12} z_{34} x} \right)^{1/8} \frac{1}{\sqrt{2}} \left[\sqrt{\sqrt{1-x}+1} \pm \sqrt{\sqrt{1-x}-1} \right] \tag{3.28}$$

$$= \frac{e^{-i\pi/8}}{\sqrt{2}} \left(\frac{1}{z_{12} z_{34} x} \right)^{1/8} \frac{1}{\sqrt{2}} \left[\sqrt{1+\sqrt{1-x}} \pm i\sqrt{1-\sqrt{1-x}} \right] \tag{3.29}$$

$$= \frac{e^{-i\pi/8}}{\sqrt{2}} \left(\frac{1}{z_{12} z_{34} x} \right)^{1/8} \frac{1}{2} \left[(1 \pm i)\sqrt{1+\sqrt{x}} + (1 \mp i)\sqrt{1-\sqrt{x}} \right] \tag{3.30}$$

$$= \frac{e^{-i\pi/8}}{\sqrt{2}} \left[e^{\pm i\pi/4} \mathcal{F}_{\mathbb{1}} + e^{\mp i\pi/4} \mathcal{F}_{\psi} \right]. \tag{3.31}$$

The matrix elements for $\mathcal{R}$ and its square are thus

$$\mathcal{R} = \frac{1}{\sqrt{2}} \begin{pmatrix} e^{i\pi/8} & e^{-3i\pi/8} \\ e^{-3i\pi/8} & e^{i\pi/8} \end{pmatrix}, \qquad \mathcal{R}^2 = e^{-i\pi/4} \begin{pmatrix} 0 & 1 \\ 1 & 0 \end{pmatrix}. \tag{3.32}$$

A double braid, or monodromy, $\mathcal{R}^2$ thus interchanges $\mathcal{F}_{\mathbb{1}}$ and $\mathcal{F}_{\psi}$ up to a phase factor. interchanged. The overall phase factor depends on the direction of the braid. The clockwise braid $\mathcal{R}^{-1}$ is given by the Hermitean conjugate of the unitary matrix $\mathcal{R}$ (the encountered branch-cuts now come with the opposite phase).

A braid of $\sigma(z_1)$ and $\sigma(z_2)$ corresponds to acting with the matrix R, or rather phase R, since the exchange for two quasiparticles in a definite fusion channel is only a phase. Under the exchange $z_1 \circlearrowleft z_2$ the cross-ratio changes to $x \to 1/x$. Pulling out fractional powers of x into/out of the square-root in $\mathcal{F}_{\mathbb{1}/\psi}$ shows that indeed under this exchange each conformal block transforms back to itself, and the overall phase follows from tracking the paths in the complex plane with respect to the branch-cuts,

$$R_{\mathbb{1}} = e^{-i\pi/8}, \qquad R_{\psi} = e^{3i\pi/8}. \tag{3.33}$$

3.2.1 What about the Berry phase?

The calculations in the previous section show the explicit braiding relation starting, in a sense, from the Moore-Read Pfaffian wavefunction, Eq. (3.2). However, it may appear that we cheated somewhere. The braiding relations seem to rely specifically on the existence of branch-cuts associated with the square-roots. However, there are no square roots present at all in the expression for the Moore-Read trial wavefunction. Furthermore, braiding was basically described by an analytic continuation in quasiparticle coordinates of the initial wavefunction. This is not necessarily the same as considering a Berry phase action upon adiabatically moving one quasiparticle around all the other ones. These issues are somewhat related. First of all, the Moore-Read trial wavefunction is unnormalized, so the normalized version contains a square root. Furthermore it was conjectured (Blok and Wen, 1992; Nayak and Wilczek, 1996) and shown for several examples in FQH settings that in the conformal

block basis there is no contribution from the Berry phase, and the only effect from adiabatic braiding is the effect as found from analytic continuation. In the Moore-Read wavefunction basis the Berry phase does have a contribution. Noting that the conventional Berry phase arises from overlaps between coherent states (Wen, 2004), which form an overcomplete basis, supports the claim that Berry phases play no role in the orthogonal basis of conformal blocks.

3.3 Edge and bulk quasiparticles in quantum Hall systems

In this section we would like to discuss the relation between quasiparticles in the bulk and quasiparticles on the edge for quantum Hall systems. The previous chapter (Ch. 2) on transport measurements in the quantum Hall effect is fully described in terms of edge dynamics. The current chapter has, so far, only considered bulk quasiparticles. What is the relation between these two?

Quasi two-dimensional systems in our physical world almost always have an edge. In principle closed systems like spheres or tori are allowed, but for the quantum Hall system we cannot physically generate the required magnetic field inside such closed systems. In other words, physical quantum Hall systems *always* have an outer edge at the boundary of the sample. There can also be inner edges, also called 'islands' or 'holes', inside the QH fluid.

A bulk quasiparticle can merge with an edge, and in doing so it disappears from the QH fluid. However, such a bulk quasiparticle carries a global topological quantum number with it. Recall that physical states with quasiparticles in it have to obey the constraint that the fusion channel of all quasiparticles in the system should be the identity channel. This is another way of saying that the true QH bulk ground state contains no quasiparticles and that the total charge of the system cannot be fractional but should be an integer (corresponding to the number of electrons). This topological constraint cannot be lost when a quasiparticle merges with an edge; since the quasiparticle itself is nevertheless lost, this information should become part of the edge itself. In other words, edges also carry a quasiparticle type, or 'sector', label, and a full specification of the physical state should thus include the fusion channel of all the bulk quasiparticles and edges in the system (or superposition thereof, depending on choice of basis). The other effect that can happen when a bulk quasiparticle merges with an edge is that some low energy mode can locally be excited on the edge. In this sense one can identify merging at time t of a quasiparticle ϕ_j with an edge as an operator $\psi_j^\dagger(x,t)$ locally creating a quasiparticle on the edge. Note that on the edge the inherited bulk quasiparticle sector also has an interpretation: this is the, possibly non-trivial, boundary condition that chiral edge-waves encounter when fully encircling the edge.

When two edges in a FQH liquid are nearby each other, it may happen that a (low-energy) ripple-wave on one edge can induce a ripple on the neighboring edge, as if a quasiparticle excitations jumps, or tunnels, between edges. From the point of view of the edges, this process would have to look like a local destruction operator $\psi_j(t,x)$ on one edge and a local creation operator $\psi_j^\dagger(t,x)$ acting on the other edge. However, such operators change the 'bulk' sector labels of these edges. The global topological constraint needs to be conserved, and this can be achieved by viewing the tunneling between edges in terms of virtual bulk

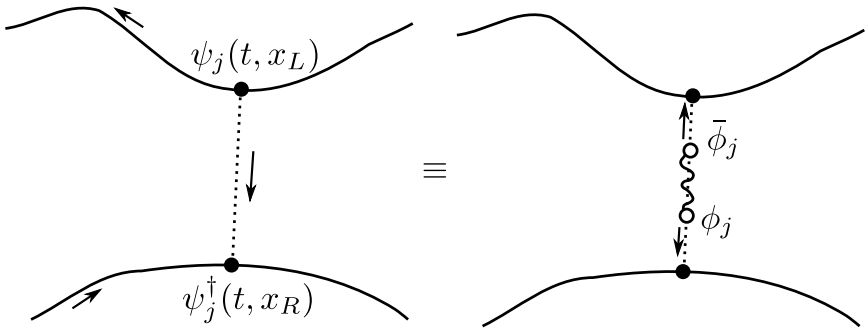

Figure 3-2: A ψ_j quasiparticle tunneling operator for tunneling between two adjacent edges corresponds to the virtual process of creation out of the vacuum of a particle anti-particle pair in the bulk which are then merged with the two opposite edges.

quasiparticles. The operator expression for such a quasiparticle tunneling process would be the virtual creation out of the vacuum of a pair of a quasiparticle and its anti-quasiparticle. The quasiparticle is merged with the new edge, and the anti-quasiparticle is merged with the old edge. This ensures that (i) on the old edge tunneling acts as a local quasiparticle destruction operator $\psi_j(x,t)$, (ii) on the new edge it acts as a local quasiparticle creation operator $\psi_j^\dagger(y,t)$, and (iii) the global topological constraint is still satisfied, because the virtual pair is in the vacuum channel. The tunneling process is illustrated in Fig. 3-2. The virtual process of pair-creation and merging with the respective edges is supposed to happen instantaneously at time t. Since the particle/anti-particle pair may braid non-trivially with the rest of the system it is necessary to specify the bulk path between the locations of the tunneling sites on the respective edges. Since tunneling amplitude generally depends exponentially on distance between the tunneling sites, the path taken is assumed to be the shortest path between the two points. By the same argument it is assumed that tunneling only takes place at points where two edges are sufficiently close to each other.

Edge quasiparticle operators suffer from the same ambiguity as bulk quasiparticle operators if the fusion channel of the operators is not specified. The fusion channels of bulk quasiparticle operators translates directly to the same fusion channel of edge quasiparticle operators, such that the fusion channel due to tunneling quasiparticles is specified by the fusion channel of their virtual bulk pair representation, which by braiding may be entangled with the rest of the bulk as well.

3.4 Quasiparticle tunneling in perturbation theory: conformal blocks disentangle the edges

We will now address the essence of conformal block decomposition for transport calculations in perturbation theory for non-abelian systems. The point is that quasiparticle tunneling creates entanglement between edges. The conformal block decomposition disentangles the edges again, in the sense that it is a basistransformation which expresses the entangled state in a basis in which the edges are not entangled.

As shown in Chapter 2, calculating transport quantities such as tunneling current and

tunneling noise in perturbation theory boils down to evaluating expectation values of products of tunneling operators in the unperturbed groundstate.

The unperturbed state is the free χLL theory for each of the edges in the system times a static bulk configuration of quasiparticles. The given location, types and fusion channel (i.e. state vector in the internal Hilbert space) of the bulk quasiparticles are assumed to be constructed in the far past and to be fixed (pinned). The edge groundstate is the state with no ripples. The groundstate of the system is the product of edge groundstates times the static bulk state vector.

Products of quasiparticle operators on a *single* edge in a *definite fusion channel* on *that* edge are readily evaluated in terms of conformal block n-point correlation functions. The 'difficulty' in evaluating products of tunneling operators in the ground state is that these tunneling operators entangle *both* the fusion channels on different edges *and* mix the bulk internal Hilbert space state vector with the edges (because quasiparticle tunneling affects edge sectors and can braid non-trivially with bulk quasiparticles). If this mixed/entangled edge-edge-bulk-state could be decomposed into a state with no entanglement between edges and bulk then the calculation would be straightforward. The key point is: *Not only does this decomposition exist, it is just a known basistransformation.* This basistransformation is a change of choice of definite fusion channel, namely the basis with definite fusion channel on each edge separate. In other words the decomposition into conformal blocks on each of the edges.

Represented schematically, we can express the tunneling current as the ground state expectation value of a sum of terms with a product of a number of quasiparticle tunneling operators $\hat{V}$

$$I_{\rm tun} = \langle {\rm groundstate}| \sum \hat{V}\hat{V}\ldots |{\rm groundstate}\rangle. \tag{3.34}$$

This perturbation expansion will of course be truncated at some order. The ground state is the fixed initial bulk B state times the ground states on each of the edges E_l ,

$$|{\rm groundstate}\rangle = |{\rm in}\rangle_B \otimes |0\rangle_{E_1} \cdots \otimes |0\rangle_{E_m} \tag{3.35}$$

The action of the quasiparticle tunneling operators $\hat{V}$ can be decomposed into a basis with quasiparticle operators in definite fusion channels on each edge and in the bulk state,

$$\begin{aligned} &\hat{V}\hat{V}\ldots|{\rm groundstate}\rangle \\ &\qquad = \hat{V}\hat{V}\ldots\Big[|{\rm in}\rangle_B \otimes |0\rangle_{E_1} \cdots \otimes |0\rangle_{E_m}\Big] \\ &\qquad = \sum |{\rm out}\rangle_B \otimes \Big[\psi\psi\ldots|0\rangle_{E_1}\Big] \cdots \otimes \Big[\psi\psi\ldots|0\rangle_{E_m}\Big]. \end{aligned} \tag{3.36}$$

An so it is obvious that the only terms that contribute to the tunneling current are the terms that obey

$$_B\langle {\rm in}|{\rm out}\rangle_B \neq 0, \qquad _{E_l}\langle 0|\psi\psi\ldots|0\rangle_{E_l} \neq 0. \tag{3.37}$$

From here onwards, one substitutes the conformal block correlation functions and performs the appropriate integrations over these correlation functions to obtain the I-V tunneling curve. The non-abelian aspect, the intertwinement of bulk and edge, has been taken care of at this point. It is also clear why this issue did not arise for abelian FQH states. For abelian

states, the bulk and edges are always unentangled and a basistransformation is unnecessary (i.e., the internal Hilbert space is one-dimensional).

3.4.1 Time-ordering and causality

It would appear that the aspect of time ordering is lost in our discussion of conformal block decomposition. The conformal block decomposition is an intrinsically two-dimensional procedure, but the physical expectation value is really three-dimensional: one time and two spatial dimensions. The question is thus how the conformal block decomposition can be valid for a product of operators that have some sort of ordering with respect to time (for instance a time-ordered product). The answer is that the conformal block decomposition only disentangles the edges but does not say anything about the ordering of operators on an edge. In other words, *the conformal block decomposition gives the same result irrespective of the ordering on the edge.*

A physical expectation value *does* have a specific ordering of the operators though, but this is not determined by the conformal block decomposition. Instead, the ordering of operators on individual edges has to be determined through other means. Ultimately it is the order in which operators appear in the perturbative expansion of the time-evolution operator which sets the ordering of operators. It would nevertheless be useful to have the pictorial representation of the conformal block decomposition include the proper ordering of operators on the edge as well. An incorrect ordering would correspond to a braid of operators that act on the same edge. A natural choice in the pictorial representation of the conformal block decomposition is then to ensure that ordered operators that act on the same individual edge do not braid with each other in the conformal block decomposition. See Fig. 3-3.

3.4.2 Validity of the formalism

We would like to note that the formalism of conformal block decomposition in perturbation theory is valid for any number of edges. Earlier works (Fendley, Fisher, and Nayak, 2007; Ardonne and Kim, 2008) focussed primarily on a setup with a single (but very long) edge, which is most relevant for a Fabry-Pérot type of setup. But the formalism discussed in this appendix should work equally well in e.g. a Mach-Zehnder type of setup (Law, Feldman, and Gefen, 2006) where there is more than one physical edge with electrodes attached to it.

One thing the formalism described here does not explicitly address is how the internal state changes after a single tunneling event. In a steady-state situation the tunneling of one quasiparticle does not influence the probability for the next quasiparticle to tunnel. In steady state, the perturbatively calculated expectation value should indeed correspond to the observed tunneling current, which of course is a time average over many tunneling events. If the internal state changes in a way that it affects the probability for a next quasiparticle to tunnel, then a calculation of the tunneling current should include the evolution of the internal state over time.

The *mathematical* framework of non-abelian anyons and conformal field theory etcetera is both very elegant and powerful, but it is also just an approximation to the physical system at low energies. The exact mathematical results are only expected to hold in the

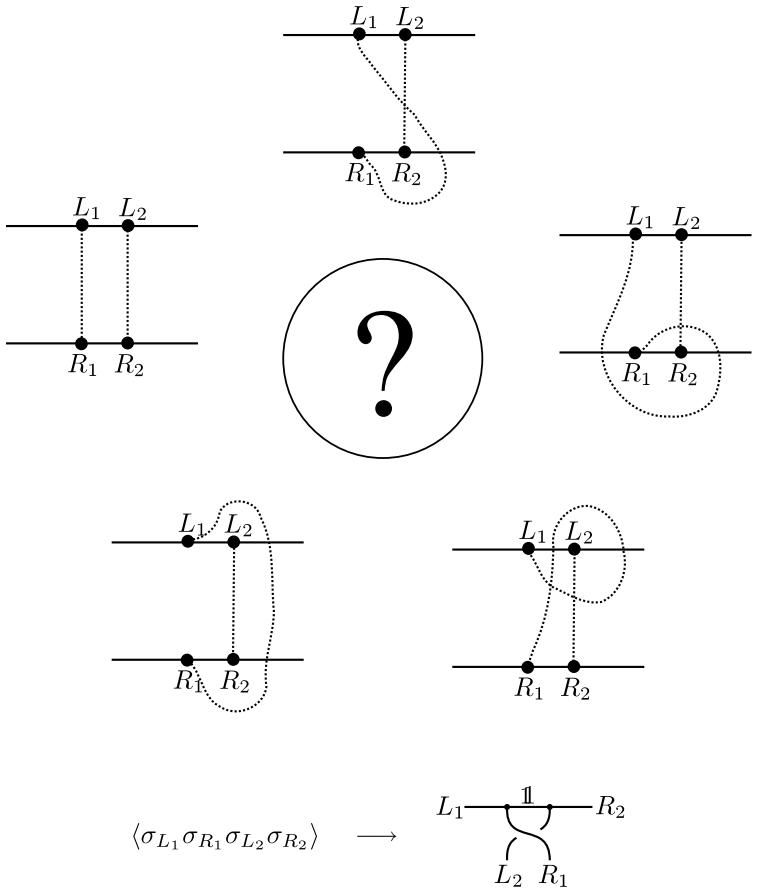

Figure 3-3: The question that may arise during the conformal block decomposition is how the ordering of operators on the individual edges is determined. This is especially important for e.g. tunneling processes that occur at *the same tunneling site* but at *different times*. The figure shows that different orderings of operators on the edge seem to give rise to different braids in the conformal block decomposition, which one is correct? The answer is that the purpose of the conformal block decomposition is to disentangle the individual edges, and the result is independent of ordering of operators on the edge, because the total fusion channel of an individual edge is invariant under braiding of quasiparticles on that edge. In other words, as far as the *conformal block decomposition* is concerned, all five different orderings shown in the figure are equivalent. However, to evaluate *the expectation value of operators* the order of the operators is important. A practical way to keep track of this ordering in the pictorial representation of the conformal block decomposition is to not allow braiding of quasiparticles that act on the same edge. This is shown in the bottom of the figure: L_1 does not braid with L_2, neither does R_1 with R_2. The only degree of freedom that is not specified is a choice of convention has to what constitutes a (counter-)clockwise braid, i.e., which side is on the front (back). Any physical result cannot depend on this choice, but for drawing pictures it is useful to pick one convention and stick with that.

thermodynamic limit of infinite system size. For finite size systems, the different basisvectors of the internal Hilbert space are in fact not independent. However, the overlap shrinks exponentially with the number of electrons in the system (i.e., the distance between bulk quasiparticles). There are situations where conformal field theory does not have all the answers. Such a situation is encountered in Sec. 4.3.1 where we have to consider the correlation function of a quasiparticle operator on an edge which is too short to have gapless modes. We require *physical* arguments to estimate the correlation function in such a case.

Chapter 4

Dynamical and scaling properties of $\nu = \frac{5}{2}$ interferometer: interference vanishes and gets restored

The material in this chapter is primarily based on Overbosch and Wen (2007).

4.1 Outline

In this chapter we calculate the tunneling conductance for the Pfaffian candidate state for the observed quantum Hall plateau at filling fraction $\nu = \frac{5}{2}$. Since this is a non-abelian system, we are required to combine the concepts from the previous chapters on transport in abelian systems (Ch. 2) and non-abelian conformal block decomposition (Ch. 3).

For a setup with a single QPC the difference between abelian and non-abelian systems is quite negligible at weak tunneling; there is a factor of $\sqrt{2}$ difference, but this factor effectively gets absorbed in other unknown factors. The real distinction between abelian and non-abelian systems manifests itself in an interferometer setup in which there are bulk quasiparticles trapped on an 'island' inside the interferometer. We calculate the tunneling conductance in linear response as function of temperature T and bias V, and we find that there is no interference when an $e/4$ quasiparticle is trapped on an island inside the interferometer. We thereby confirm within a dynamical edge theory the result by Bonderson *et al.* (2006a); Stern and Halperin (2006), see also Sec. 1.3, and we obtain the scaling properties of the tunneling current and conductance as functions of T and V. Such a non-linear I-V curve had not been calculated for any non-abelian FQH state before.

Next, we consider consider a higher order quasiparticle tunneling process that can potentially restore some interference even when an $e/4$ quasiparticle is trapped inside the interferometer. The interference vanishes to leading order $|\Gamma_1\Gamma_2|$ in the tunneling amplitude strengths Γ_j. One higher order process that would lead to non-zero interference would be of order $|\Gamma_1\Gamma_2|^2$. Another type of tunneling process that could influence the (dis)appearance of interference is tunneling of quasiparticles on and off the central island. If we would allow

$e/4$ quasiparticles to tunnel this would be like a decay-process, which is not valid for a steady state situation. Instead, we consider the tunneling between island and the edge of the neutral fermionic quasiparticle ψ that exists in the state as well.

There are several reasons why this neutral ψ-ψ-tunneling is an interesting process and might be more relevant to calculate than e.g. a process of order $|\Gamma_1\Gamma_2|^2$:

- ψ-ψ-tunneling can be incorporated in a calculation in steady-state and leading order perturbation theory.
- this process provides an elegant example of out-of-equilibrium non-abelian expectation values which require a Keldysh contour treatment and a non-trivial conformal block decomposition.
- ψ-ψ-tunneling could be the dominant form of tunneling: through detailed numerical calculations (Wan, Yang, and Rezayi, 2006; Wan *et al.*, 2008) it was found that the neutral excitations have a much lower energy scale than charged excitations (i.e., neutral mode has a slower edge velocity than charged mode).
- hypothetical observation of ψ-ψ-tunneling indicates that the presumed topologically protected qubit states are sensitive to spin-flips.
- the interference due to ψ-ψ-tunneling has the same oscillation interference period as the system with an even number of trapped quasiparticles, whereas an order $|\Gamma_1\Gamma_2|^2$ tunneling process has double that frequency.
- ψ-ψ-tunneling is not more involved to calculate compared to $|\Gamma_1\Gamma_2|^2$ processes.
- this process might help understand the more complicated process of fusion of a bulk quasiparticle with one of the edges.

In other words, by studying the ψ-ψ-tunneling process we are testing the robustness of the leading order 'even-odd' effect that was proposed by Bonderson *et al.* (2006a); Stern and Halperin (2006). From a topological quantum computation stand-point this process considers the stability of topological qubits.

One aspect that we do not focus on in this chapter is the effect of edge velocities as source of decoherence for the observed interference. Interferometers cannot be built arbitrarily large since finite temperature and finite edge velocity will set a length scale beyond which coherence becomes lost. Although we do acknowledge that the neutral edge velocity in the Pfaffian state might be quite slow (i.e., this translates to small coherence length with temperature), this is not exclusively a non-abelian effect. The same decoherence should occur for interferometers in abelian systems that have slow edge velocities. In this chapter we want to emphasize the non-abelian aspects of the problem, and as far as edge velocities go we consider the regime where these are very large and decoherence effects due to temperature do not yet show up. Finite edge velocities can nevertheless straightforwardly be included in the formalism. In chapter 6 we do focus our attention on slow edge velocities.

Figure 4-1 summarizes the main results for this chapter. In Sec. 4.2 we express the tunneling conductance of the $\nu = \frac{5}{2}$ interferometer in terms of the dynamical edge theory, and we obtain the expected vanishing interference when a central $e/4$ quasiparticle is present.

We show in Sec. 4.3 that the interference can be restored by allowing tunneling between the central island and one of the edges, and provide a more detailed calculation. We conclude with a summary. We will repeat some material from previous chapters where we think this is appropriate.

4.2 Interferometer for the Pfaffian state with vanishing interference

4.2.1 Tunneling conductance in FQH interferometer, average and amplitude

The 'Fabry-Pérot'-type interferometer concept that is used for generic quantum Hall fluids is depicted in the inset of Fig. 4-1(b). Two edges, one left- and one right-moving, of a quantum Hall fluid are brought closer together through the application of quantum point contacts; an applied bias voltage between the two edges will then induce a tunneling current of quasiparticles at these point contacts. In case of two or more point contacts, the multiple ways in which a quasiparticle can tunnel can cause interference of these paths; the presence of a non-trivial central island between the point contacts can affect the interference due to the fractional statistics of the quasiparticles.

The edge states of the Moore-Read Pfaffian state are described by a free chiral charged boson plus free chiral Majorana fermion theory (Moore and Read, 1991; Wen, 1993; Milovanović and Read, 1996). The corresponding conformal field theory is a central charge $c = 1$ plus a $c = \frac{1}{2}$ theory. Edge excitations can be described in terms of edge quasiparticle operators acting on the groundstate. Each quasiparticle type, or sector, corresponds to an irreducible representation of the algebra of the electron operators. In CFT language electron operators are certain primary fields of the $c = 1 + \frac{1}{2}$ theory. The different quasiparticle sectors are labeled by more general primary fields of the $c = 1 + \frac{1}{2}$ theory. The non-abelian part of the Moore-Read Pfaffian state comes from the $c = \frac{1}{2}$ Ising contribution which carries a primary field σ with fusion rules $\sigma \times \sigma = \mathbb{1} + \psi$, $\psi \times \psi = \mathbb{1}$, $\sigma \times \psi = \sigma$, where ψ is the neutral fermion field. The $c = 1$ part is described by a bosonic field ϕ.

The Hamiltonian we consider is a copy of the free edge theory for each edge (Wen, 1993) plus tunneling operators which destroy a quasiparticle on one edge and create it on the edge on the opposite side of a point contact, $H = H_{\text{free}} + H_{\text{tun}}$. We restrict ourselves here to tunneling of the most relevant operator with the smallest fractional charge, the charge $e^* = e/4$ quasiparticle with operator form $\sigma e^{\frac{i}{2}\phi}$ (Wen, 1993). In chapter 5 we discuss scaling dimensions and relevancy for other quasiparticle operators in the spectrum as well. With $\omega_J = e^* V$ the applied (Josephson) bias voltage between edges L and R, and Γ_1 and Γ_2 the tunneling amplitudes at the two point contacts, the tunneling Hamiltonian becomes

$$\begin{aligned} H_{\text{tun}}(t) = {} & \Gamma_1 e^{i\omega_J t} \sigma_L(t, x_1) e^{\frac{i}{2}\phi_L(t,x_1)} \sigma_R(t, x_1) e^{-\frac{i}{2}\phi_R(t,x_1)} \\ & + \Gamma_2 e^{i\omega_J t} \sigma_L(t, x_2) e^{\frac{i}{2}\phi_L(t,x_2)} \sigma_R(t, x_2) e^{-\frac{i}{2}\phi_R(t,x_2)} \\ & + \text{H.c.}. \end{aligned} \tag{4.1}$$

The tunneling current operator j_{tun} is given by ie^* times H_{tun} from Eq. (4.1) with appro-

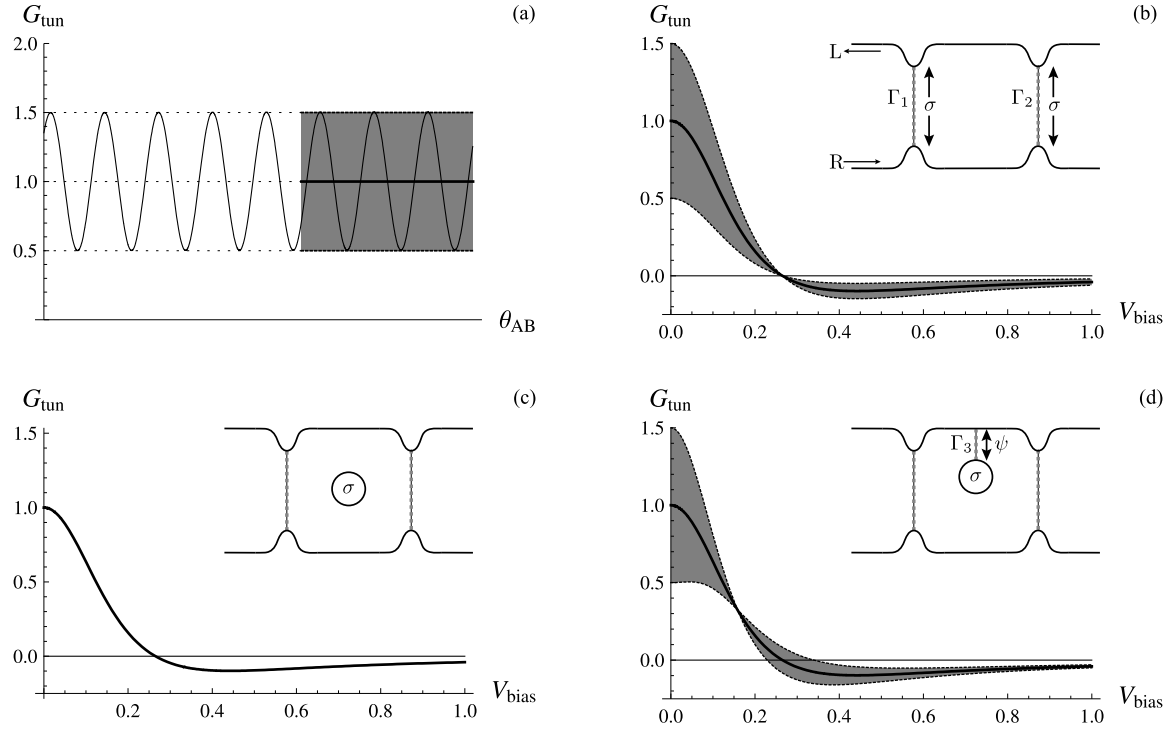

Figure 4-1: Sketch of main predictions for interference behavior in tunneling conductance $G_{\rm tun}$, for fixed temperature T and in the weak-tunneling regime. (a) At fixed bias voltage $V_{\rm bias}$ interference oscillations may be observed in $G_{\rm tun}$ as the Aharonov-Bohm phase $\theta_{\rm AB}$ is changed (e.g. changing the area of the interferometer, or the magnetic field), and *average* (thick line) and *oscillation amplitude* (grayed area) of the interference oscillations can be determined. (b) Behavior of average and amplitude of interference oscillations of $G_{\rm tun}$ as a function of $V_{\rm bias}$ for interferometer with no island. Both average and amplitude are given by same function $f_{(0)}(V_{\rm bias})$. (c) For setup with a σ-quasiparticle at the central island the interference in $G_{\rm tun}$ vanishes completely, i.e., the amplitude of oscillations is zero and only the average remains. (d) Interference is restored when the central island with the σ-quasiparticle can have ψ-ψ-tunneling to one of the edges. However, average and amplitude now scale differently with bias, average like $f_{(0)}(V_{\rm bias})$ and amplitude like $f_{(1)}(V_{\rm bias})$. This difference in scaling can be used to distinguish situations (b) and (d) when experimentally some interference is observed; as a function of T (b) and (d) also scale differently (not shown). $V_{\rm bias}$ is given in units of $2\pi T/e^*$ and units of $G_{\rm tun}$ are arbitrary, with average and oscillation amplitude of $G_{\rm tun}$ at zero bias normalized to 1 and 0.5 respectively.

priate minus signs in the Hermitean conjugated part.

The tunneling current can be calculated in linear response (i.e., leading order perturbation theory) in the tunneling amplitudes Γ_1 and Γ_2 by expressing the tunneling current in terms of a time-integral of time-ordered ground state correlation functions of CFT primary fields, which are known exactly both at zero temperature and finite temperature. This was discussed in detail for abelian states in chapter 2, see e.g. Eqs. (2.2),(2.7). The two-particle correlation function for the $e/4$ operators has, just as for the abelian states, a power-law form (at $T = 0$)

$$\langle \sigma(t_1, x_1) e^{\frac{i}{2}\phi(t_1,x_1)} \sigma(t_2, x_2) e^{\frac{i}{2}\phi(t_2,x_2)} \rangle_{L/R} = \frac{1}{\{\delta + i[t_1 - t_2 \pm (x_1 - x_2)]\}^{1/4}}. \tag{4.2}$$

This is the result for the free theory on each of the edges; the $e/4$ quasiparticles have quasiparticle exponent $g = 1/4 = 1/8 + 1/8$, contributions $1/8$ coming from both the charged ϕ sector and the neutral σ/ψ sector.

However, the expectation value that appears in the linear response for the tunneling current is not of the form of Eq. (4.2). Instead, the lowest order contribution has a term that mixes two σ_R and two σ_L operators (we focus on the non-abelian σ operators for now)

$$\langle \sigma_L(t, x_1) \sigma_R(t, x_1) \sigma_L(t', x_2) \sigma_R(t', x_2) \rangle \tag{4.3}$$

To tackle this expectation value, we need the conformal block decomposition as described in chapter 3. The conformal block decomposition factors out the correlation function of tunneling operators into a product of correlation functions (in definite fusion channel) for each edge. Since except for quasiparticle tunneling we assume no other interaction between the edges, these correlations can be evaluated in the respective groundstates of the free edge theories. The only edge correlation functions that are non-zero are those where the fusion channel of all the operators on that edge is the identity channel.

The conformal block decomposition for the four σ operators in Eq. (4.3) is shown pictorially in Fig. 4-2, in which we use the conventional notation of conformal blocks/fusion channel decompositions in terms of trivalent graphs with edges labeled by a quasiparticle sector (i.e., $\mathbb{1}$, ψ or σ). The edge quasiparticle tunneling operators are associated with bulk quasiparticles created in pairs out of the vacuum in the identity fusion channel. These bulk quasiparticles are braided until quasiparticles are ordered by edge. Then the fusion channel per edge is determined. The braiding operation is given in terms of the braid matrix $\mathcal{R}$ which is worked out in detail in Ch. 3. In the conformal block decomposition we ignore phase factors in front of basis-vectors. The phase associated with tunneling is very sensitive to the exact path taken, and thus such a phase is better captured by including it in the tunneling amplitudes Γ_i.

The resulting conformal block decomposition has the full identity channel (identity channel for each of the edges) in it, and hence has a non-zero expectation value,

$$\begin{aligned}\langle \sigma_L(t, x_1) \sigma_R(t, x_1) \sigma_L(t', x_2) \sigma_R(t', x_2) \rangle \\ = \frac{1}{\sqrt{2}} \langle \sigma_L(t, x_1) \sigma_L(t', x_2) \rangle \langle \sigma_R(t, x_1) \sigma_R(t', x_2) \rangle.\end{aligned} \tag{4.4}$$

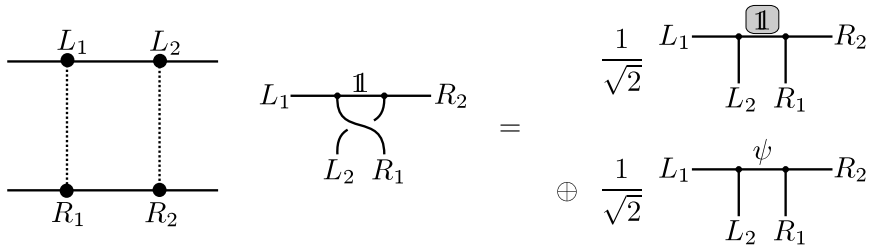

Figure 4-2: Conformal block decomposition when two σ quasiparticles tunnel between left- and right-moving edges on opposite sides of a FQH liquid. The left picture indicates the tunneling paths. Such a process involves the action of four σ quasiparticle operators, labeled by L_1, R_1, L_2 and R_2. In the middle and the right pictures, a graphical representation of fusions is used where all legs (internal and external) are labeled by a quasiparticle type $\mathbb{1}$, ψ or σ. The conformal block decomposition is a basistransformation from a state where the pair L_1 and R_1 is in the identity channel, and likewise the pair L_2 and R_2 (the middle picture), to a basis where L_1 and L_2 (R_1 and R_2) are in a definite fusion channel (the right picture). This fusion channel can be either $\mathbb{1}$ or ψ. The basistransformation is constructed through application of the braid matrix $\mathcal{R}$. Note that we are ignoring phase-factors here (as they can be absorbed into the coupling constants Γ_i), hence the direct-sum symbol on the right-hand-side instead of the literal sum. Only those states in which all edges, i.e., in this case both the left and the right edge, simultaneously contain the identity channel give rise to a non-zero expectation expectation value. Such a state appears (once) in the current decomposition, for which the identity channel is highlighted.

To identify the presence of the full identity channel, one can drop all the legs that correspond to $\mathbb{1}$ in the right picture of Figure 4-2. Then we see that in the full identity channel, (L_1, L_2) legs and (R_1, R_2) legs form their own connected graphs.

With the non-abelian aspect, the conformal block decomposition, taken care of at this point, the tunneling current can be calculated using the known methods for the abelian states. Following formalism described in chapter 2 (based on Chamon *et al.*, 1997) we find for the tunneling current

$$I_{\rm tun}(T,V) = |\Gamma_{\rm eff}|^2 T^{-\frac{1}{2}} F_{(0)}\left(\frac{e^*V}{2\pi T}\right). \tag{4.5}$$

This form is valid both for a single QPC and an interferometer setup with two QPCs. For precise comparison with Eqs. (2.36) and (2.42) we have to identify $F_{(0)}(z) \equiv F_{g=1/4}(z)$, $\delta x \equiv 0$ and furthermore

$$\text{for } N=1: \quad |\Gamma_{\rm eff}|^2 = \frac{1}{\sqrt{2}}(e/4)|\Gamma|^2(2\pi)^{-1/2} \tag{4.6}$$

$$\begin{aligned}\text{for } N=2: \quad |\Gamma_{\rm eff}|^2 =& \frac{1}{\sqrt{2}}(e/4)(2\pi)^{-1/2}\Big[|\Gamma_1|^2 + |\Gamma_2|^2 \\ &+ 2{\rm Re}\Big(\Gamma_1\Gamma_2^* e^{i\theta_{\rm AB}}\Big) H_{g=1/4}(T,V,x)\Big].\end{aligned} \tag{4.7}$$

Note that the only distinction between the result for an abelian quasiparticle with $e^* = e/4$

and $g = 1/4$ and this non-abelian result is the overall factor $\frac{1}{\sqrt{2}}$ coming from the conformal block decomposition Eq. 4.4. Unless the Γ_j are known to high accuracy this distinction is not observable. The difference between abelian and non-abelian is quite striking though when bulk quasiparticles are present.

First however, we would like to express Eq. (4.7) in a form that focuses on the scaling behavior as a function of T and V. Also, to compare more directly with experimental settings, instead of the tunneling current we would like to write the differential tunneling conductance. $G_{\rm tun} = \frac{\partial I_{\rm tun}}{\partial V}$,

$$G_{\rm tun}(T,V) = |\Gamma_{\rm eff}|^2 T^{-\frac{3}{2}} f_{(0)}\left(\frac{e^*V}{2\pi T}\right), \tag{4.8}$$

where $f_{(0)}(z) = F'_{(0)}(z)$ and we absorbed all overall constant factors that we are less interested in into the tunneling amplitudes Γ_i. Separating out the contributions with interference oscillations from the others

$$\begin{aligned} G_{\rm tun}(T,V) &= G^{\rm ave}_{\rm tun}(T,V) + G^{\rm osc}_{\rm tun}(T,V)\cos(\theta_{\rm AB}+\theta_0), \\ G^{\rm ave}_{\rm tun}(T,V) &= \left(|\Gamma_1|^2+|\Gamma_2|^2\right) T^{-\frac{3}{2}} f_{(0)}\left(\frac{e^*V}{2\pi T}\right), \\ G^{\rm osc}_{\rm tun}(T,V) &= 2|\Gamma_1\Gamma_2|\, T^{-\frac{3}{2}} f_{(0)}\left(\frac{e^*V}{2\pi T}\right). \end{aligned} \tag{4.9}$$

$G^{\rm osc}_{\rm tun}(T,V)$ describes the amplitude of the interference oscillation, and $G^{\rm ave}_{\rm tun}(T,V)$ the average differential tunneling conductance. We note that both $G^{\rm osc}_{\rm tun}(T,V)$ and $G^{\rm ave}_{\rm tun}(T,V)$ scale as $T^{-3/2}$. In fact, they both depend on V/T in the same way. This is plotted in Fig. 4-1(b).

Note that, as announced, we made a simplification here by assuming that the distance x between the two point contacts is smaller than the thermal decoherence length. In other words, since $H_g(T,V,x) = 1+\mathcal{O}(x^2)$, this is the limit in which x is small enough such that we can ignore both $H_g(T,V,x)$ and its derivative with V. If x is not much smaller the thermal decoherence length then the full form of $H_g(V,T,x)$, Eq. (2.30), would be required for the precise form of the tunneling conductance as function of V and T. This would not alter the predictions about vanishing/restored interference and overall scaling with temperature though.

4.2.2 Vanishing interference with σ quasiparticle on central island

The non-abelian statistics of the quasiparticles can be probed if the interferometer contains a small central island (or bulk quasiparticle) in the σ sector, as depicted in the inset of Fig. 4-1(c). Since quasiparticles in the σ sector can only exist in pairs, there has to be an additional σ-quasiparticle somewhere else in the FQH fluid, either on another island, on an edge, or as a true bulk quasiparticle. Our only assumption is that it should be located outside the interferometer. An interference path that loops around the central island will now have a different conformal block decomposition, and this affects the interference.

The conformal block decomposition in the presence of a small central island with a $e/4$ σ quasiparticle trapped on it is illustrated in Fig. 4-3. The main difference with the

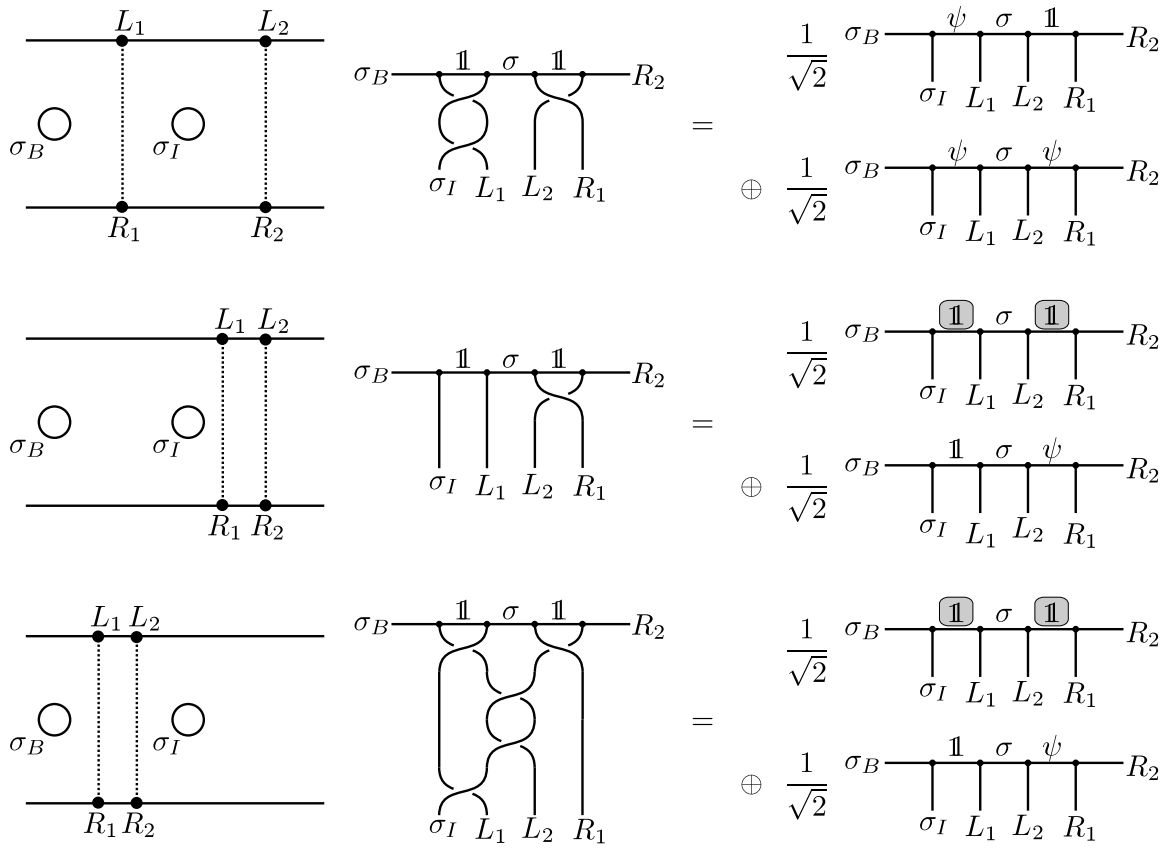

Figure 4-3: Conformal block decomposition when a σ quasiparticle is present on a central island, which can be constructed from consecutive braidings $\mathcal{R}$ of the σ operators. When σ quasiparticle tunneling takes place on *both* sides of the central island the full identity channel disappears from the decomposition (top row). This term represents the interference between the two different paths to tunnel between left- and right edge, and now had a zero expectation value: the interference vanishes. The contributions from tunneling at a *single* point contact, i.e., tunneling of two σ quasiparticles at the QPC right of the island (middle row) or left of the island (bottom row), still contain the full identity channel and hence are still non-zero. The conformal block now not only contains the left edge (with L_1 and L_2) and the right edge (with R_1 and R_2) but also the bulk (which includes the island quasiparticle σ_I and the necessary σ_B which is assumed to be outside the interferometer).

situation before, i.e., Fig. 4-2, is that the central σ_I is fully encircled by σ_{L_1} for the case with tunneling quasi-particles on both sides of the island (top row in Fig. 4-3). If a charge $e/4$ non-abelian quasiparticle is moved around another $e/4$ non-abelian quasiparticle, the two particles will each gain a neutral fermion (Das Sarma, Freedman, and Nayak, 2005; Bonderson *et al.*, 2006a; Stern and Halperin, 2006; Fendley *et al.*, 2007). In Sec. 3.2 we show explicitly that fusion channels $\mathbb{1}$ and ψ are interchanged upon a double braid $\mathcal{R}^2$. As there is no channel in the full identity representation at all three edges (left-, right- and island-edge) the expectation value of this operator is zero.

If one calculates the tunneling conductance for the case with a σ-quasiparticle present inside the interferometer one finds

$$G_{\rm tun}(T,V) = G^{\rm ave}_{\rm tun}(T,V), \qquad G^{\rm osc}_{\rm tun}(T,V) = 0. \tag{4.10}$$

The average tunneling conductance is still given by Eq. (4.9), but the interference term has vanished, see Fig. 4-1(c). This follows from the conformal block decomposition, because the operator that caused interference before, the term that involved tunneling at the two different point contacts, now has a zero expectation value. The average tunneling conductance is given by the terms where tunneling operators act only on one of the two point contacts and thus not enclose the central σ quasiparticle (as depicted in middle and bottom rows of Fig. 4-3).

An alternative explanation is that in encircling the island a σ-quasiparticle flips a global internal pseudospin and 'internal-spin-up' and 'internal-spin-down' do not interfere. Also one can explain the vanishing interference as being able to tell which path the tunneling quasiparticle took, because this information can be determined from a hypothetical measurement of the sectors of the system before and after a tunneling event.

If more than one σ quasiparticle is trapped inside the interferometer (on e.g. multiple small islands, or as pure bulk quasiparticles) one observes the 'even-odd' effect: the interference will vanish when the number of quasiparticles is *odd*, and interference is expected to be seen when the number of quasiparticles is *even*.[1]

4.3 Interference restored through ψ-ψ-tunneling

In the presence of a σ quasiparticle on the central island the interference vanished to leading order in Γ_1 and Γ_2. Here we will consider the situation where the the central island is close to one of the edges (which we choose to be the left-moving/top edge). We will include a tunneling process between the central island and the left edge. For simplicity we restrict ourselves to the tunneling of the neutral fermions only, because this process leaves the sector of the island unaltered and furthermore this is a charge-neutral operation. We will see that such higher order tunneling processes can potentially restore some interference.

[1] In the case of two or more quasiparticles there is another conceptual step that needs to be considered, namely that measuring the tunneling current constitutes a projective measurement. This aspect is discussed in Overbosch and Bais (2001); Bonderson *et al.* (2008). It is only after the projection has taken place that the even-odd effect result holds.

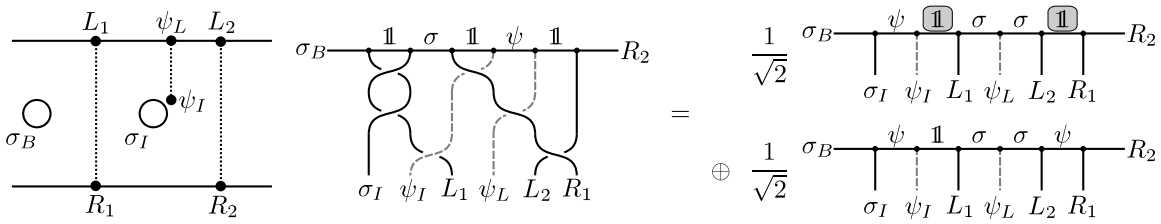

Figure 4-4: Conformal block decomposition when a neutral ψ quasiparticle tunnels between left edge and central island. The additional exchange of a ψ gives the contribution with σ quasiparticles tunneling on *both* sides of the island a non-zero expectation value, since the full identity channel now appears in the decomposition: $\mathbb{1}$ on right edge, left edge *and* in the bulk simultaneously. Not shown are processes where two σ operators tunnel on a single side of the island; such contributions have a zero expectation value in the presence of the tunneling ψ quasiparticle.

The tunneling of the neutral fermions is described by the tunneling Hamiltonian

$$H_{\text{tun}} \to H_{\text{tun}} + \Gamma_3 \psi_L(t, x_3)\psi_I(t), \tag{4.11}$$

where the tunneling amplitude Γ_3 is real-valued to ensure hermiticity of the Hamiltonian (the ψ quasiparticle is its own anti-particle).

Inclusion of the operator $\psi_L\psi_I$ in the Hamiltonian has the potential to restore interference because the fusion channel now has the full identity channel in it, as shown in Fig. 4-4. This follows straightforwardly from the braiding matrix for the σ particles as explained in Sec. 3.2 (braiding a σ and a ψ only gives a phase). Hence the corresponding operator has a non-zero expectation value, whereas without the additional $\psi_L\psi_I$ contribution the expectation value is zero.

We find a contribution to the tunneling conductance to leading order in Γ_3 which contains some non-zero interference. The average value of the conductance is still unaltered to leading order, but the oscillation amplitude now behaves as

$$G_{\text{tun}}^{\text{osc}}(T, V) = 2|\Gamma_1\Gamma_2|\Gamma_3\, T^{-2}\, f_{(1)}\left(\frac{e^*V}{2\pi T}\right). \tag{4.12}$$

Compared with Eq. (4.9), the interference oscillation amplitude now has a different power of T, T^{-2} instead of $T^{-3/2}$, and a different dependence on V/T through a dimensionless function $f_(1)(y)$, as depicted in Fig. 4-1(d).

If the tunneling amplitudes Γ_i are unknown (i.e., only known to limited accuracy because e.g. experimental control is poor) the different scaling of the interference with temperature and bias is a way to tell one situation [interference with no central σ, Fig. 4-1(b)] from the other [interference with a central σ but also ψ-ψ-tunneling, Fig. 4-1(d)].

As mentioned in the outline, an observation of ψ-ψ-tunneling would indicate that the topologically protected zero-mode space is sensitive to 'spin/qubit' flips. It also help us to understand how the destruction of interference by non-abelian statistics is restored as the non-abelian particle between the two point contacts is moved near an edge. Tunneling of a neutral ψ between island and edge is not the only mechanism through which interference

can be restored. Higher order contributions in Γ_1 and Γ_2 will have a non-zero interference term, for instance at order $|\Gamma_1|^2|\Gamma_2|^2$, as for such a term the central island is effectively encircled twice (i.e., an even number of times) by the tunneling quasiparticle. However, the Aharonov-Bohm phase is included twice as well, and such a term would show a different oscillation period when varying θ_{AB}.

4.3.1 Calculation of the leading island tunneling contribution

We will now derive the result Eq. (4.12) in detail.

The steady state tunneling current I_{tun} is calculated by expanding the time evolution operator, starting from an initial state $|0\rangle$

$$\begin{aligned} I_{\mathrm{tun}}(t) &= \langle\varphi(t)|\, j_{\mathrm{tun}}\, |\varphi(t)\rangle \\ |\varphi(t)\rangle &= \mathcal{T}\{e^{-i\int_{-\infty}^{t} dt'[H_0+H_{\mathrm{tun}}(t')]}\}|0\rangle, \end{aligned} \tag{4.13}$$

where $\mathcal{T}\{\ldots\}$ indicates time-ordering. Up to second order in H_{tun} this becomes

$$\begin{aligned} &I_{\mathrm{tun}}(t) = \\ &-i\int_{-\infty}^{t} dt'\,\langle 0|[j_{\mathrm{tun}}(t), H_{\mathrm{tun}}(t')]|0\rangle + \int_{-\infty}^{t} dt_1 \int_{-\infty}^{t} dt_2 \Big(-\langle 0|\mathcal{T}\{j_{\mathrm{tun}}(t)H_{\mathrm{tun}}(t_1)H_{\mathrm{tun}}(t_2)\}|0\rangle \\ &\quad -\langle 0|\mathcal{T}\{j_{\mathrm{tun}}(t)H_{\mathrm{tun}}(t_1)H_{\mathrm{tun}}(t_2)\}|0\rangle^* + \langle 0|H_{\mathrm{tun}}(t_1)j_{\mathrm{tun}}(t)H_{\mathrm{tun}}(t_2)|0\rangle\Big) + \ldots. \end{aligned} \tag{4.14}$$

One term that appears in Eq. (4.14) is a correlation of the form

$$\langle 0|\mathcal{T}\{\sigma_L(t_1)\sigma_L(t_2)\sigma_R(t_1)\sigma_R(t_2)\psi_L(t_3)\psi_I(t_3)\}|0\rangle. \tag{4.15}$$

From the conformal block decomposition shown in Fig. 4-4, we see that $\sigma_L\sigma_L\sigma_R\sigma_R\psi_L\psi_I$ contains the full identity channel if there is an $e/4$ non-abelian quasiparticle between the two junctions. Thus the above correlation is non-zero.

After the conformal block decomposition, the correlation function is factorized into correlation functions on each edge, which then takes the typical form

$$\langle\sigma\sigma\psi\rangle_L\langle\sigma\sigma\rangle_R\langle\psi\rangle_I\langle e^{\frac{i}{2}\phi}e^{-\frac{i}{2}\phi}\rangle_L\langle e^{\frac{i}{2}\phi}e^{-\frac{i}{2}\phi}\rangle_R. \tag{4.16}$$

We would like to argue that we can set $\langle\psi(t)\rangle_I = 1$. On long edges, in the groundstate, surely $\langle\psi\rangle$ would be zero as follows from CFT. However, the central island is a very short edge. The edge excitations for this small island are not gapless, but form a discrete spectrum. The effect of the operator ψ_I at low energies will then be to change the quasiparticle sector of the island, but not to excite any edge modes. We thus expect the groundstate expectation value of this operator to be constant and one. Note that in the thermodynamic limit changing a σ quasiparticle sector by adding/removing a neutral ψ costs no energy (recall fusion rule $\sigma\times\psi = \sigma$).

Next, we address time-ordering. According to the conformal field theory, the time-

ordered two-point and three-point-function (at zero temperature) are given by

$$\langle 0|\mathcal{T}\{\sigma_R(t_1)\sigma_R(t_2)\}|0\rangle = \frac{1}{(\delta + i|t_1 - t_2|)^{1/8}}, \tag{4.17}$$

$$\langle 0|\mathcal{T}\{\sigma(t_1)\sigma(t_2)\psi(t_3)\}|0\rangle = \frac{1}{\sqrt{2}}\frac{(\delta + i|t_1 - t_2|)^{3/8}}{(\delta + i|t_1 - t_3|)^{1/2}(\delta + i|t_2 - t_3|)^{1/2}}. \tag{4.18}$$

Recall that in these correlators δ is a short-distance cutoff. The leading order contribution in the tunneling current is the familiar linear response result. But note that the next contribution contains both time-ordered and non-time-ordered parts. The non-time-ordered part is basically a Keldysh contour-ordered term; to compute its expectation value we have to analytically continue the time-ordered correlation functions. We would like to have an expression for *any* ordering of the times t_1, t_2 and t_3, which we obtain by removing the absolute value bars,

$$\langle 0|\sigma_L(t_1)\sigma_L(t_2)\psi_L(t_3)|0\rangle\langle 0|\sigma_R(t_1)\sigma_R(t_2)|0\rangle = \frac{(\delta + i(t_1 - t_2))^{1/4}}{(\delta + i(t_1 - t_3))^{1/2}(\delta + i(t_2 - t_3))^{1/2}}. \tag{4.19}$$

If we include the contributions from the charged sectors as well, the total correlation function simplifies considerably because of a cancellation: the numerator in Eq. (4.19) gets cancelled by the product of the ϕ two-point functions.

The total scaling dimension of the remaining operators is 1. From the scaling consideration in the $\int dt_1 \int dt_2$ integral, we find that such an operator will contribute $\delta I_{\rm tun} \propto T^{-1}$, or more precisely

$$\delta I_{\rm tun} = \frac{1}{\sqrt{2}}\frac{4e^*}{\pi T} 2{\rm Re}\Big(\Gamma_1\Gamma_2^* e^{i\theta_{\rm AB}}\Big)\,\Gamma_3\,F_{(1)}\left(\frac{e^*V}{2\pi T}\right), \tag{4.20}$$

where the scaling function $F_{(1)}(y)$ will be given below.

Working out the double-integrals in Eq. (4.14), a tedious but somewhat straightforward task that we not explicitly include in this thesis, it turns out that the two time-ordered contributions depend on the cutoff and only the non-time-ordered part contributes in the limit of zero δ. The contribution we find to first order in Γ_3 in the tunneling current, working at finite temperature (by making imaginary time periodic with period $1/T$ which maps (Shankar, 1990) $(\delta + it)^g \to \{\sin[\pi T(\delta + it)]/\pi T\}^g$) and setting $x_i = 0$, is Eq. (4.20) with $F_{(1)}$ given by

$$F_{(1)}(y) = \int_0^\infty du_1 \sin(2yu_1) \int_0^{u_1} du_2 \frac{1}{\sqrt{\sinh u_2 \sinh(u_1 - u_2)}}. \tag{4.21}$$

We find that we can approximate the integral over u_2 reasonably well with the function $\pi/\cosh\frac{u_1}{2\sqrt{2}}$. By taking the derivative with respect to V, $f_{(1)}(y) = F'_{(1)}(y)$, and absorbing constants into the Γ_i we arrive at the expression Eq. (4.12) for the oscillation amplitude of the tunneling conductance. Note that the Γ_3 contribution is pure interference *only*, there is no contribution to the average conductance.

4.3.2 Flow to fixed point

Since the Γ_3 contribution to the interference oscillation amplitude increases more rapidly than the average conductance as T goes to zero (T^{-2} versus $T^{-3/2}$), we expect the present result to be unstable towards lowering of the temperature. And we can ask the question what fixed point this setup flows to; more carefully worded: by lowering the temperature and at the same time making Γ_1 and Γ_2 smaller as well such that tunneling between left and right edges is still weak, what interference pattern does this flow to? Since in our setup the $e/4$ non-abelian quasiparticle present on the island is not affected by the ψ-ψ tunneling, the junction may flow to a non-trivial fixed point.

To determine the behavior of the interference pattern at arbitrary coupling requires a (numerical approximation to an) exact solution, which in general is a lot harder to obtain than the leading order weak tunneling contribution. However, near the strong coupling fixed point a perturbative calculation might be possible again, and one can interpolate between weak and strong fixed points to estimate the behavior for arbitrary coupling. For tunneling in generic abelian FQH state this was studied by Moore and Wen (2002). Similarly, we expect that there is a strong coupling limit for this non-abelian ψ-ψ tunneling process. Identifying such a fixed point would would likely allow one to estimate the behavior of the interference pattern for arbitrary ψ-ψ tunneling amplitude. Because of the non-abelian nature of the neutral ψ, we expect this strong coupling fixed point to lie beyond the realm of the known abelian fixed points.

4.4 Summary

In this chapter we calculate the scaling behavior of the non-linear I-V tunneling curves for a two-point-contact tunneling junction between two edges of the $\nu = \frac{5}{2}$ non-abelian fractional quantum Hall state. Using the conformal block decomposition rules for the tunneling operators, we can calculate the non-linear I-V tunneling curves for the cases with and without an $e/4$ non-abelian quasiparticle between the two contacts. It was suggested that the presence of the $e/4$ quasiparticle between the two contacts destroys the interference between the two tunneling paths. We show how to obtain such a result within a quantitative dynamical edge theory. Such a dynamical understanding allows us to calculate how the interference reappears as the $e/4$ quasiparticle is moved closer to an edge. In particular, we consider the effect of a ψ-ψ tunneling between the island (which traps an $e/4$ quasiparticle) and an edge. We find that such a coupling between the island and the edge makes the interference pattern reappear. The scaling behavior of the induced interference pattern is calculated as well.

Related literature

Tunneling between bulk island and edge was considered as well in Rosenow, Halperin, Simon, and Stern (2008). Their setup is symmetric between top L and bottom R edges; however it also includes two $e/4$ particles inside the interferometer, and as such the problem they study is different from the one in this chapter, although somewhat related.

Shortly after our paper (Overbosch and Wen, 2007) first appeared, another candidate

trial wavefunction for the $\nu = \frac{5}{2}$ FQH state was introduced: the 'anti-Pfaffian' (Lee *et al.*, 2007; Levin *et al.*, 2007). Following shortly, a quantitative dynamical edge calculation was performed by Bishara and Nayak (2008), in which the authors explore a two point contact interferometer setup for both the Pfaffian and anti-Pfaffian candidate states and calculate I-V-curves, taking finite edge velocities into account. They find the even-odd effect for both states. Furthermore they emphasize that a slow neutral edge velocity sets a decoherence length scale for the interferometer arm lengths. Recent numerical results (Wan *et al.*, 2008) indicate that the neutral mode velocity is indeed slow compared to the charged mode velocity. Strictly speaking, the results in our paper are valid in the regime where decoherence due to edge velocities does not yet play yet, and for the Pfaffian state only; however, our results and those of Bishara and Nayak (2008) can straightforwardly be extended to include ψ-ψ-tunneling in these more general cases as well.

Other proposals to probe non-abelian fractional statistics have been made for noise measurements in the $\nu = \frac{5}{2}$ state (Ardonne and Kim, 2008), and for interferometry in the $k = 3$ Read-Rezayi state (Bonderson, Shtengel, and Slingerland, 2006b; Chung and Stone, 2006; Fidkowski, 2007).

Chapter 5

Phase transitions on the edge of the $\nu = \frac{5}{2}$ Pfaffian and anti-Pfaffian quantum Hall state

The material in this chapter is primarily based on Overbosch and Wen (2008).

5.1 Outline

The physics of a quantum Hall bulk state can be probed through transport measurements on the edge. We described this in detail in chapter 2 for tunneling current and noise in perturbation theory for abelian quantum Hall systems. From the discussion on non-abelian quantum Hall systems, chapters 3 and 4, we see that the non-abelian effects do not yet come into play when tunneling takes place on a single site. In other words, through measurements on tunneling at a single QPC, quasiparticle charge e^* and exponent g can be fitted. These are parameters that can distinguish between different candidate states, and it does not matter whether the physical state is abelian and non-abelian. It is primarily the propagation of quasiparticles along the edge, i.e., chiral Luttinger liquid theory (Wen, 1992), which determines the I-V-characteristics at a single QPC, where non-abelian braiding does not play a role.

As far as the filling fraction $\nu = \frac{5}{2}$ state goes, it is currently still unclear what the true nature of the bulk state is; many candidate states, or trial wavefunctions, exist, some of which predict non-abelian statistics, others predict less exotic abelian statistics (Halperin, 1983; Moore and Read, 1991; Wen, 1991b, 2000; Lee *et al.*, 2007; Levin *et al.*, 2007). We will briefly review these candidates here. The recent experimental data on transport on a single QPC in the $\nu = \frac{5}{2}$ state (Dolev *et al.*, 2008; Radu *et al.*, 2008) is most consistent with a quasiparticle charge $e^* = 1/4$ and exponent $g = 1/2$.

In this chapter we introduce two other candidates for the $\nu = \frac{5}{2}$ FQH *edge*. First, starting from the existing anti-Pfaffian bulk state (Lee *et al.*, 2007; Levin *et al.*, 2007), we consider interactions between the counterpropagating edge modes. As we change the interaction strength, we find that there is a transition to a new phase on the edge, with different values for e^* and g. Note that this is really a phase transition on the edge, since

the bulk state does not change. By appropriately tuning the edge interactions one should be able to observe this quantum phase transition through e.g. a change in e^* and g.

We call this new phase the 'Majorana-gapped' phase, as the anti-Pfaffian Majorana mode becomes gapped. The Majorana-gapped phase has 2 and 1/2 right-moving edge branches and 1 left-moving edge branches, while the standard edge phase for the anti-Pfaffian state has 3 right-moving edge branches and 1 and 1/2 left-moving edge branches. During the transition from the standard edge phase to the Majorana-gapped phase, half a left-moving edge branch (a Majorana fermion mode) pairs up with half a right-moving edge branch and this opens up an energy gap.

Second, we start with the edge reconstructed (Chamon and Wen, 1994) Pfaffian bulk state, which has 2 and 1/2 branches of right movers and 1 branch of left movers. Such an edge can also undergo a phase transition into a Majorana-gapped phase which has 2 branches of right movers and 1/2 branch of left movers. The values of e^* and g can be changed by the phase transition.[1] We find that the quasiparticle tunneling exponent changes from $g = 1/4$ to $g = 1/2$ for the edge reconstructed Pfaffian state, and changes from $g = 1/2$ to $g = 0.55 - 0.75$ for the anti-Pfaffian state, in the new Majorana-gapped phases.

The above result is for the clean edge. In the presence of impurities, the picture is different. In that case, as we change the interaction strength between different edge branches beyond a threshold, a right-moving Majorana fermion mode pairs up with a left-moving Majorana fermion mode and they become localized. If we assume that the localized modes do not contribute to tunneling between the edges, then we can treat those localized modes as if they are gapped. Under this assumption, the clean edge and dirty edge behave similarly.

We like to stress that in order to have the gapping or the localization phase transition, it is necessary to include the supposedly completely filled lowest Landau level in the framework, or to include the additional edge branches from the edge reconstruction. The new phases require that the different edge modes have substantial interactions with each other.

Numerical simulations for small-size closed (i.e., compact) systems (Morf, 1998; Rezayi and Haldane, 2000), which by construction ignore edge effects, suggested that the Moore-Read Pfaffian trial wavefunction is the most likely candidate for the actual $\nu = \frac{5}{2}$ FQH bulk state. To compare with actual experiments, which obviously have an edge, it is necessary, as our examples in this paper shows, to include the edge-aspect as well. This is emphasized also in a very recent numerical study (Wan *et al.*, 2008) which considers a disc-geometry with an edge, and a varying confining potential; for a sharp edge the Pfaffian is found to be favored, but for a smooth edge the groundstate is a different state which bears the marks of some form of edge reconstruction.

The 'Majorana-gapping' transition is a quantum phase transition on the edge only which does not affect the bulk state. Such a kind of edge-only quantum phase transition has been studied by Kao, Chang, and Wen (1999). Here we find a new type of edge-only quantum phase transition where we lose (gain) a fractional branch of right-movers (right-movers) through the transition.

The organization of this chapter is as follows. We review the different candidates for

[1] Here, with a change of e^* we mean that another quasiparticle with a different charge becomes the most dominant quasiparticle which is observed in experiments. The phase transition does not change the fixed charge e^* of a given quasiparticle; it can change the exponent g for all quasiparticles.

Table 5.1: Seven different candidates states for the $\nu = \frac{5}{2}$ FQH system with number of edge branches, expected quasiparticle charge e^* and exponent g for dominant tunneling quasiparticles, and exponent g_e for electron operator. Here, we have included the 2 right-moving branches from the underlying $\nu = 2$ IQH state. The subscripts L and R indicate the left-moving and right-moving edge branches. Exponent g generally seems to be increasing with total number of edge branches. The listed electron operator exponents g_e ignore the $\nu = 2$ IQH electrons. The two Majorana-gapped phases have a dominant $e^* = e/2$ quasiparticle in addition to a quarter charge quasiparticle.

state	# of branches	e^*/e	g	g_e
$K = 8$	$1_R + 2_R$	1/4	0.125	∞
Pfaffian	$\frac{3}{2}_R + 2_R$	1/4	0.25	3
331	$2_R + 2_R$	1/4	0.375	3
$U(1) \times SU_2(2)$	$\frac{5}{2}_R + 2_R$	1/4	0.5	3
anti-Pfaffian	$1_R + \frac{3}{2}_L + 2_R$	1/4	0.5	3
Majorana-gapped edge-rec. Pfaffian	$2_R + \frac{1}{2}_L + 2_R$	1/4 1/2	0.5 0.5	3
Majorana-gapped anti-Pfaffian	$\frac{5}{2}_R + 1_L$	1/4 1/2	0.55-0.75 0.5-0.7	1.8-2.0

the $\nu = \frac{5}{2}$ state in Sec. 5.2. Section 5.3 is the core of our paper. Here we show that for the anti-Pfaffian state there exists an operator which for certain density-density interactions becomes relevant and can drive a phase transition. In the new phase a pair of counterpropagating Majorana modes becomes gapped. For the new phase we determine the quasiparticle spectrum and which of these quasiparticles is the most relevant. In Sec. 5.4 we apply the same formalism to the edge reconstructed Pfaffian state. We discuss and summarize our results in Sec. 5.5.

5.2 List of candidate states for $\nu = \frac{5}{2}$ ($\nu = \frac{1}{2}$) FQH state.

The Majorana-gapped phase at the edge of the anti-Pfaffian state is just one of many possible edge states at filling fraction $\nu = \frac{5}{2}$. Therefore, in this section, we will review some known theoretical edge candidate states for filling fraction $\nu = \frac{5}{2}$. Or, to be more precise, for filling fraction $\nu = \frac{1}{2}$ modulo completely filled Landau levels.

It is well known that, at a given filling fraction, FQH states may have many different internal structures – topological orders (Blok and Wen, 1990a; Read, 1990; Wen and Niu, 1990; Fröhlich and Kerler, 1991; Fröhlich and Zee, 1991; Wen and Zee, 1992; Fröhlich and Studer, 1993; Wen, 1995). So it is not clear a priori which topological order describes a particular experimentally observed $\nu = \frac{1}{2}$ ($\nu = \frac{5}{2}$) FQH state. The following five topological orders are simple and are more likely to describe the observed $\nu = \frac{1}{2}$ ($\nu = \frac{5}{2}$) FQH states. These topological orders are:

(A) The electrons first pair into charge $2e$ bosons and the charge $2e$ bosons then condense

into the Laughlin state described by the following wave function:

$$\prod_{i<j}(Z_i - Z_j)^8 e^{-\frac{1}{4}\sum_i |Z_i|^2}.$$

The effective theory of this state has a form (Blok and Wen, 1990a; Wen and Niu, 1990; Wen and Zee, 1992)

$$\mathcal{L} = \sum_{IJ} K_{IJ} \frac{1}{4\pi} a_{I\mu} \partial_\nu a_{J\lambda} \epsilon^{\mu\nu\lambda}, \tag{5.1}$$

with K a 1×1 matrix $K = 8$.

(B) The charge $2e/3$ quasiparticles on top of the $\nu = \frac{1}{3}$ Laughlin state condense into a second level hierarchical FQH state (Blok and Wen, 1990b; Wen and Zee, 1992; Yang, Su, and Su, 1992). The effective theory of such a state is given by Eq. (5.1) with $K = \begin{pmatrix} 3 & -2 \\ -2 & 4 \end{pmatrix}$. Since $\begin{pmatrix} 3 & 1 \\ 1 & 3 \end{pmatrix} = W \begin{pmatrix} 3 & -2 \\ -2 & 4 \end{pmatrix} W^T$ with $W = \begin{pmatrix} 1 & 1 \\ 1 & 0 \end{pmatrix}$, such a state has the same topological order as the 331 double layer state (Wen and Zee, 1992).

(C) The FQH state proposed by Moore and Read (1991) and described by the Pfaffian wave function

$$\Psi_{\rm Pf}(\{z_i\}) = \mathcal{A}\Big(\frac{1}{z_1 - z_2}\frac{1}{z_3 - z_4}\cdots\Big)\prod_{i<j}(z_i - z_j)^2 e^{-\frac{1}{4}\sum_i |z_i|^2}, \tag{5.2}$$

where $\mathcal{A}$ is the antisymmetrization operator. See also Eq. (3.2) in section 3.1.1.

(D) The anti-Pfaffian state, which is the particle-hole conjugate of the Pfaffian state (Lee *et al.*, 2007; Levin *et al.*, 2007). An explicit wavefunction for the anti-Pfaffian can be given in terms of an integral (one can think of the anti-Pfaffian as fully filling a Landau-level from which a Pfaffian wavefunction then needs to be integrated out).

(E) The FQH state proposed by Wen (1991b); Blok and Wen (1992) and described by the wave function

$$\Psi(\{z_i\}) = [\chi_2(\{z_i\})]^2 \prod_{i<j}(z_i - z_j) e^{-\frac{1}{4}\sum_i |z_i|^2}, \tag{5.3}$$

where $\chi_2(\{z_i\})$ is the fermion wave function of two filled Landau levels. We provide a more detailed description of the edge theory of this state in appendix 5.A.

Other topological orders at $\nu = \frac{1}{2}$ have more complicated internal structures and are unlikely to appear. For convenience, we will use $K = 8$, 331, Pfaffian, anti-Pfaffian, and $U(1) \times SU_2(2)$ to denote the above five topological orders respectively.

The $K = 8$ and the 331 states are abelian FQH states, whose quasiparticles all have abelian statistics. The bulk low energy effective theories for the two FQH state are given by $U(1)$ Chern-Simons (CS) theory, Eq. (5.1). The edge excitations of the $K = 8$ state are described by a single density mode (or more precisely, a $U(1)_R$ Kac-Moody (KM) algebra,

where the subscript R indicates that the excitations are right moving). The number of low energy edge excitations for the $K = 8$ state is the same as one filled Landau level, as measured by the low temperature specific heat. Thus we say that the $K = 8$ state has one branch of edge excitations. The edge excitations of the 331 state are described by two density modes (which form a $U(1)_R \times U(1)_R$ KM algebra). Using the similar definition in terms of specific heat, the 331 state has two branches of edge excitations.

The Pfaffian, anti-Pfaffian, and $U(1) \times SU_2(2)$ states are non-abelian states. Some of their quasiparticles have non-abelian statistics. The edge excitations of the Pfaffian state are described by a density mode (the $U(1)_R$ KM algebra) and a free chiral Majorana fermion (the $Ising_R$ conformal field theory), or in other word, by a $U(1)_R \times Ising_R$ conformal field theory (CFT). Such an edge state has one and a half branches of right-moving edge excitations as measured by specific heat. The edge excitations of the anti-Pfaffian state are described by $U(1)_R \times U(1)_L \times Ising_L$ CFT. The edge excitations for the anti-Pfaffian state have one and a half branches of left-moving edge excitations and one branch of right-moving edge excitations. For the $U(1) \times SU_2(2)$ state, the bulk effective theory is a $U(1) \times SU_2(2)$ CS theory and the edge excitations are described by $U(1)_R \times SU_2(2)_R$ KM algebra. The edge state has two and a half branches of right-moving excitations.

The theory of edge excitations for both abelian and non-abelian FQH states were well developed (Wen, Wu, and Hatsugai, 1994; Wen, 1995, 1999; Lee *et al.*, 2007; Levin *et al.*, 2007). In Table 5.1 we list the relevant results; e^* is the quasiparticles charge and g is the exponent in the corresponding quasiparticle Green's function: $\langle \psi^\dagger_{\rm qp} \psi_{\rm qp} \rangle \sim 1/t^g$. In terms of scaling dimensions Δ the exponent g is twice the scaling dimension of the quasiparticle operator.

The results we find in this paper for the Majorana-gapped edge phases of the anti-Pfaffian and edge-reconstructed Pfaffian states are also included in the table. Note that the anti-Pfaffian edge state and its Majorana-gapped edge state are two edge phases of the same anti-Pfaffian bulk FQH state (and similarly for the Pfaffian edge states). For the Majorana-gapped anti-Pfaffian phase we find that the exponent of the quasiparticle Green's function is non-universal; the exact value of g depends on the interaction. Nevertheless there are two dominant quasiparticles, one with $e^* = 1/4$ and the exponent g in the range $g \in [0.55-0.75]$, and one with $e^* = 1/2$ and $g \in [0.5 - 0.7]$.

5.3 Majorana-gapped phase of the anti-Pfaffian

This section contains the main results for this chapter. We show in detail how to calculate scaling dimensions of quasiparticle operators for the anti-Pfaffian state in the presence of density-density interactions. We identify a charge-transfer operator that can be relevant. This operator is a product of a left-moving Majorana fermion and a right-moving complex fermion. Condensation of this operator gaps the left-moving Majorana mode and half of the right-moving fermionic mode.

In the new phase, dubbed 'Majorana-gapped' phase, several quasiparticle operators have become gapped as well, and we determine the spectrum of ungapped quasiparticles. Next, we find the quasiparticle with the lowest scaling dimension which is expected to dominate tunneling. Finally, we consider the effect of impurities.

5.3.1 Non-universality for non-chiral edges

Fractional quantum Hall states which are described by fully chiral edge theories are called 'universal', because correlation function exponents are independent of the the exact microscopic details of e.g. the interaction between different edge branches.

This situation is no longer the case for FQH state described by an edge theory with branches moving in opposite directions, i.e., a non-chiral edge. In this case the scaling dimensions of operators depend on the exact form of the interaction between the different edge branches, and a more detailed analysis is required to predict the fate of e.g. tunneling exponents.

In some cases (i.e., for some regions in the space of all possible interactions) the result is that the tunneling exponents are indeed non-universal, in other cases the properties of the system are dominated by a certain fixed point for which the tunneling exponents do acquire universal values. In this sense one can construct a phase diagram in 'interaction-space'.

Such an analysis typically focusses on two types of interactions: density-density-interactions, which determine the scaling dimensions of all quasiparticle operators, and charge-transfer operators. Charge-transfer operators move charge between the different edge branches, and as such it is also the mechanism through which different edge branches equilibrate. Charge-transfer operators violate no symmetry and are allowed to appear in the action. If a charge-transfer operator has a relevant scaling dimension, the condensation of this operator can lead to a different phase.

The effect of a charge-transfer operator can be more drastic than to merely adjust values for tunneling exponents, and can cause instabilities (Haldane, 1995). For example in the $\nu = \frac{9}{5}$ state, it was shown (Kao *et al.*, 1999) that condensation of a charge-transfer operator leads to a transition on the edge where a pair of counterpropagating (previously gapless) edge modes becomes gapped; in the resulting $\nu = \frac{9}{5}$ phase the single electron operator by itself is no longer gapless.

5.3.2 K-matrix, action, electron operators, quasi-particles

The edge theory of the anti-Pfaffian is described by one (charge-neutral) Majorana branch λ, and four (charge-carrying) bosonic branches ϕ_i. In our setup three of the bosonic branches are right-moving; the Majorana branch and the fourth bosonic branch are left-moving. We adopt a basis where the left-moving branch appears first, i.e., $(\phi_4, \phi_1, \phi_2, \phi_3)$; in this basis the K-matrix of the bosonic modes is given by

$$K = \mathrm{Diag}(-2, 1, 1, 1). \tag{5.4}$$

The action for this system is

$$S = \frac{1}{4\pi} \int dx d\tau \left[iK_{ij} \partial_x \phi_i \partial_\tau \phi_j + V_{ij} \partial_x \phi_i \partial_x \phi_j + \lambda (v_\lambda \partial_x - \partial_\tau) \lambda \right]. \tag{5.5}$$

The generic quasiparticle operator has a form of a bosonic vertex operator $e^{i\vec{l}\cdot\vec{\phi}}$ times a Majorana operator. Majorana (CFT primary field) operators are the identity operator $\mathbb{1}_\lambda$, the Majorana fermion operator λ and the spin operator σ_λ. The charge and the bosonic

Table 5.2: Allowed quasiparticles in the $\nu = \frac{5}{2}$ anti-Pfaffian are labelled by four integers m_j and a Majorana sector ($\mathbb{1}_\lambda$, λ, or σ_λ). The corresponding vertex operators are $e^{i(m_1\phi_1+m_2\phi_2+m_3\phi_3)}$ for the three right-moving branches and the left-moving branch ϕ_4 is explicitly listed in the table. The quasiparticle charge q is also given.

λ-sector	ϕ_4	q
$\mathbb{1}_\lambda$	$e^{im_4\phi_4}$	$m_1+m_2+m_3-\frac{m_4}{2}$
λ	$e^{im_4\phi_4}$	$m_1+m_2+m_3-\frac{m_4}{2}$
σ_λ	$e^{i(m_4-\frac{1}{2})\phi_4}$	$\frac{1}{4}+m_1+m_2+m_3-\frac{m_4}{2}$

contribution to the (mutual) statistics of such a quasiparticle operator can be determined from the inverse of the K-matrix:

$$\theta = \pi\,\vec{l}\cdot K^{-1}\cdot\vec{l}, \quad q = \vec{t}\cdot K^{-1}\cdot\vec{l}, \quad \theta_{jk} = \pi\,\vec{l}_j\cdot K^{-1}\cdot\vec{l}_k, \tag{5.6}$$

where θ is the statistical phase, q is the charge, $\vec{t} = (1,1,\ldots,1)$ is the so-called charge vector and unit of charge is $e = -|e|$. The Majorana branch is charge-neutral and commutes with the bosonic branches. Its contribution to mutual statistics is[2]

$$\frac{1}{\pi}\theta_{\lambda\lambda} = \pm 1, \qquad \frac{1}{\pi}\theta_{\lambda\sigma} = \pm\frac{1}{2}, \tag{5.7}$$

where we fix the sign to be $+1$ for right-moving branches and -1 for left-moving ones.

The quasiparticle spectrum is obtained by first identifying physical electron operators, which have charge e and fermionic statistics. For the anti-Pfaffian state we are considering here, the physical electron operators are $e_1 = e^{i\phi_1}$, $e_2 = e^{i\phi_2}$, $e_3 = e^{i\phi_3}$, $e_4 = \lambda e^{-2i\phi_4}$, and any combination of these e_i with total charge e.

The remainder of the quasiparticle spectrum is formed by those quasiparticle operators that are local with respect to all these electron operators, i.e., the phase induced by moving a quasiparticle around any electron operators should be a multiple of 2π. The allowed quasiparticles can straightforwardly be found from these rules and are listed for convenience in Table 5.2.

5.3.3 Calculating scaling dimension of quasiparticle operators, boost parameters

For the matrices K and V in the action, Eq. (5.5), there exist a (non-orthogonal) basis $\tilde{\phi}$ such that K is a pseudo-identity and V is diagonal. In such a basis, the scaling dimension Δ of a quasiparticle operator $e^{i\tilde{l}\cdot\tilde{\phi}}$ would be given by $\Delta = \frac{1}{2}\tilde{l}^2$. In general, with K given and fixed, the scaling dimension of quasiparticle operators thus depends on the precise form of the 4-by-4 matrix V in the basis ϕ.

[2]For purposes of finding the quasiparticle spectrum we do not need to consider mutual statistics of two σ operators. Since the σ is a non-abelian anyons, the mutual statistics of two σ operators is of course not just a phase but a matrix; concrete examples for braiding σ operators were given in Ch. 3.

A parametrization of the most generic density-density interaction V requires ten real parameters. With a suitable choice of parameters the scaling dimension depends on only three of these parameters. This goes as follows (Moore and Wen, 1998; Kao *et al.*, 1999).

Let M_1 be the matrix that brings K into pseudo-identity form,

$$\tilde{K} = M_1^T K M_1 = -\mathbb{1}_{N^-} \oplus \mathbb{1}_{N^+}, \tag{5.8}$$

where $N^{\pm}$ is the number of positive/negative eigenvalues of K, in our case $N^- = 1$, $N^+ = 3$. Next we diagonalize V with a matrix $M_2 \in SO(N^-, N^+)$,

$$\tilde{V} = M_2^T M_1^T V M_1 M_2 = \mathrm{Diag}(v_4, v_1, v_2, v_3). \tag{5.9}$$

Note that M_2 leaves $\tilde{K}$ invariant. Furthermore, M_2 can be decomposed in a pure boost B and a pure rotation $R \in SO(N^-) \times SO(N^+)$, $M_2 = BR$.

In our case we use[3]

$$M_1 = \begin{pmatrix} \sqrt{\frac{1}{2}} & 0 & 0 & 0 \\ 0 & 0 & \frac{1}{\sqrt{2}} & -\frac{1}{\sqrt{2}} \\ 0 & \sqrt{\frac{2}{3}} & \frac{1}{\sqrt{6}} & \frac{1}{\sqrt{6}} \\ 0 & \frac{1}{\sqrt{3}} & -\frac{1}{\sqrt{3}} & -\frac{1}{\sqrt{3}} \end{pmatrix}, \tag{5.10}$$

and $B \in SO(1,3)$ is the familiar pure boost from the Lorentz-group,

$$B = \begin{pmatrix} \gamma & \beta_1\gamma & \beta_2\gamma & \beta_3\gamma \\ \beta_1\gamma & \frac{\beta_1^2\gamma^2}{\gamma+1} + 1 & \frac{\beta_1\beta_2\gamma^2}{\gamma+1} & \frac{\beta_1\beta_3\gamma^2}{\gamma+1} \\ \beta_2\gamma & \frac{\beta_1\beta_2\gamma^2}{\gamma+1} & \frac{\beta_2^2\gamma^2}{\gamma+1} + 1 & \frac{\beta_2\beta_3\gamma^2}{\gamma+1} \\ \beta_3\gamma & \frac{\beta_1\beta_3\gamma^2}{\gamma+1} & \frac{\beta_2\beta_3\gamma^2}{\gamma+1} & \frac{\beta_3^2\gamma^2}{\gamma+1} + 1 \end{pmatrix}, \tag{5.11}$$

with $\gamma = 1/\sqrt{1 - (\beta_1^2 + \beta_2^2 + \beta_3^2)}$. An explicit specification of R is not required at this point.

What is important from this decomposition is that the scaling dimension of operator $e^{i\vec{l}\cdot\vec{\phi}} = e^{i\tilde{l}\cdot\tilde{\phi}}$ is now given by $\Delta = \frac{1}{2}\vec{l}\cdot\tilde{\Delta}\cdot\vec{l}$, where

$$\tilde{\Delta} = M_1 B^2 M_1^T. \tag{5.12}$$

In our case, V is parametrized by four (eigenvalues v_j) plus three (rotation $R \in SO(3)$) plus three (boost parameters β_j) equalling a total of ten parameters. But the scaling dimension depends only on the three boost parameters β_j: one parameter for each pair of counterpropagating edge modes. The scaling dimension in the bosonic sector of any quasiparticle operator thus becomes a function of a vector $\vec{\beta} = (\beta_1, \beta_2, \beta_3)$ inside the unit 3D-ball $\beta^2 < 1$ (cf. $|v| < c$).

[3]The extra rotation incorporated in our M_1 is added for later convenience, such that the β_3 axis becomes an axis with higher symmetry.

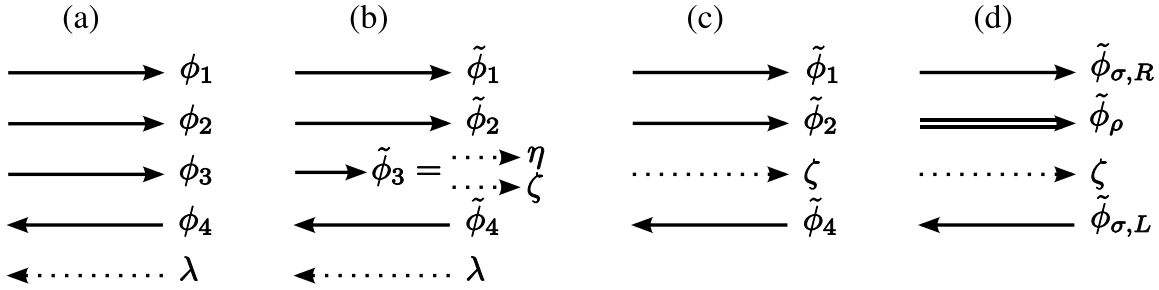

Figure 5-1: Different representations of the gapless branches in the anti-Pfaffian and Majorana-gapped phases. (a) In the basis ϕ the anti-Pfaffian has three right-moving bosonic branches (solid lines) and two left-moving modes, one bosonic and one Majorana mode (dotted line). (b) After a basistransformation to basis $\tilde{\phi}$ the right-moving charge-neutral mode $\tilde{\phi}_3$ can be expressed as two right-moving Majorana modes η and ζ. (c) In the Majorana-gapped phase, the modes λ and η acquire a gap and are dropped. (d) An additional basistransformation explicitly separates the charge mode, $\tilde{\phi}_\rho$ (double solid line), from the neutral modes ($\tilde{\phi}_{\sigma,L/R}$).

There is also a contribution to the scaling dimension from the Majorana sector (see e.g. Di Francesco *et al.*, 1997),

$$\Delta_\lambda = \frac{1}{2}, \qquad \Delta_\sigma = \frac{1}{16}, \tag{5.13}$$

which simply needs to be added to the bosonic scaling dimension of a quasiparticle operator to obtain the total scaling dimension. Here we note that the density-density interactions between the Majorana sector and the boson sectors are always irrelevant and we ignore those interactions in our calculations of scaling dimensions. We will consider other interactions between the Majorana sector and the boson sectors below.

5.3.4 Majorana mode becomes gapped through 'null' charge-transfer operator

Now that we know how to calculate scaling dimensions, we can probe $\vec{\beta}$-space for charge-transfer operators with low scaling dimension. Charge-transfer operators are total charge zero operators, which typically move electrons between the different branches. Since they violate no symmetry or conservation, charge-transfer operators are in principle allowed to appear in the action, Eq. (5.5), and if relevant (in Renormalization Group sense) can cause a transition to another phase.

In $\vec{\beta}$-parameter-space surfaces of constant scaling dimension typically are of ellipsoidal shape, for example

$$\Delta_{+e_2-e_3} = 1 + \frac{2\beta_1^2}{1-\beta^2}, \quad \Delta_{+e_1-e_4} = \frac{2\left(\beta_2 + \frac{\beta_3}{\sqrt{2}} + \sqrt{3}\right)^2}{3\left(1-\beta^2\right)}, \tag{5.14}$$

where $+e_i - e_j$ stands for the combination of an e_i creation and an e_j destruction operator, which transfers charge e between branches i and j.

Regions inside parameter space where charge-transfer operators are relevant ($\Delta < 2$) are thus ellipsoids inside the unit ball $\beta^2 < 1$.

One charge transfer operator we are particularly interested in is $\lambda e^{i(2\phi_4-\phi_1+\phi_2+\phi_3)} \equiv \hat{n}$, that is, the operator which simultaneously destroys e_1 and e_4 and creates e_2 and e_3. Its scaling dimension is

$$\Delta_{-e_1-e_4+e_2+e_3} = 1 + \frac{3\left(\sqrt{\frac{2}{3}} - \beta_3\right)^2}{1-\beta^2}. \tag{5.15}$$

There is a whole *disc* in $\vec{\beta}$-space for which the scaling dimension of $\hat{n}$ is identically 1, namely when $\beta_3 = \sqrt{2/3}$ (with $\beta_1^2 + \beta_2^2 < 1/3$).

On this disc the bosonic part of the operator $\hat{n}$ has the scaling dimensions and statistics of a charge-neutral right-moving complex fermion, which we write as a combination of two Majorana fermions η and ζ, such that $\hat{n} = \lambda(\eta + i\zeta)$. Note that $\hat{n}$ resembles the 'neutral null vector' from the $\nu = \frac{9}{5}$ FQH case, as in it is a zero-charge operator with equal left and right conformal dimensions, $h = \bar{h}$.

We are now approaching the step where the Majorana mode acquires a gap. Clearly this is a key ingredient in our procedure. But the argument of gapping itself is almost trivial: consider a system with two counterpropagating fermions ψ_1 and ψ_2, with dispersion relation $E_{1/2}(k) = \pm vk$, which has gapless excitations at zero energy; adding a coupling $\sum_x \Gamma\psi_1^\dagger(x)\psi_2(x) + \text{H.c.}$ changes the dispersion to $E_\pm(k) = \sqrt{\Gamma^2 + (vk)^2}$ and opens up a gap at zero energy.

Let us assume the interaction V is such that the operator $\hat{n}$ is relevant, and include $\hat{n}$ and its Hermitian conjugate in the action Eq. (5.5) with a *constant* coupling Γ, i.e., we are not considering disorder at this point. Then the effect of this term, $\Gamma(\hat{n} + \hat{n}^\dagger) = 2\Gamma\lambda\eta$, is that the counterpropagating Majorana modes λ and η become gapped whereas ζ is left untouched. *In other words the left-moving Majorana mode and a right-moving bosonic mode disappear and a right-moving Majorana mode emerges.*

Figure 5-2 shows the volume of parameter space in which $\hat{n}$ is a relevant operator. A schematic representation of the branches and different bases before and after Majorana-gapping is given in Fig. 5-1.

Before we continue to determine the quasiparticle spectrum in the Majorana-gapped system we would like to note that the operator $\hat{n}$ is not unique; due to the permutation symmetry between branches ϕ_1, ϕ_2 and ϕ_3 there is a total of three such operators $\hat{n}$.

5.3.5 Quasiparticle spectrum in gapped system

With the gapping of the λ Majorana fermion, some of the quasiparticle operators in the original spectrum, Table 5.2, have likely developed a gap as well and have disappeared from the low-energy spectrum. For the Majorana-gapped phase we would like to find out (i) which quasiparticles have survived the gapping and (ii) which of these survivors have the lowest scaling dimension and are thus expected to dominate e.g. tunneling processes.

To obtain the quasiparticle spectrum we follow the same procedure as for any other χLL FQH edge system: we identify the physical electron operators and determine those quasiparticles which are single-valued with respect to the electron operators. The non-standard part is how to remove the degree of freedom associated with the now-gapped λ

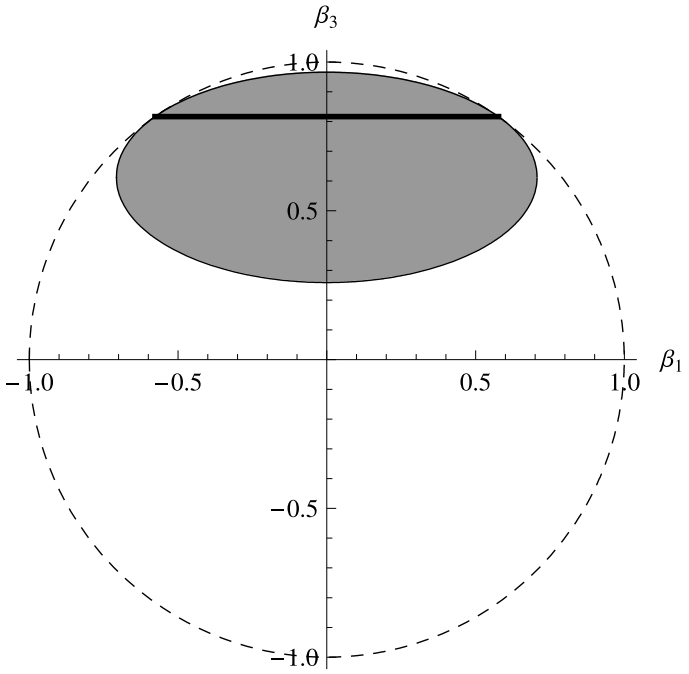

Figure 5-2: Shown is the cross-section, at $\beta_2 = 0$, of the parameter space unit ball $|\vec{\beta}|^2 < 1$. The scaling dimension of the 'null' operator $\hat{n}$, the charge-transfer operator which induces the transition to the Majorana-gapped phase, is identically one at the disc $\beta_3 = \sqrt{2/3} \approx 0.82$ (indicated by thick black line). This null operator $\hat{n}$ is relevant in a substantial volume of $\vec{\beta}$ parameter space; the grey area indicates the ellipsoidal volume where $\hat{n}$ had scaling dimension $\Delta \leq 3/2$, i.e., the region where $\hat{n}$ is relevant even in the presence of disorder.

Majorana fermion and insert the now-emerged ζ Majorana fermion.

Setting $\beta_3 = \sqrt{2/3}$, the following steps will find the quasiparticle spectrum for arbitrary β_1 and β_2 ($\beta_1^2 + \beta_2^2 < 1/3$). To illustrate the procedure we will use the example where $\beta_1 = 0 = \beta_2$, for which the intermediate basis-dependent values are relatively simple.

We transform the basis from ϕ to $\tilde{\phi}$ such that $\tilde{K}$ is the pseudo-identity, $\tilde{V}$ is diagonal, and $\hat{n} = \lambda e^{+i\tilde{\phi}_3}$, which is achieved by M_1 and B, Eqs. (5.10) and (5.11), and $R = \mathrm{Diag}(1, 1, -1, -1)$. As far as the electron operators go, e_4 contains a λ operator and hence becomes gapped, so we drop e_4 from the spectrum. The three remaining physical electron operators have the following form in the basis $\tilde{\phi}$,

$$e_1 = e^{i(+\frac{\sqrt{2}}{\sqrt{3}}\tilde{\phi}_4 + \frac{\sqrt{2}}{\sqrt{3}}\tilde{\phi}_2 - \tilde{\phi}_3)}, \tag{5.16}$$

$$e_2 = e^{i(-\frac{\sqrt{2}}{\sqrt{3}}\tilde{\phi}_4 + \frac{1}{\sqrt{2}}\tilde{\phi}_1 - \frac{1}{\sqrt{6}}\tilde{\phi}_2 + \tilde{\phi}_3)}, \tag{5.17}$$

$$e_3 = e^{i(-\frac{\sqrt{2}}{\sqrt{3}}\tilde{\phi}_4 - \frac{1}{\sqrt{2}}\tilde{\phi}_1 - \frac{1}{\sqrt{6}}\tilde{\phi}_2 + \tilde{\phi}_3)}. \tag{5.18}$$

For the operator $e^{+i\tilde{\phi}_3} = \eta + i\zeta$ we expect that gapping will get rid of the η-part and effectively leave a Majorana operator ζ times some overall phase: $e^{i\tilde{\phi}_3} \to \zeta$. Note that this includes all three electron operators for which we thus make the identification

$$e_1 \simeq \zeta\, e^{i(+\frac{\sqrt{2}}{\sqrt{3}}\tilde{\phi}_4 + \frac{\sqrt{2}}{\sqrt{3}}\tilde{\phi}_2)}, \tag{5.19}$$

$$e_2 \simeq \zeta\, e^{i(-\frac{\sqrt{2}}{\sqrt{3}}\tilde{\phi}_4 + \frac{1}{\sqrt{2}}\tilde{\phi}_1 - \frac{1}{\sqrt{6}}\tilde{\phi}_2)}, \tag{5.20}$$

$$e_3 \simeq \zeta\, e^{i(-\frac{\sqrt{2}}{\sqrt{3}}\tilde{\phi}_4 - \frac{1}{\sqrt{2}}\tilde{\phi}_1 - \frac{1}{\sqrt{6}}\tilde{\phi}_2)}. \tag{5.21}$$

Next, we look for quasiparticles which are single-valued with respect to these three electron operators, with the generic form $e^{i(\tilde{l}_4\tilde{\phi}_4 + \tilde{l}_1\tilde{\phi}_1 + \tilde{l}_2\tilde{\phi}_2)}$ times a ζ-sector Majorana operator $\mathbb{1}_\zeta$, ζ, or σ_ζ.

Solving for allowed $\tilde{l}_4$, $\tilde{l}_1$ and $\tilde{l}_2$ now is a computationally trivial task of solving a set of three linear equations given by the mutual statistics equations, Eqs. (5.6) and (5.7). The resulting expressions for the $\tilde{l}_j$ will involve various square roots, which tend to become more ugly for generic values for β_1 and β_2. However, the mutual statistics equations are basis-invariant, and hence can be solved in any basis. As it turns out, these equations become really simple in the original ϕ basis.

Making the identifications $\zeta \simeq e^{+i\tilde{\phi}_3}$ and $\sigma_\zeta \simeq e^{+i\frac{1}{2}\tilde{\phi}_3}$ we can transform back to the original basis ϕ. In this basis, the generic quasiparticle operator has the form $e^{i(l_4\phi_4 + l_1\phi_1 + l_2\phi_2 + l_3\phi_3)}$. Single-valuedness with the three electron operators forces l_1, l_2, and l_3 to be integers m_j; l_4 is determined by the constraint

$$-l_4 - l_1 + l_2 + l_3 = \begin{cases} 0 & \text{for } \mathbb{1}_\zeta\text{-sector}, \\ 1 & \text{for } \zeta\text{-sector}, \\ \frac{1}{2} & \text{for } \sigma_\zeta\text{-sector}, \end{cases} \tag{5.22}$$

which will assure the appropriate coefficient of $\tilde{\phi}_3$ for each Majorana sector in the $\tilde{\phi}$ basis.

So the result is that the quasiparticle spectrum in the Majorana-gapped phase can be

Table 5.3: Quasiparticle spectrum in the Majorana-gapped phase. Quasiparticles are identified by three integers m_1, m_2, m_3 and a ζ-Majorana sector. The corresponding vertex operator are easiest expressed in the *ungapped* basis ϕ, where the ϕ_1, ϕ_2 and ϕ_3 contributions are still $e^{i(m_1\phi_1+m_2\phi_2+m_3\phi_3)}$. The three m_j and the Majorana sector fix the coefficient of ϕ_4, as shown in the table. The quasiparticle charge q is listed, as well as a correction to the scaling dimension, $\Delta_{\rm cor}$, as explained in the text.

ζ-sector	ϕ_4	q	$\Delta_{\rm cor}$
$\mathbb{1}_\zeta$	$e^{i(-m_1+m_2+m_3)\phi_4}$	$\frac{3}{2}m_1+\frac{1}{2}m_2+\frac{1}{2}m_3$	0
ζ	$e^{i(-m_1+m_2+m_3-1)\phi_4}$	$\frac{1}{2}+\frac{3}{2}m_1+\frac{1}{2}m_2+\frac{1}{2}m_3$	0
σ_ζ	$e^{i(-m_1+m_2+m_3-\frac{1}{2})\phi_4}$	$\frac{1}{4}+\frac{3}{2}m_1+\frac{1}{2}m_2+\frac{1}{2}m_3$	$-\frac{1}{16}$

labelled by three integers m_1, m_2 and m_3, and a Majorana ζ-sector, as shown in Table 5.3. Note that these expressions are *independent* of β_1 and β_2. The charge is given by $q = l_1+l_2+l_3-\frac{1}{2}l_4$.

Even the scaling dimension can be calculated in the ϕ basis for all β_1 and β_2, however, in the σ_ζ sector the calculation $\frac{1}{2}\tilde{l}_3^2$ would assign a scaling dimension of $\frac{1}{8}$ to the σ-operator; we know this should be $\frac{1}{16}$ for a Majorana σ operator, and so scaling dimension calculations need to be corrected for this. This stems from the identification $\sigma_\zeta \simeq e^{+i\frac{1}{2}\tilde{\phi}_3}$, which gives the correct statistics and is valid for the purpose of enumerating the quasiparticle spectrum, but may not be true as operator equality.

5.3.6 Dominant quasiparticles in gapped system, charge separation

Having determined the quasiparticle spectrum, we now look for the most dominant quasiparticles.

As far as (non-)universality goes, the gapping of the pair of Majorana modes has removed one pair of counterpropagating bosonic modes from the system, and with it one boost-parameter. Two counterpropagating pairs remain with corresponding boost parameters β_1 and β_2.

And so in principle we now have to repeat our procedure of looking for dominant charge-transfer operators on the disc $\beta_1^2+\beta_2^2<1/3$. However, so far we have considered the most general density-density interaction V. We expect the interaction to show traces of the underlying Coulomb interaction; especially, we expect that there will be a single charge mode which will separate itself from the other (neutral) modes.

Here we will consider the limit where the charged mode is completely separated from the neutral modes. This decouples one of the right-moving bosonic modes from the left-moving one and eliminates one boost parameter. The condition for charge-separation is $\beta_2 = (\sqrt{2}\beta_3-\sqrt{3})/4 = -1/(4\sqrt{3})$. The one remaining boost parameter is β_1, with $|\beta_1| < \sqrt{5}/4 = \sqrt{1-\beta_2^2-\beta_3^2}$.

So we continue our analysis of scaling dimensions of operators on the line β_1. A plot of scaling dimensions for several quasiparticle operators is given in Fig 5-3. See also appendix 5.B for some more details. Upon closer inspection though, there is some regularity

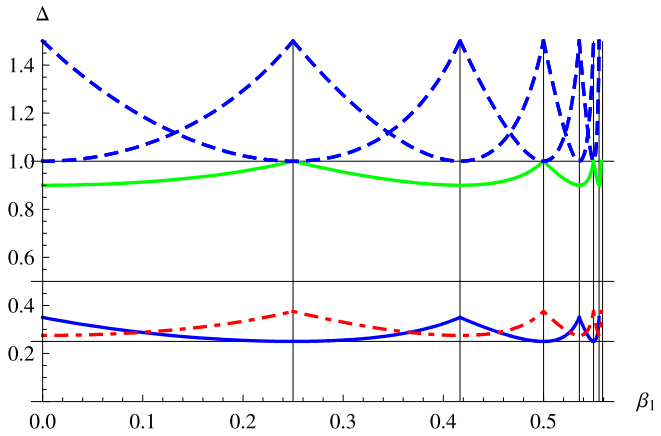

Figure 5-3: The scaling dimension of several important quasiparticles in the Majorana-gapped phase as function of boost parameter β_1. Plotted are charge-transfer operators with scaling dimension $\Delta < 3/2$ (dashed blue lines), electron operator with lowest scaling dimension (solid green line), and two operators with lowest scaling dimension of all operators: a charge $q = 1/4$ quasiparticle (dashed-dotted red line) and a charge $q = 1/2$ quasiparticle (solid blue line). Notice that there is a pattern which repeats itself for $\beta_1 > 0.25$, turning into a series with shrinking width as β_1 approaches its maximum allowed value $\beta_1 = \sqrt{5}/4 \approx 0.56$. Note that there are many quasiparticle operators with scaling dimensions smaller than 1.5 that we did not include on this graph.

in the spectrum. For instance, charge-transfer operators can have a minimal scaling dimension of one, which is obtained for $\beta_1 = 0, \pm\frac{1}{4}, \pm\frac{5}{12}, \pm\frac{1}{2}, \pm\frac{15}{28}, \ldots$ which appears to form an on-going series, and in between such points the same 'spectrum' of scaling dimensions is repeated.

So it seems we only need to consider the interval $0 \leq \beta_1 \leq 1/4$. At $\beta_1 = 0$ the most dominant quasiparticle operator is a charge $q = 1/4$ σ_ζ-sector operator, with scaling dimension $\Delta = 0.275$. Upon increasing β_1 the scaling dimension increases monotonically to a value of $\Delta = 0.375$ at $\beta_1 = 1/4$. At $\beta_1 = 1/4$ the quasiparticle operator with the lowest scaling dimension is a charge $q = 1/2$ $\mathbb{1}_\zeta$-sector operator with $\Delta = 0.25$. Its scaling dimension increases monotonically in the opposite direction, reaching a maximum at $\beta_1 = 0$ of $\Delta = 0.35$.

It is tempting to suggest that the charge-transfer operator with the smallest scaling dimension will dominate and fix the system to be either at the $\beta_1 = 0$ or at the $\beta_1 = 1/4$ point. However, since both charge-transfer operators have scaling dimension between 1 and 3/2 on the interval, they are both relevant, and it depends on the strength of the coefficient if one dominates over the other. Similarly, in our analysis we cannot single out a most dominant quasiparticle, it is simply too close to call. In that sense we find the Majorana-gapped charge-separated phase to be non-universal: there are two dominant quasiparticles, with charges of 1/4 and 1/2 and scaling dimensions ranging between 0.25 and 0.375.

5.3.7 Only strong interaction leads to Majorana-gapped phase

Having identified the Majorana-gapped phase, we can ask what kind of interaction will lead to such a phase. In the Majorana-gapped charge-separated phase the interaction is characterized by 5 remaining parameters: if we pick $\tilde{\phi}_2$ as the charged mode these are the three $\tilde{V}$ eigenvalues v_4, v_1 and v_3, an angle α for rotations between branches $\tilde{\phi}_1$ and $\tilde{\phi}_3$, and the boost parameters β_1.

A crucial ingredient for the Majorana-gapped phase is to include the two filled (lowest) Landau level modes. If these two modes are spatially well-separated on the edge from the inner two modes one would expect the interactions to be small between these blocks of edge branches. We find that the interaction required for the Majorana-gapped phase is such that this kind of separation of two modes is not possible: all right-moving branches have to interact with the left-moving branch with similar strength.

5.3.8 Disorder: localization instead of gapping

The assumption we made so far was that the charge-transfer coupling strength Γ was uniform along the edge. A more realistic assumption would be to consider $\Gamma = \Gamma(x)$ to be fluctuating with position due to random disorder. Also, with disorder we do not need to worry about momentum mismatch between different edge modes.

With disorder present, we expect instead of the gapping of the pair of left and right moving Majorana modes, λ and η, that they will become localized. Here we will assume that the localized modes do not contribute to the tunneling between edges. In particular, they do not affect the value of exponent g. So as long as the calculation of g is concerned, we treat the localized modes as if the are gapped. Thus the above calculation of g also applies to the disordered edge with localization.

5.4 Majorana-gapped phase of the edge-reconstructed Pfaffian state

We now apply the same mechanism of Majorana gapping on a different state: the edge-reconstructed Pfaffian state. By itself the Pfaffian (Moore and Read, 1991) state is fully chiral and gapping of pairs of counterpropagating modes cannot occur. However, the edge might be unstable towards edge reconstruction (Chamon and Wen, 1994). Edge reconstruction effectively adds pairs of counterpropagating charged bosonic modes to the edge. Here we will analyze the state in which edge reconstruction has introduced one such pair of edge modes to the Pfaffian state.

In the edge-reconstructed Pfaffian there are three bosonic modes ϕ_1, ϕ_2 and ϕ_3, and one neutral Majorana mode λ. The left-moving branch is ϕ_1, the other branches are right-moving. The K-matrix is $K = \mathrm{Diag}(-1, 1, 2)$. Electron operators are $e_1 = e^{i\phi_1}$, $e_2 = e^{i\phi_2}$ and $e_3 = \lambda e^{-2i\phi_3}$.

The 'null' operator $\lambda e^{i(2\phi_1+\phi_2+2\phi_3)}$ is a charge-transfer operator with equal left and right conformal dimensions $h = \bar{h} = \frac{1}{2}$. Introducing boost parameters $\vec{\beta} = (\beta_1, \beta_2)$, similar to Eq. (5.11), we can parametrize scaling dimensions of quasiparticle operators. The scaling dimension of $\lambda e^{i(2\phi_1+\phi_2+2\phi_3)}$ becomes one at the point $\beta_1 = -1/2$, $\beta_2 = -1/\sqrt{2}$.

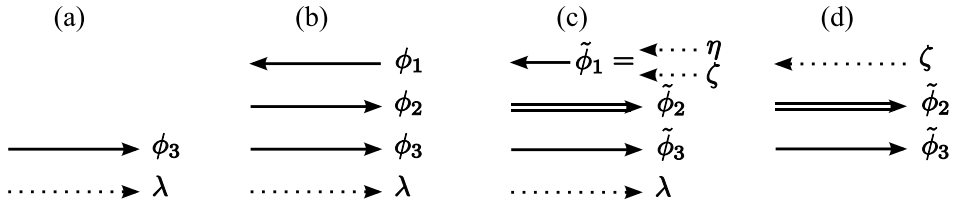

Figure 5-4: Schematic representation of the bases in the various steps of the Majorana gapping of the edge reconstructed Pfaffian; (a) is the Pfaffian state without edge reconstruction, with a right-moving bosonic branch and a right-moving Majorana branch. In (b), edge reconstruction has introduced an additional pair of left- and right-moving bosonic mode. After a basistransformation from ϕ to $\tilde{\phi}$, in (c), branch $\tilde{\phi}_1$ can be written as a combination of two left-moving Majorana branches ζ and η, and $\tilde{\phi}_2$ is the charge mode. Finally, after the Majorana-gapping two of the Majorana modes, λ and η have disappeared, leaving as left-moving mode only a Majorana mode ζ.

We perform a basistransformation from ϕ to $\tilde{\phi}$; in this basis $\tilde{K} = \mathrm{Diag}(-1,1,1)$, $\lambda e^{i(2\phi_1+\phi_2+2\phi_3)} = \lambda e^{i\tilde{\phi}_1}$, and the $\tilde{\phi}_2$ branch carries all the charge. If the null operator is relevant it will gap the right-moving Majorana mode λ and half of the left-moving bosonic mode $\tilde{\phi}_1$ leaving a left-moving Majorana mode ζ, as illustrated in Fig. 5-4.

In the Majorana-gapped phase, the gapless physical electron operators are $e_1 = \zeta e^{i(\sqrt{2}\tilde{\phi}_2)}$ and $e_2 = e^{i(\sqrt{2}\tilde{\phi}_2+\tilde{\phi}_3)}$; e_3 acquires a gap. The quasiparticle spectrum can be labeled by two integers m_1 and m_2 and a ζ Majorana sector, as follows, with charge and scaling dimension included:

$$\mathbb{1}_\zeta\text{-sector}: \quad e^{i\frac{m_1}{\sqrt{2}}\tilde{\phi}_2+(m_2-m_1)\tilde{\phi}_3}, \quad q=\tfrac{m_1}{2}, \Delta = \tfrac{m_1^2}{4}+\tfrac{(m_2-m_1)^2}{2}, \tag{5.23}$$

$$\zeta\text{-sector}: \quad \zeta\, e^{i\frac{m_1}{\sqrt{2}}\tilde{\phi}_2+(m_2-m_1)\tilde{\phi}_3}, \quad q=\tfrac{m_1}{2}, \Delta = \tfrac{m_1^2}{4}+\tfrac{(m_2-m_1)^2}{2}+\tfrac{1}{2}, \tag{5.24}$$

$$\sigma_\zeta\text{-sector}: \quad \sigma_\zeta\, e^{i\frac{m_1+\frac{1}{2}}{\sqrt{2}}\tilde{\phi}_2+(m_2-m_1-\frac{1}{2})\tilde{\phi}_3}, \quad q=\tfrac{m_1+\frac{1}{2}}{2}, \Delta = \tfrac{(m_1+\frac{1}{2})^2}{4}+\tfrac{(m_2-m_1-\frac{1}{2})^2}{2}. \tag{5.25}$$

Note that here the Majorana-gapping effectively removes all pairs of counterpropagating bosonic modes that existed before. Hence the scaling dimensions of all operators becomes fixed. In other words, there is no remaining boost parameter degree of freedom.

In the Majorana-gapped edge-reconstructed there are *three* operators with smallest scaling dimension $\Delta = \frac{1}{4}$: one charge $q = 1/2$ operator ($m_1 = m_2 = 1$ in $\mathbb{1}_\zeta$-sector), and two charge $q = 1/4$ operators ($m_1 = 0$, $m_2 = 0, 1$ in the σ_ζ-sector). The electron operator with smallest scaling dimensions has $\Delta = \frac{3}{2}$.

5.5 Summary and Discussion

5.5.1 Tunneling through bulk in new edge phase

To detect the phase transition to the Majorana-gapped phase on the edge of the anti-Pfaffian state one would have to observe a change in quasiparticle tunneling exponent g. This presents a dilemma: even though g itself is an intrinsic property of the edge, a measurement

of g requires the quasiparticle to tunnel through the bulk. But in the bulk the phase transition does not occur, so is it even possible for the quasiparticle to tunnel? We assume that edge quasiparticles in the Majorana-gapped phase can indeed tunnel through the bulk and we do not run into obvious inconsistencies (of e.g. having a quasiparticle charge on the edge which does not exist in the bulk). Whether or not this assumption is fully justified is not yet understood.

5.5.2 Charge transfer in the bulk

We would like to note that that operator $\lambda e^{i(2\phi_4-\phi_1+\phi_2+\phi_3)}$ not only appears in the edge effective Hamiltonian, the corresponding operator also appears in the 2D bulk effective Hamiltonian for the 2D anti-Pfaffian state. Such a bulk operator transfers charges between different condensates (note that the anti-Pfaffian state is formed by several condensates: the spin-down electrons in the first Landau level, the spin-up electrons in the first Landau level, the spin-up electrons in the second Landau level, etc). With such an operator present in the bulk Hamiltonian,[4] one naturally expects that the 2D anti-Pfaffian state has $1_L + (5/2)_R$ branches of the edge excitations. The $(3/2)_L + 3_R$ branches of the edge excitations proposed in Lee *et al.* (2007); Levin *et al.* (2007) can be viewed as a result of edge reconstruction of the $1_L + (5/2)_R$ edge (Chamon and Wen, 1994).

5.5.3 Effects of spin conservation

So far we have ignored the effect of spin conservation. In the presence of magnetic field, the z-component of spin S_z is still conserved. By examining the spin quantum number of the charge transfer operator $\lambda e^{i(2\phi_4-\phi_1+\phi_2+\phi_3)}$ in the anti-Pfaffian state, we find that it carries $S_z = 1$. Therefore, the S_z conservation prevents $\lambda e^{i(2\phi_4-\phi_1+\phi_2+\phi_3)}$ from appearing in the edge Hamiltonian. In this case the Majorana-gapped phase for the anti-Pfaffian state cannot appear. Thus to have the Majorana-gapped phase for the anti-Pfaffian state we either need to break the S_z conservation, or to consider the $\nu = \frac{9}{2}$ anti-Pfaffian state where there exists a charge transfer operator which carries $S_z = 0$.

The charge transfer operator for the edge reconstructed Pfaffian state has $S_z = 0$. Thus the S_z conservation will not prevent the appearance of the Majorana-gapped phase. The Majorana-gapped phase is more likely to appear for edge reconstructed Pfaffian state.

5.5.4 Determining the true nature of the $\nu = \frac{5}{2}$ state

Glancing at Table 5.1 we have to conclude that the quest to determine the nature of the observed $\nu = \frac{5}{2}$ FQH state is far from over. The first experimental results (Dolev *et al.*, 2008; Radu *et al.*, 2008) suggest that likely $e^* = e/4$ and $g = 0.5$. If these are confirmed to be the correct values we can scratch a few candidates off the list; but we would not be able to distinguish between the anti-Pfaffian, $U(1) \times SU_2(2)$ and Majorana-gapped edge-reconstructed Pfaffian states. Electron tunneling is expected to be the same for these three states as well.

[4] Deep inside the bulk there is a large energy gap between different Landau levels, i.e., the cyclotron energy $\hbar\omega_c$. If a charge-transfer operator acts between different Landau levels its effect will be suppressed except where the Landau level splitting is small: at the edge.

Additional measurements which would probe the number of left- and right-moving edge branches would be required to settle this issue. For instance a thermal Hall conductance (Kane and Fisher, 1997) measurement distinguishes between the three states with $e^* = e/4$ and $g = 0.5$.

As far as the presence of non-abelian statistics goes the prospect is somewhat brighter, as five out of the seven candidate states are non-abelian. Furthermore the non-abelian statistics is carried by similar Ising spin fields in all these cases, hence experimental setups based on interference should give qualitatively similar results (i.e., the even-odd effect)

5.5.5 Conclusions

In this chapter we have studied the effect of a charge transfer process described by neutral bosonic operators in the $\nu = \frac{5}{2}$ anti-Pfaffian state and edge reconstructed Pfaffian state. On the edge, such operators have a form $\lambda e^{i(2\phi_4-\phi_1+\phi_2+\phi_3)}$ or $\lambda e^{i(2\phi_1+\phi_2+2\phi_3)}$. Such operators transfer charges between edge branches and create/annihilate a Majorana fermion λ. The operator respects all the symmetries and is local with respect to all the electron operators. Thus such an operator is allowed in the effective edge Hamiltonian. We find that, for a certain range of interactions between the edge branches, the operators $\lambda e^{i(2\phi_4-\phi_1+\phi_2+\phi_3)}$ or $\lambda e^{i(2\phi_1+\phi_2+2\phi_3)}$ represent relevant perturbations. The effect of such a relevant perturbation opens up a gap for a pair of left and right moving Majorana fermion modes.

For the anti-Pfaffian state, before the 1D gapping transition at the edge, the state has 3/2 branches of left-movers and 3 branches of right-movers. After the gapping transition, the same 2D anti-Pfaffian state has 1 branch of left-movers and 2 and 1/2 branches of right-movers. For the edge reconstructed Pfaffian state, before the 1D gapping transition at the edge, the state has 1 branches of left-movers and 2 and 1/2 branches of right-movers. After the gapping transition, the same state has 1/2 branch of left-movers and 2 branches of right-movers.

The phase transition changes the scaling dimension of quasiparticle operators on the edge, which can in principle be observed in experiment. For FQH edge states with counterpropagating edge modes it was known that interactions between the edge branches have to be taken into account to determine the phase of the edge. It was previously shown that under certain conditions a full left- and right-moving branch could pair up and open up a gap (Kao *et al.*, 1999). Here, we showed that half a left- and right-moving branch can pair and become gapped.

This formalism might be generalized further. We see that on the edge of FQH states under certain conditions pairs of counterpropagating modes can appear (edge reconstruction) or disappear (like the Majorana-gapped phase). Under the current formalism these two processes are treated separately, but it is suggestive to look for a formalism that treats these two on equal footing under a unified theory of phase transitions on the edge.

Gapping of modes requires strong interaction between different modes, and edge reconstruction requires a smooth confining potential to create distance between edge branches. These two statements seem to carry the same message, but right now we cannot quantitatively equate the two statement. Another concrete question we cannot answer at this point is whether the charged mode, which presumably separates from the other modes, will be located on the inner or the outer side of the edge.

A perhaps less ambitious and more concrete question one may ask at this point is whether the quasiparticle spectrum that we found in Sec. 5.3.5 can be confirmed via a more direct calculation. In our work, the existence of e.g. a quasiparticle σ_ζ in the Majorana-gapped phase was postulated; presumably this quasiparticle operator is directly related to the quasiparticle operator σ_λ in the ungapped phase; after all, where else could σ_ζ come from? The σ_λ-σ_λ correlation function might very well turn into a σ_ζ-σ_ζ correlation function when the charge-transfer operator is relevant. This is something that could potentially be shown rigorously through a direct calculation of the correlation functions.

5.A Appendix: The $U(1) \times SU_2(2)$ edge state

The edge excitations of the $U(1) \times SU_2(2)$ state is described by a charge density mode $\rho(x)$, an S^z density mode $\tilde{\rho}(x)$, plus a Majorana fermion $\lambda(x)$:

$$\begin{aligned}
[\rho_k, \rho_{k'}] &= \frac{\nu}{2\pi} k \delta_{k+k'}, \qquad \nu = \frac{1}{2} \\
[\tilde{\rho}_k, \tilde{\rho}_{k'}] &= \frac{1}{2\pi} k \delta_{k+k'}, \\
\{\lambda_k, \lambda_{k'}\} &= \delta_{k+k'}, \qquad \lambda_k^\dagger = \lambda_{-k} \\
H &= 2\pi \sum_{k>0} [V \rho_{-k} \rho_k + \tilde{V} \tilde{\rho}_{-k} \tilde{\rho}_k)] + \sum_{k>0} V_\lambda k \lambda_{-k} \lambda_k
\end{aligned} \tag{5.26}$$

There are three electron operators given by

$$\begin{aligned}
\Psi_{e,3}(x) &= \lambda(x) e^{2i\phi(x)} \\
\Psi_{e,1}(x) \pm i\Psi_{e,2}(x) &= e^{\pm i\tilde{\phi}(x)} e^{2i\phi(x)}
\end{aligned}$$

The $e/4$ quasiparticle operators are given by

$$\begin{aligned}
\psi_{q,1} &= \sigma(x) e^{i\frac{1}{2}\tilde{\phi}(x)} e^{i\frac{1}{2}\phi(x)} \\
\psi_{q,2} &= \sigma(x) e^{-i\frac{1}{2}\tilde{\phi}(x)} e^{i\frac{1}{2}\phi(x)}
\end{aligned}$$

We find that

$$\langle \psi^\dagger(x,t) \psi(x',t') \rangle \sim (z - z')^{-g}$$

with

$$g = \frac{1}{8} + \frac{1}{4} + \frac{1}{8} = \frac{1}{2}.$$

5.B Appendix: Symmetries for scaling dimensions

In section 5.3.6, after the Majorana gapping for the case of the anti-Pfaffian we look to determine the dominant quasiparticles in the spectrum of quasiparticles that remain. The scaling dimension of these quasiparticle operators is a function of β_1 and β_2 on a disc-region

$\beta_1^2 + \beta_2^2 < 1/3$. One might guess that the scaling dimension of quasiparticle operators has some symmetry on this disc, and the obvious choice would be circular symmetry in which the scaling dimensions is a function of the radial coordinate $r \equiv \sqrt{\beta_1^2 + \beta_2^2}$. However, this turns out not to be the case. Instead, there is a $\mathbb{Z}_3$ symmetry of rotations by $2\pi/3$ around the central axis $r = 0$.

The $\mathbb{Z}_3$ symmetry can be traced back to the permutation symmetry among the three right-moving bosonic branches. On the β_1-β_2-plane, the symmetry means that for every quasiparticle with a certain scaling dimension at a given coordinates $(\beta_1, \beta_2) = r(\cos\theta, \sin\theta)$ there is a quasiparticle operator in the spectrum with the same charge and scaling dimension and same radial coordinate r, but with $\theta \to \theta \pm 2\pi/3$.

On the boundary of the β_1-β_2 plane there are three points where the scaling dimension of a charge e quasiparticle operator (*not* a physical electron operator though) tends to zero. That would represent a true instability with interesting physics in it. However, it is unlikely that the interaction is such that the physics of these three points on the disc is realized. First of all, at the boundary the boost parameters approach the 'speed of light' and the strength of the interactions diverges. Furthermore, we do expect charge separation to occur, as discussed in section 5.3.6. This fixes β_2 and limits the region in β-space to a line as function of β_1. We conjecture separation of the charged mode; this was studied in more detail and showed to be true for other FQH systems (Kane, Fisher, and Polchinski, 1994; Wen, 1995; Lee *et al.*, 2007; Levin *et al.*, 2007).

On the β_1 line fixed by Majorana gapping ($\beta_3 = \sqrt{2/3}$) and separation of the charged mode ($\beta_2 = -1/(4\sqrt{3})$), a first inspection of scaling dimensions of quasiparticle operators yields a large amount of operators with relatively small scaling dimension, see Fig. 5-5. One thing that is very clear is that there is no single operator which obviously has the lowest scaling dimension, instead there is a seemingly infinite series of operators with scaling dimension smaller than a half. Upon closer inspection, the whole spectrum repeats itself periodically with β_1, with the period becoming smaller and smaller as β_1 approaches its limiting value. In the main text we highlighted in Fig. 5-3 the important operators from Fig. 5-5.

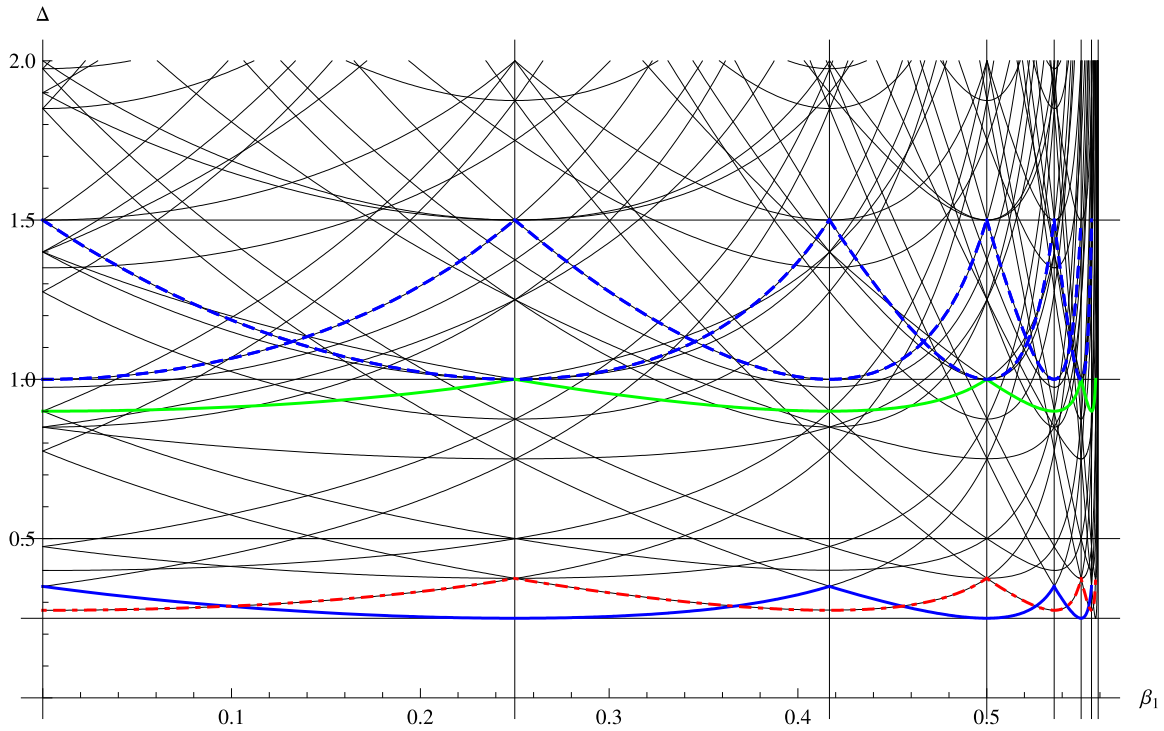

Figure 5-5: Scaling dimensions of a large number of quasiparticle operators, as function of boost parameter β_1; this is essentially the same plot as Fig. 5-3, but with a lot more operators included; colored curves are the same as in Fig. 5-3. Notice how the entire spectrum-pattern repeats itself with β_1, with period becoming smaller and smaller (obviously, only a finite number of curves is drawn in this figure).

Chapter 6

Probing the neutral velocity in the quantum Hall effect with a long point contact

The material in this chapter is primarily based on Overbosch and Chamon (2008).

6.1 Outline

In this chapter we propose a setup through which slow edge velocities in quantum Hall systems can be detected. This is a subject that is not exclusive for non-abelian states, and it could very well turn out to be more useful for abelian states. Nevertheless, the issue of more than one edge velocity is important for the current experimental $\nu = \frac{5}{2}$ setups. If there is a slow edge velocity present, this will lead to thermal decoherence and this puts an upper bound on the size of interferometer setups in which interference can be observed (Bishara and Nayak, 2008). Also, showing the mere existence of more than one edge mode is very interesting by itself, as this has not been observed for *any* quantum Hall state yet.

The problem of tunneling between two infinitely long edges at a *single* site is mathematically well-defined. In chapters 2–4 we show in detail how tunneling current (and its derivative with bias voltage, the tunneling conductance) can be calculated as function of applied bias voltage V and temperature T in linear response theory for all quantum Hall states, both abelian and non-abelian, as long as basic information about the state, such as quasiparticle exponents, is known.

Experimentally, tunneling is induced by attempting to create a constriction in the quantum Hall fluid using a quantum point contact: by applying a voltage on gates the edges of the quantum Hall fluid are squeezed closer together, as introduced in Sec. 1.1. If the distance between the two edges is on the order of a few magnetic lengths, tunneling is expected to occur, if only because the single particle wavefunctions will start to have some small, but non-zero, overlap.

An experimentally measured tunneling conductance might very well not coincide with the theoretical linear response result, for several reasons:

1. the linear response result is valid for weak tunneling only and breaks down for strong

tunneling. Experimentally, a decent amount of tunneling is necessary to be able to observe the tunneling conductance, which might be beyond the regime where linear response is valid. The linear response result might be improved by including higher order terms in perturbation theory; a full numerical solution for arbitrary tunneling strength was calculated for the Laughlin states, in particular $\nu = \frac{1}{3}$ (Fendley *et al.*, 1995), but has not been constructed for e.g. the $\nu = \frac{5}{2}$ state yet.

2. the application of a point contact locally changes the electron density as well. In the neighborhood of the point contact the filling fraction might be different from that in the bulk, whereas the linear response result is based on the assumption that the quantum Hall state is the same everywhere between the edges. The implications of a locally different filling fraction for the conductance were recently studied by Rosenow and Halperin (2008).

3. the constriction created by the point contact cannot be infinitely sharp to define a true single tunneling *point* of measure zero, rather tunneling is expected to occur over a small (but non-zero) range of points. This is the subject of this chapter: we study the effects of tunneling at a point contact of finite size..

We find that coherent tunneling inside a *long* quantum point contact (QPC) gives rise to a resonance in the tunneling current at zero temperature for a bias voltage $V_{\rm res}$ given by

$$\frac{eV_{\rm res}}{\hbar} = \frac{vW}{l_B^2}. \tag{6.1}$$

Here W is the width of the long QPC and v is the slowest edge velocity associated with the tunneling quasiparticle. The resonance becomes sharper for longer length L of the QPC. At finite temperature T the resonance will be reduced and for temperature $2\pi T > e^*V_{\rm res}$ it will be washed out, with e^* the quasiparticle charge. A sharp resonance in the tunneling current will lead to a strong peak followed by a strong dip in the tunneling conductance at non-zero bias. We estimate that slow edge velocities between 25 and 1000 m/s can be observed this way.

The origin for the resonance has a simple explanation. The interference of a tunneling quasiparticle at two locations separated by distance x is guided by two phases: on the one hand there is the Aharonov-Bohm phase $(e^*/e)xW/l_B^2$ that basically multiplies the quasiparticle's charge e^* with the flux enclosed in the area Wx; on the other hand there is the phase $\omega_J t$ that is introduced by an applied bias voltage V, with Josephson frequency $\omega_J = e^*V/\hbar$. For a distance x between two tunneling sites the associated phase is then $\omega_J x/v$ where v is the edge velocity with which the quasiparticle propagates along the edge. The resonance occurs at the stated voltage $V_{\rm res}$ when the two phases become equal and give rise to constructive interference.

If there are multiple edge velocities associated with propagation of the quasiparticle along the edge, there are in principle multiple phases $\omega_J x/v_i$, one for each velocity. We are especially interested in a situation where there are two velocities: one fast velocity associated with the charged mode, and one slow velocity associated with the neutral mode(s). For the charged mode the edge velocity is expected on general grounds to be on the order of the Fermi velocity $\sim 10^5$m/s. With a width $W \sim 10l_B$ and $l_B \sim 10$nm we would

find $V_{\rm res} \sim 0.1$V; the current that would have to be driven through the sample at such a voltage would surely destroy the quantum Hall state (at temperature on the order of of tens of millikelvin). A resonance due to such a fast velocity is thus not likely experimentally accessible. A neutral mode velocity is not bound to the Fermi velocity though, and can in principle be orders of magnitude smaller. It is such a slow neutral mode edge velocity that we propose to detect.

First, we will consider the zero temperature limit of a very long quantum point contact in section 6.2, taking the continuum limit of a system of many tunneling sites. Next, in section 6.3, we consider the situation at finite temperature and at finite lengths. We provide plots for the expected behavior of the $\nu = \frac{5}{2}$ Pfaffian and anti-Pfaffian cases, and the $\nu = \frac{2}{3}$ state. In section 6.4 we estimate the range of edge velocities that can be observed through the proposed setup. We conclude in section 6.5.

6.2 Tunneling at a long QPC in linear response at $T = 0$

The tunneling current due to N (discrete) tunneling sites in linear response theory (Chamon *et al.*, 1997) is discussed in detail in chapter 2. We repeat here the main expression for the tunneling current, Eq. (2.7), and explicitly include the edge velocity as well,

$$I_{\rm tun}(\omega_J) = e^* \sum_{i,j=1}^{N} \frac{\Gamma_i \Gamma_j^* + \Gamma_i^* \Gamma_j}{2} \int_{-\infty}^{\infty} dt e^{i\omega_J t} P_g(t + x_{ij}/v) P_g(t - x_{ij}/v) - (\omega_J \leftrightarrow -\omega_J). \tag{6.2}$$

As a reminder, $x_{ij} = x_i - x_j$ and quasiparticle propagator $P_g(t)$ is given by

$$P_g(t) = \begin{cases} \dfrac{1}{(\delta + it)^g} & \text{for } T = 0,\ \delta = 0^+, \\ \dfrac{(\pi T)^g}{(i \sinh \pi T t)^g} & \text{for } T \neq 0. \end{cases} \tag{6.3}$$

We will generalize Eq. (6.2) by making the discrete number of tunneling sites into a continuous distribution, $\Gamma_i \to \gamma(x)$, and to separate contributions from charged and neutral modes, which come with distinct edge velocities $v_{c/n}$ and tunneling exponents $g_{c/n}$,

$$I_{\rm tun}(\omega_J) = e^* \int dx dy\, \gamma(x)\gamma^*(y) \int_{-\infty}^{\infty} dt\, e^{i\omega_J t} P_{g_c}\big(t + \frac{x-y}{v_c}\big) P_{g_c}\big(t - \frac{x-y}{v_c}\big) \times \\ P_{g_n}\big(t + \frac{x-y}{v_n}\big) P_{g_n}\big(t - \frac{x-y}{v_n}\big) - (\omega_J \leftrightarrow -\omega_J). \tag{6.4}$$

See Fig. 6-1 for a sketch of the setup. Since quasiparticles can tunnel back and forth between the two opposite edges it seems unrealistic for a bulk quasiparticle to become trapped inside this area as it would likely instantly get 'sucked' into one of the two edges. Therefore, we will consider no bulk quasiparticles to be present under the QPC, and all interference is due to coherent tunneling between the edges. We do assume that the entire bulk has the same filling fraction, and the edges are the modes associated with that bulk

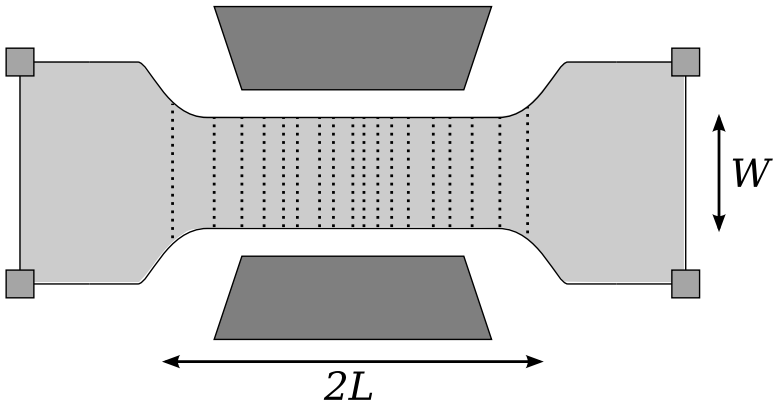

Figure 6-1: Tunneling between two edges in a long quantum point contact does not occur at a single site, but rather over a range of positions x along the edge. The width W is expected to be of the order of a few magnetic lengths, and it is unlikely that any bulk quasiparticles can be statically trapped inside this narrow region.

state.

The form we choose for the tunneling amplitude $\gamma(x)$ explicitly contains the Aharonov-Bohm phase linear in x,

$$\gamma(x) = \frac{\Gamma_0}{\sqrt{\pi}L_0} e^{-\frac{x^2}{L^2}} e^{i\frac{x}{L}\frac{e^*}{e}N_\Phi}, \qquad N_\Phi = \frac{WL}{l_B^2}. \tag{6.5}$$

Here N_Φ is 2π times the number of flux quanta enclosed in the area WL; Γ_0/L_0 is a measure of the tunneling amplitude strength per unit length, which is assumed to be small enough to warrant the weak-tunneling approximation. We included a Gaussian envelope to provide a smooth cut-off scale at length L. The exact form of the cut-off is not important when L is large, and this is the regime we are interested in, because temperature will introduce another, smaller, cut-off length-scale; the Gaussian form simplifies the integration over x and y since

$$\int_{-\infty}^{\infty} dx \int_{-\infty}^{\infty} dy\, \gamma(x)\gamma(y)^* e^{-i(x-y)u} = \frac{|\Gamma_0|^2}{L_0^2} L^2 e^{-\frac{1}{2}[(e^*/e)N_\Phi - Lu]^2}. \tag{6.6}$$

For the case when L is not so large (i.e., $L/l_B \sim 1$), it is not entirely clear how realistic an approximation $\gamma(x)$ in Eq. (6.5) is to an actual experimental x-dependent tunneling amplitude for a FQH system under a point contact. Very likely $\gamma(x)$ depends strongly on the width $W(x)$, the local distance between the opposite edges. As tunneling is concerned, tunneling probabilities typically scale exponentially with distance. However, in terms of wave-function overlap, in the Landau-gauge the overlap of single particle wavefunctions is Gaussian with respect to the distance. Tunneling might also be affected by the local electron density; the assumption is that under the QPC the system is still on the same FQH plateau, but likely closer to the boundary of the plateau than outside the QPC in the 'true' bulk.

The x and y dependence in Eq. (6.2) can be brought in the form of Eq. (6.6) through

the (inverse) Fourier transforms of $P_g(t)$, see Eqs. (2.8)–(2.13) in section 2.1,

$$\tilde{P}_g(\omega) = \int_{-\infty}^{\infty} dt e^{i\omega t} P_g(t), \tag{6.7}$$

$$\tilde{P}_g(\omega) = \begin{cases} \theta(\omega)|\omega|^{g-1}\dfrac{2\pi}{\Gamma(g)} & \text{for } T = 0, \\ (2\pi T)^{g-1} B(\dfrac{g}{2} + i\bar{\omega}, \dfrac{g}{2} - i\bar{\omega}) e^{\pi\bar{\omega}} & \text{for } T \neq 0, \quad \bar{\omega} = \dfrac{\omega}{2\pi T}. \end{cases} \tag{6.8}$$

The tunneling current then becomes

$$I_{\rm tun} = e^*|\Gamma_0|^2 \frac{L^2}{L_0^2} \int \frac{d\omega_1}{2\pi}\frac{d\omega_2}{2\pi}\frac{d\omega_3}{2\pi} d\omega_4 \delta(\omega_J - \omega_1 - \omega_2 - \omega_3 - \omega_4) \tilde{P}_{g_n}(\omega_1)\tilde{P}_{g_n}(\omega_2) \times \\ \tilde{P}_{g_c}(\omega_3)\tilde{P}_{g_c}(\omega_4) e^{-\frac{1}{2}\alpha^2\left[1-\left(\frac{V_1-V_2}{V_{\rm res}} + \frac{V_3-V_4}{V_{\rm res}}\frac{v_n}{v_c}\right)\right]^2} - (\omega_J \leftrightarrow -\omega_J), \tag{6.9}$$

where $\alpha \equiv (e^*/e)N_\Phi$ and $e^*V_j \equiv \omega_j$, and $V_{\rm res}$ is defined with respect to the neutral velocity.

We can simplify this expression a little further by working in the limit $v_c \gg v_n$ to

$$\boxed{\lim_{v_c\to\infty} I_{\rm tun} = e^*|\Gamma_0|^2 \frac{L^2}{L_0^2} \int \frac{d\omega_1}{2\pi}\frac{d\omega_2}{2\pi} \tilde{P}_{g_n}(\omega_1)\tilde{P}_{g_n}(\omega_2)\tilde{P}_{2g_c}(\omega - \omega_1 - \omega_2) e^{-\frac{1}{2}\alpha^2\left[1-\frac{V_1-V_2}{V_{\rm res}}\right]^2}.} \tag{6.10}$$

Note that the power-law form of the quasiparticle propagator leads to a simple convolution product of $\tilde{P}_g(\omega)$,

$$\int_{-\infty}^{\infty} \frac{d\omega}{2\pi} \tilde{P}_{g_1}(\omega)\tilde{P}_{g_2}(\omega_0 - \omega) = \tilde{P}_{g_1+g_2}(\omega_0). \tag{6.11}$$

Let us consider Eq. (6.10) at zero temperature and in the limit of large L. For large L the Gaussian reduces to a delta function that sets $V_{\rm res} = V_1 - V_2$, or in terms of dimensionless variable $Z \equiv V/V_{\rm res}$ it sets $(V_1/V - V_2/V) = 1/Z$. The step functions in $P_g(\omega)$ at $T = 0$ restrict $0 \le V_1/V + V_2/V \le 1$. So in the large L limit we already see the tunneling current is zero for voltages $Z < 1$. For arbitrary Z:

$$I_{\rm tun} \to e^*|\Gamma_0|^2 \frac{(L/l_B)}{(W/l_B)(e^*/e)} \frac{(2\pi)^{3/2}}{\Gamma(g_n)^2\Gamma(2g_c)} \frac{(e^*V_{\rm res})^{2g-1}}{Z} \mathcal{I}[Z; g_n, g_c], \tag{6.12}$$

$$\mathcal{I}[Z; g_n, g_c] \equiv \int_{1/Z}^{\frac{1}{2}(1+1/Z)} ds\, s^{g_n-1} \left(s - \frac{1}{Z}\right)^{g_n-1} \left(1 + \frac{1}{Z} - 2s\right)^{2g_c-1}. \tag{6.13}$$

An analytical expression for $\mathcal{I}[Z; g_n, g_c]$ is given in appendix 6.A. Writing $Z = 1 + \epsilon$ the function $\mathcal{I}[Z; g_n, g_c]$ diverges as $\epsilon^{2g_c+g_n-1}$ when Z approaches one. For large voltages, $Z \gg 1$, the Z dependence is

$$\frac{\mathcal{I}[Z \gg 1; g_n, g_c]}{Z} \sim \begin{cases} Z^{-2g_n} & g_n < \frac{1}{2} \\ \frac{\log Z}{Z} & g_n = \frac{1}{2} \\ \frac{1}{Z} & g_n > \frac{1}{2} \end{cases}. \tag{6.14}$$

Quick summary of the long QPC ($L \gg l_B$) at zero temperature $T = 0$ is that the tunneling current is zero for voltages $V < V_{\rm res}$ with a divergence at $V = V_{\rm res}$ with power $2g_c + g_n - 1$ and a power law decay at $V \gg V_{\rm res}$. Plots for the $\nu = \frac{5}{2}$ Pfaffian, anti-Pfaffian and the $\nu = \frac{2}{3}$ are shown in Fig. 6-3 in the next section.

6.3 Finite temperature

Next two things we will consider is finite length L and non-zero temperature T. We expect that either will smoothen the divergence at $Z = 1$. Note that the ratio $I_{\rm tun}/L$ is independent of the length L in the limit of large L and at zero temperature, and this is a useful quantity to compare different lengths L.

We treat finite length L first. Starting from Eq. (6.10), we substitute the zero temperature quasiparticle correlation functions $\tilde{P}_g$ and find

$$\frac{I_{\rm tun}(T=0, L<\infty)}{L} = \frac{e|\Gamma_0|^2}{(L_0/l_B)^2}(e^*V_{\rm res})^{2g-1}\big(\frac{e^*}{e}\big)\big(\frac{L}{l_B}\big)\frac{2\pi}{\Gamma(g_n)^2\Gamma(2g_c)}Z^{2g-1}\times \int\limits_{0\le\bar{V}_1+\bar{V}_2\le 1} d\bar{V}_1\, d\bar{V}_2\, \bar{V}_1^{g_n-1}\bar{V}_2^{g_n-1}(1-\bar{V}_1-\bar{V}_2)^{2g_c-1}e^{-\frac{1}{2}(\frac{e^*}{e}\frac{W}{l_B}\frac{L}{l_B})^2[1-(\bar{V}_1-\bar{V}_2)Z]^2}. \quad (6.15)$$

Required integration is over a two-dimensional triangle $\bar{V}_1 \ge 0$, $\bar{V}_2 \ge 0$, $\bar{V}_1 + \bar{V}_2 \le 1$, where $\bar{V}_i = V_i/V$ are dimensionless integration variables. Note though that the integrand is singular (but integrable) at every point along the boundary of the integration domain, hence the actual numerical implementation of the integration can be a little tricky.

Next, we stay in the limit of very large L, but work at finite temperature T; i.e., we use the finite temperature form for $\tilde{P}_g$ in Eq. (6.10) where the Gaussian becomes a delta function,

$$\frac{I_{\rm tun}(T\neq 0, L\gg l_B)}{L} = \frac{e|\Gamma_0|^2}{(L_0/l_B)^2}(e^*V_{\rm res})^{2g-1}\frac{1}{(2\pi)^2}\frac{1}{(W/l_B)}\left(\frac{L_T}{l_B}\right)^{3-2g}\sinh\big[\pi Z(L_T/l_B)\big]\times \int_{-\infty}^{\infty} dS_1\, B\Big[\frac{g_n}{2}\pm iS_1(L_T/l_B)\Big]\, B\Big[\frac{g_n}{2}\pm iS_2(L_T/l_B)\Big]\, B\Big[g_c\pm i(Z-S_1-S_2)(L_T/l_B)\Big], \quad (6.16)$$

and $S_2 \equiv S_1 - 1$; S_i is a dimensionless integration dummy corresponding to $V_i/V_{\rm res}$. Here we introduced a dimensionless ratio L_T/l_B that appears naturally in the above expression,

$$\frac{L_T}{l_B} \equiv \frac{e^*V_{\rm res}}{2\pi T}, \qquad L_T = \frac{v_n}{2\pi T}\frac{e^*}{e}\frac{W}{l_B} \quad (6.17)$$

The reason to call this dimensionless ratio $e^*V_{\rm res}/(2\pi T)$ a length scale 'L_T', instead of something more neutral like 'Y', is because we found that the effect of finite temperature is *remarkably similar* to that of finite length in the following sense:

$$\frac{1}{L}I_{\rm tun}(T,\neq 0, L\gg l_B) \simeq \frac{1}{L_T}I_{\rm tun}(T=0, L=L_T) \quad (6.18)$$

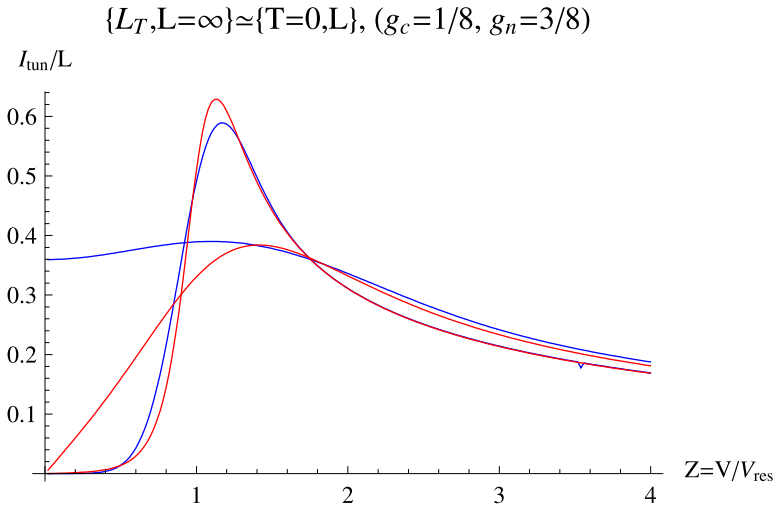

Figure 6-2: Tunneling current as function of dimensionless voltage $V/V_{\rm res}$. Blue curves are for zero temperature and finite length $L/l_B = 2$ and $L/l_B = 1/2$, as given by Eq. (6.15); red curves are for finite temperatures, $L_T/l_B = 2$ and $L_T/l_B = 1/2$, and infinite length L, i.e. Eq. (6.16); other parameters are $g_c = 1/8$, $g_n = 3/8$, $e^* = e/4$, $W = 10l_B$. The two curves are surprisingly similar, except for voltages V that are much smaller than temperature T: here zero temperature goes like $Z^{2g_n+2g_c-1}$ and finite temperature behaves linear in Z (i.e. Ohmic). Units on the vertical axis are such that constant prefactors equal one, i.e., $1 \equiv \frac{e|\Gamma_0|^2}{(L_0/l_B)^2}(e^*V_{\rm res})^{2g-1}$.

Figure 6-2 is a clear example of the resemblance between finite temperature and finite length. It was already emphasized by Bishara and Nayak (2008) that v/T sets a temperature decoherence length scale; they define a temperature decoherence length as $L_\phi = v_n/(2\pi T g_n)$ (for $v_c \to \infty$). Their definition differs from ours by a factor of order one. We find that our definition matches better in producing overlapping curves, although we do notice some dependence on g_n as well.

We plot curves for tunneling current and conductance at zero temperature and finite temperature in Fig. 6-3. To be concrete, we show plots for the cases of the Pfaffian, anti-Pfaffian, and $\nu = \frac{2}{3}$ states. The various curves depend intrinsically on g_n, g_c and e^*. For the Pfaffian these are predicted to be $g_n = 1/8$, $g_c = 1/8$, $e^* = e/4$ (Moore and Read, 1991; Wen, 1993). For the anti-Pfaffian the neutral exponent is larger, $g_n = 3/8$, $g_c = 1/8$, $e^* = e/4$ (Lee *et al.*, 2007; Levin *et al.*, 2007). The $\nu = \frac{2}{3}$ state is an abelian state for which the edge is expected to consist of two counterpropagating branches, with $g_n = 1/2$, $g_c = 1/6$, $e^* = e/3$ (Kane *et al.*, 1994). The $\nu = \frac{2}{3}$ state is one of the more stable abelian states for which separation of charge and neutral modes is predicted, and may be a good candidate to probe experimentally.

All three cases we consider in Fig. 6-3 show a pronounced peak in the tunneling current. At zero temperature the peak occurs right at $Z = 1$, with power-law decay for $Z > 1$. For finite temperatures the peak in tunneling current is shifted to slightly higher values of Z. The sharp peak in the tunneling current leads to a peak and a dip in the tunneling

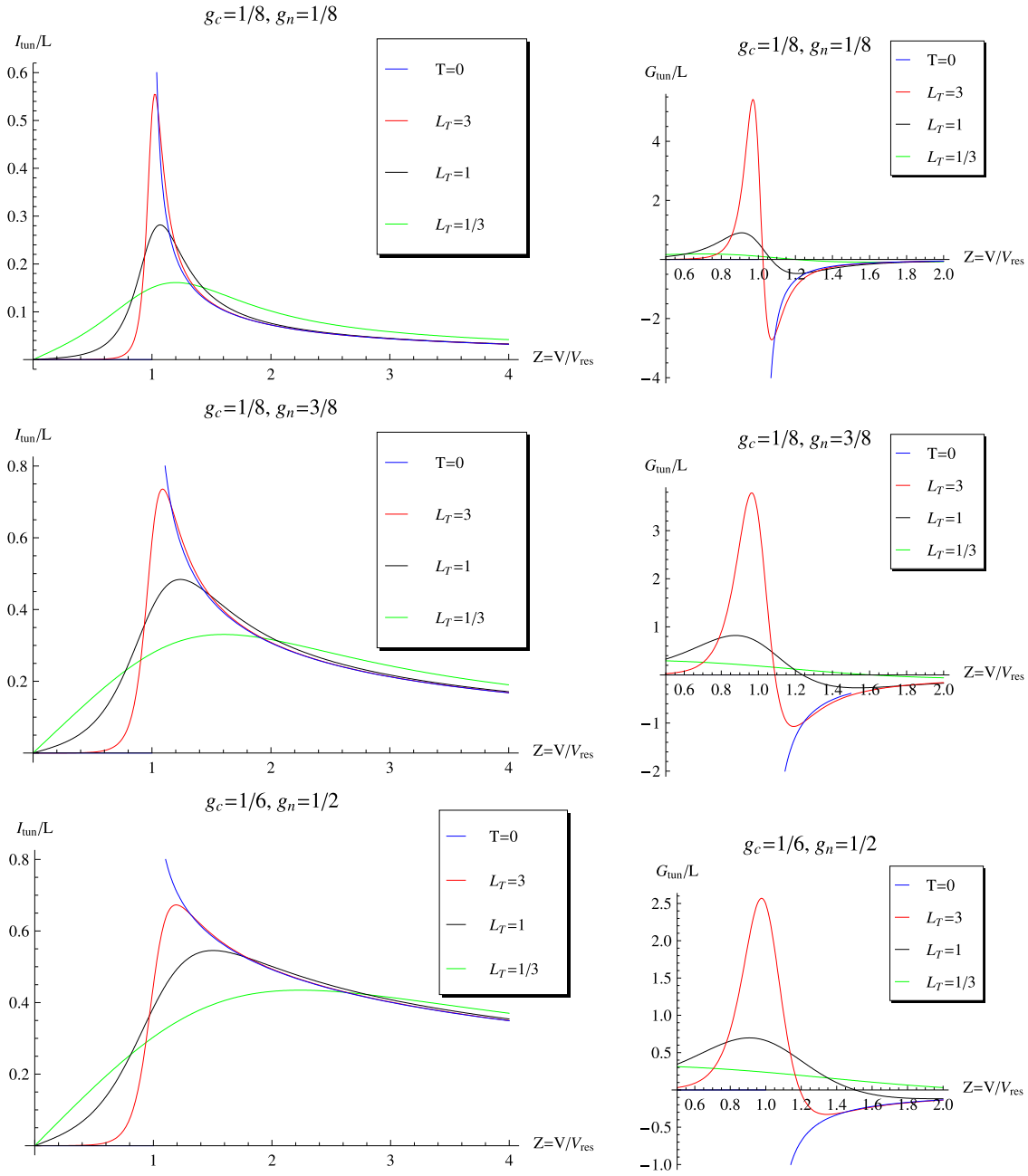

Figure 6-3: Tunneling current and tunneling conductance for the Pfaffian (top row), anti-Pfaffian (middle row), and $\nu = \frac{2}{3}$ (bottom row) states, plotted for several temperatures 'L_T' (in units of l_B) in the limit of very large real length L. At zero temperature there is nothing for $Z < 1$ and a divergence right at $Z = 1$. Units on vertical axes are the same as in Fig. 6-2, $1 \equiv \frac{e|\Gamma_0|^2}{(L_0/l_B)^2}(e^*V_{\rm res})^{2g-1}$.

conductance. It would appear that for smaller values of g_n the peak is more pronounced.

6.4 Estimating the observation window

The important question to ask now is which range of slow edge velocities can realistically be observed. The lower bound is set by temperature. The length scale $L/l_B \approx 1$ is the cross-over region where the resonance disappears. Exactly for which value L/l_B the resonance is still observable is a matter of personal taste, and also depends on the precise value of W/l_B; one could argue that as long as the position of the peak in the conductance dI_{tun}/dV is at finite bias and not at zero bias there is still trace of a resonance at non-zero voltage. The lower bound $v_{\min}$ on the slow edge velocity is then given by

$$v_{\min} \simeq \frac{2\pi}{(\frac{e^*}{e})(\frac{W}{l_B})} \frac{k_B T}{\hbar} l_B. \tag{6.19}$$

For typical values, $T_{\text{base}} = 10\text{mK}$, $l_B = 10\text{nm}$, $W/l_B = 10$, $e^* = e/3$, we find $v_{\min} \simeq 25\text{m/s}$. The upper bound $v_{\max}$ on the windows for which the resonance can be observed is given by the maximum voltage that can be applied to the quantum Hall system without destroying it due to e.g. heating (a current $I = V/R_H$ has to flow through the system). This maximum voltage $V_{\max}$ is not as clear-cut and may depend on sample, specific experimental setup, and filling fraction. In terms of this $V_{\max}$ we have

$$v_{\max} = \frac{1}{(\frac{W}{l_B})} \frac{eV_{\max}}{\hbar} l_B. \tag{6.20}$$

To give a numerical estimate, for $eV_{\max} = 750 k_B T_{\text{base}}$ one would find $v_{\max} = 1000\text{m/s}$. Note, that 750 times base temperature would equal a temperature of 7.5 Kelvin; the intrinsic excitation gap of the bulk typically is (much) smaller than that, although it is not immediately clear how this would affect $V_{\max}$.

We expect the effect to be more dramatic when at zero bias the tunneling current is truly zero. This would suggest to design an experiment to take place at the middle of a quantum Hall plateau. Shot noise experiments typically require a decent amount of tunneling current at zero bias for a noise signal to be observable, and such measurements are often taken at the outer edge of a quantum Hall plateau (Dolev *et al.*, 2008) where tunneling occurs more frequently. Instead, our proposed setup is built around a true weak-tunneling regime: the individual tunneling amplitudes need to be very small and in the weak tunneling regime, the *total tunneling current however does not need to be small* and is in fact allowed to be quite substantial.

Also note that since the resonance occurs at a finite bias voltage, the tunneling conductance is allowed to be quite large as well. The only upper bound on the tunneling current, the integrated tunneling conductance, is given by the Hall conductance, i.e., the maximum amount of current that the edge channel can conduct. In other words, as long as the ratio of tunneling current to total current is small enough, e.g. $I_{\text{tun}}/I_{\text{sup}} \lesssim 1/10$, our predictions should hold *quantitatively*. If the resonance is stronger than that, one would expect to see the long QPC pinch-off at the resonance bias voltage and open up again at larger bias

voltages.

Finally, the tunneling noise should show the same behavior as the tunneling current. Since the entire formalism is based on the linear response result, the general relation between tunneling current and its noise, Eq. (2.55), should hold as well:

$$S_{\rm tun}(T,V) = 2e^* I_{\rm tun}(T,V) \coth \frac{e^*V}{2T}. \tag{6.21}$$

This relation is even true if the tunneling amplitude $\gamma(x)$ does not have the exact form as in Eq. (6.5).

What would happen if the resonance bias voltage $V_{\rm res}$ does *not* lie in the observational window? Well, in that case one would expect tunneling current to behave as a function of V/T (true both for very small $V_{\rm res}$ and very large $V_{\rm res}$; in other words any feature in the tunneling current or tunneling conductance is expected to scale as the dimensionless ratio of voltage over temperature. Any feature that scales differently with temperature and voltage than V/T is an indication that there is an additional physical scale to be considered (or that the system is in a state of too high energy for which a scaling form does not hold).

6.5 Summary and Discussion

In this chapter we propose a measurement setup to excite a potential resonance in fractional quantum Hall states which possess a slow edge velocity. The quantum Hall state is tuned to resonance by a long quantum point contact at finite bias voltage. We calculate the shape of the resonance in linear response in the limit where the charged mode velocity v_c is much larger than the neutral mode velocity v_n. We plot curves for tunneling current and tunneling conductance at zero and finite temperatures, and at very large and intermediate lengths L of the QPC. Our result should be valid for both abelian an non-abelian quantum Hall states alike, as long as there is more than one edge branch.

A hypothetical observation of such a resonance would foremost provide an estimate of the value of the slow edge velocity, which is expected to be the neutral velocity. The remaining uncertainty is due to the presumably not exactly known width of the QPC. We estimate a window of edge velocities that would be observable in this setup, but a priori we cannot predict for *any* fractional quantum Hall state if its neutral edge velocity lies inside this window.

If such a resonance would be observed in a particular fractional quantum Hall state, this would open up possibilities to determine more properties about this specific quantum Hall state. A combination of a measurement of tunneling current (conductance) and tunneling noise would provide a good estimate of the fractional charge e^* of the tunneling quasiparticle, see Eq. (6.21). The exact shape of the resonance provides information about both the neutral and charged quasiparticle exponents g_n and g_c.

The lower bound of the value of the edge velocity that can be observed is given by temperature. Temperature sets a natural decoherence length L_T, Eq. (6.17). The upper bound on the window of observation of v_n is given by the maximum amount of current that can be driven through the system without destroying the quantum Hall state. This would suggest to set up a measurement at the middle of the quantum Hall plateau as opposed to

near the edges of the plateau, to avoid unwanted heating.

The existence of the resonance is due to constructive interference of coherent tunneling quasiparticles. An observation of the resonance would thus also show that interference of quasiparticles is realizable. The interference becomes constructive when two phases become equal; the first phase is the Aharonov-Bohm phase, the second phase is the phase set by the bias voltage. The second phase is not immediately obvious, as it is buried in expressions with fouriertransforms and beta functions. However, a simple plot, like those for $H_g(T, \omega, x)$ in Fig. 2-2 in chapter 2, show that a bias voltage does induce an oscillation linear in x.

What our proposed measurement setup cannot probe is the *direction* of the edge velocity. For instance for the $\nu = \frac{2}{3}$ state the neutral mode is predicted to move in the opposite direction of the charged mode; unfortunately our current setup is symmetric under a change of the sign of the edge velocity and unable to probe this physically interesting aspect of the quantum Hall states. We assumed a priori that the charged mode edge velocity v_c is too fast to observe in this setup as well.

6.A Appendix: Integral $\mathcal{I}[Z; g_n, g_c]$

In this appendix we provide an exact expression for the function

$$\mathcal{I}[Z; g_n, g_c] \equiv \int_{1/Z}^{\frac{1}{2}(1+1/Z)} ds\, s^{g_n-1} \left(s - \frac{1}{Z}\right)^{g_n-1} \left(1 + \frac{1}{Z} - 2s\right)^{2g_c-1}, \tag{6.22}$$

that was introduced in Eq. (6.13). An exact, but not very enlightening, expression for $\mathcal{I}[Z; g_n, g_c]$ exists in terms of hypergeometric functions,

$$\begin{aligned}\mathcal{I}[Z; g_n, g_c] = &\frac{2^{-2g_n} Z^{1-2g_n} \Gamma\left(\frac{1}{2} - g_n\right) \Gamma(g_n)\, {}_2F_1\left[1 - 2g_c, g_n; 2g_n; \frac{2}{Z+1}\right] \left(1 + \frac{1}{Z}\right)^{2g_c-1}}{\sqrt{\pi}} \\ &+ \frac{Z^{1-2g_n}(Z+1)^{2g_n-1} \Gamma(2g_c) \Gamma\left(g_n - \frac{1}{2}\right) \Gamma(g_n)\, \left(1 + \frac{1}{Z}\right)^{2g_c-1}}{2\sqrt{\pi}\Gamma(2g_c + 2g_n - 1)} \times \\ &\qquad {}_2F_1\left[1 - g_n, 2 - 2(g_c + g_n); 2 - 2g_n; \frac{2}{Z+1}\right]. \end{aligned} \tag{6.23}$$

There are two special cases to consider. First, when $g_n = \frac{1}{2}$ the above expression Eq. (6.23) is ill-defined; instead we have

$$\mathcal{I}[Z; g_n = \frac{1}{2}, g_c] = \sqrt{\pi} \left(\frac{Z-1}{Z}\right)^{2g_c} \frac{Z}{\sqrt{Z^2-1}} \Gamma(2g_c) \Gamma(2g_c + \frac{1}{2})\, {}_2F_1\left[\frac{1}{2}, 2g_c; 2g_c + \frac{1}{2}; \frac{Z-1}{Z+1}\right]. \tag{6.24}$$

The other special case is when $g_c + g_n = \frac{1}{2}$, because in this case the hypergeometric functions simplify to mere powers,

$$\mathcal{I}[Z; g_n + g_c = \frac{1}{2}] = \frac{4^{-g_n} Z \left(Z^2 - 1\right)^{-g_n} \Gamma\left(\frac{1}{2} - g_n\right) \Gamma(g_n)}{\sqrt{\pi}}. \tag{6.25}$$

The behavior of $\mathcal{I}[Z; g_n, g_c]$ near $Z = 1$ and for $Z \to \infty$ follows from standard series expansions of the above expressions. For $Z = 1 + \epsilon$ the function behaves as $\epsilon^{2g_c+g_n-1}$ for small ϵ. A large Z expansion is primarily determined by the neutral mode exponent g_n, where we find

$$\mathcal{I}[Z; g_n, g_c] = \frac{4^{-g_n}\Gamma\left(\frac{1}{2} - g_n\right)\Gamma(g_n)}{\sqrt{\pi}} Z^{1-2g_n} + \frac{2^{1-2g_n}\Gamma(2g_c)\Gamma(2g_n-1)}{\Gamma(2g_c+2g_n-1)} + \mathcal{O}\left(\frac{1}{Z}\right), \quad g_n \neq \frac{1}{2}, \tag{6.26}$$

$$\mathcal{I}[Z; g_n, g_c] = \log Z + \log 2 - \gamma - \Psi[2g_c] + \mathcal{O}\left(\frac{1}{Z}\right), \quad g_n = \frac{1}{2}; \tag{6.27}$$

γ is the Euler gamma constant and $\Psi[z] = \Gamma[z]'/\Gamma[z]$ the digamma function.

The form, Eq. (6.22), already resembles the definition of the hypergeometric function in terms of an integral (Abramowitz and Stegun, 1964, p. 558),

$${}_2F_1[a, b; c; z] \equiv \frac{\Gamma(c)}{\Gamma(b)\Gamma(c-b)} \int_0^1 dt\, t^{b-1}(1-t)^{c-b-1}(1-tz)^{-a}. \tag{6.28}$$

An alternative expression we can find for $\mathcal{I}[Z; g_n, g_c]$ is then

$$\mathcal{I}[Z; g_n, g_c] = \\ 2^{-g_n}\frac{\Gamma(2g_c)\Gamma(g_n)}{\Gamma(2g_c+g_n)} Z^{2-2g_n-2g_c}(Z-1)^{2g_c+g_n-1}\, {}_2F_1\left[1-g_n, g_n; 2g_c+g_n; -\frac{1}{2}(Z-1)\right]. \tag{6.29}$$

This expression is especially useful near $Z = 1$, where a simple power expansion becomes possible.

Chapter 7

Discussion

In this final chapter we reflect, in section 7.1, on the validity of perturbative results for e.g. the tunneling current, as described in chapters 2 and 3 and put to use in chapters 4 and 6. In section 7.2 we put the results in this thesis in a broader perspective by discussing some recent results reported by others. We conclude in section 7.3

7.1 Perturbation theory to any order

We discuss the possible limitations of calculating transport in (non-)abelian fractional quantum Hall states in perturbation theory.

7.1.1 Breakdown of linear response

In this thesis we rely heavily on perturbation theory, especially the leading order linear response results, in the calculation of the tunneling current that is induced at point contacts. A question one might ask is under what conditions the perturbative results are valid, and when they breakdown. Let us consider a concrete example, the tunneling conductance of a single point contact in linear response, Eq. (2.39), which we rewrite slightly and explicitly include Planck's constant as well,

$$G_{\text{tun}}(T, \omega = e^*V) = \left[\frac{e^2}{h}\right]\left[\frac{|\Gamma|^2}{(2\pi T)^{2-2g}}\right]\left[2\pi(e^*/e)^2 f_g\left(\frac{\omega}{2\pi T}\right)\right]. \tag{7.1}$$

The first factor on the right-hand-side, e^2/h, is the unit of conductance. The last factor is dimensionless. This implies that the middle factor is dimensionless as well, and that the tunneling amplitude Γ has to have units of T^{1-g}.

Next consider a situation where the tunneling conductance is measured at some temperature T and zero bias, $\omega = 0$, and the weak-tunneling assumption is valid; in other words, the tunneling conductance is much smaller than one over the Hall resistance, $G_{\text{tun}}(T, V = 0) \ll 1/R_H \sim e^2/\hbar$. This obviously requires that tunneling amplitude Γ is such that $|\Gamma|^2/(2\pi T)^{2-2g} \ll 1$. Now consider lowering the temperature *a lot*.

By lowering the temperature at fixed tunneling amplitude strength Γ the tunneling conductance $G_{\text{tun}}(T, V = 0)$ will increase, and for some temperature become greater than

$1/R_H$; at that point the tunneling conductance result becomes unphysical. Most likely the perturbative result became invalid at a temperature somewhere along the way.

Well, perturbation theory is not limited the linear response, and the full machinery of perturbation theory for any (non)-abelian fractional quantum Hall state is described in this thesis. So, if the leading order perturbative result fails, why not include a few higher order terms. This is indeed possible, and the following type of series expansion would appear:

$$G_{\rm tun}(T, V=0) = \frac{e^2}{\hbar}\left\{ \left[\frac{|\Gamma|^2}{(2\pi T)^{2-2g}}\right] f_{(1)} + \left[\frac{|\Gamma|^2}{(2\pi T)^{2-2g}}\right]^2 f_{(2)} + \left[\frac{|\Gamma|^2}{(2\pi T)^{2-2g}}\right]^3 f_{(3)} + \dots \right\}. \tag{7.2}$$

The coefficients $f_{(j)}$ are dimensionless, and we restrict ourselves to zero bias for now. In other words, perturbation theory to arbitrary order becomes an expansion in terms of a parameter

$$\theta_B \equiv \frac{|\Gamma|^2}{(2\pi T)^{2-2g}}, \tag{7.3}$$

where θ_B is a measure of the tunneling (or Backscattering) amplitude strength compared to temperature. When $\theta_B = 0$ there is no current tunneling, and for all $\theta_B < 1$ the series expansion is convergent, as the coefficients $f_{(j)}$ are well-behaved at any order (true for $V \neq 0$ as well). However, when $\theta_B > 1$ the series is always divergent.

7.1.2 Example: series expansion of the arctangent

To illustrate our line of thought, consider the function $h(\theta) = \frac{1}{\pi/2}\arctan\theta$ for $\theta \geq 0$; this function increases monotonically from 0 to 1 along the positive θ-axis, $h(\theta = 0) = 0$, $h(\theta = 1) = \frac{1}{2}$, $\lim_{\theta\to\infty} h(\theta) = 1$. See also Fig. 7-1.

The series expansion for $h(\theta)$ is

$$h(\theta) = \frac{2}{\pi}\left(\theta - \frac{\theta^3}{3} + \frac{\theta^5}{5} - \frac{\theta^7}{7}\right) + \mathcal{O}(\theta^9). \tag{7.4}$$

The series expansion for $h(\theta)$ converges for $\theta < 1$, but diverges for $\theta > 1$. The arctangent can nevertheless till be calculated through a convergent series for values of θ larger than one, through the identity

$$\arctan\theta = \frac{\pi}{2} - \arctan\frac{1}{\theta}. \tag{7.5}$$

In other words, we also have the series expansion for large x

$$h(\theta) = 1 - \frac{2}{\pi}\left(\frac{1}{\theta} - \frac{1}{3\theta^3} + \frac{1}{5\theta^5} - \frac{1}{7\theta^7}\right) + \mathcal{O}\Big(\frac{1}{\theta^9}\Big), \tag{7.6}$$

which converges for $\theta > 1$ and diverges for $\theta < 1$.

For the arctangent, Eq. (7.5) is the analytic continuation of the function into the complex plane beyond the initial radius of convergence. Once the analytic continuation form is known

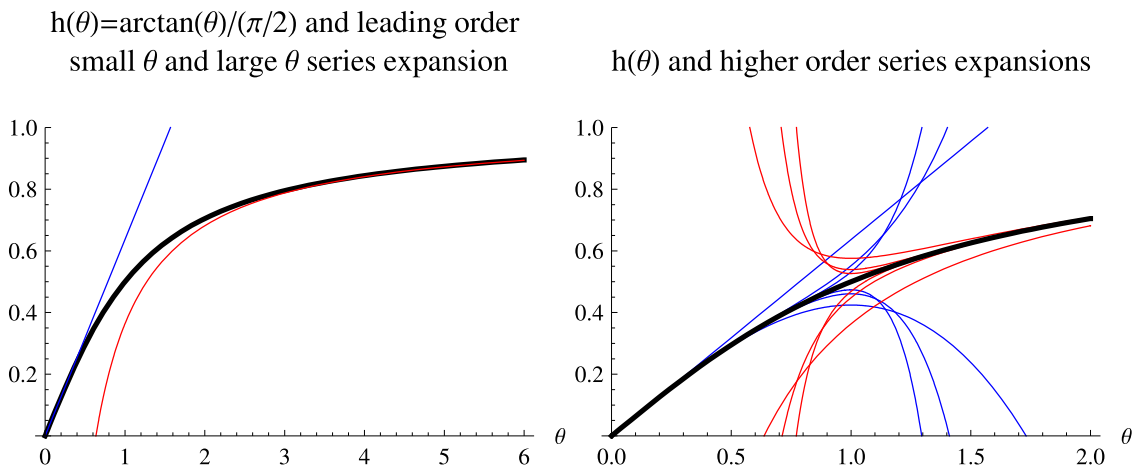

Figure 7-1: The perturbation expansion of the function $h(\theta) = \frac{2}{\pi}\arctan\theta$ is very similar to that of the tunneling conductance (current). The function $h(\theta)$ is very-well behaved for all $\theta \geq 0$; a perturbative expansion in small θ will always diverge when $\theta > 1$ (and converge when $\theta \leq 1$); an expansion in large θ will diverge when $\theta < 1$ (converge when $\theta \geq 1$). This is illustrated in the figures. The two series expansions are related to each other by analytic continuation. An interpolation between the two expansions in the region $\theta \approx 1$ already gives a decent approximation to the actual function.

the function $h(\theta)$ can be calculated in perturbation theory for all θ to arbitrary accuracy.

The behavior of the arctangent is very similar to the behavior of the perturbative expansion of the tunneling conductance (or current). Perturbation expansion will yield a series in powers of θ_B which only converges for $\theta_B < 1$, however there is a unique analytic continuation that relates the values for $\theta_B < 1$ to those for $\theta_B > 1$.

For the Laughlin states $\nu = \frac{1}{m}$ such a relation can be shown analytically at the zero temperature limit, where the tunneling conductance becomes a function of $\theta_V = |\Gamma|^2/V^{2-2g}$ (Fendley *et al.*, 1995); the series expansion can be expressed as a hypergeometric function in θ_V, and for the generic hypergeometric function the analytic continuation (from argument z to argument $1/z$) is known (Abramowitz and Stegun, 1964).

7.1.3 Arbitrary order, causality, numerics, physics

So we can conjecture (we cannot prove this at this point, but it seems very likely) that including higher order terms in the perturbative series will converge towards the exact solution of the tunneling conductance (or current, or current noise) for all bias voltages V as long as the expansion parameter θ_B is smaller than one.

For $\theta_B > 1$ there are two options available. Either do a series expansion in electron tunneling (i.e., large θ_B perturbative expansion), or determine the appropriate analytic continuation to relate the curve at $\theta_B < 1$ to that at $\theta_B > 1$. Of course, finding the form for the analytic continuation is non-trivial, especially if the terms in the expansion have been obtained numerically. The effect of finite bias V is unclear at this moment as well (i.e., does analytic continuation at $V = 0$ determine that at $V \neq 0$).

Good news is that all higher order terms in the series expansion are *always* finite. If the short-scale cut-off δ is kept there is *no divergence in any integral* at finite temperature. In other words, if one can write down the integral, it can be calculated numerically.

A systematic treatment to write down the corresponding integrals does not exist however. We have shown in this thesis that any term can be calculated even for non-abelian state through the conformal block decomposition, but even for a single term this was quite an involved task, as seen in chapter 4. What one would need is some sort of analog of a Feynman diagram language.

Perhaps such a diagrammatic can capture the essence of causality as well; in Sec. 4.3 one can see from the detailed calculation that interference due to ψ-ψ-tunneling is restored from a contribution where the Γ_3 tunneling process takes place in between a Γ_1 and a Γ_2 process, which signals causality. In the actual calculation this comes about through complex phases in which all non-causal contributions cancel in the end. One would guess that the restrictions due to causality can be made more apparent, and that this could simplify a calculation.

An alternative approach to find the exact tunneling conductance curve for any θ_B would be to find a numerically exact solution. This was done for the Laughlin states by Fendley *et al.* (1995), who used a mapping to a sine-Gordon model for which it was known how to construct a numerical solution (we have not been able to reproduce their result though). In principle, a numerically exact solution should be possible since the problem of a tunneling at a single site between chiral edge modes is an 'integrable' problem. However, at this point it is unclear how to construct an exact numerical solution for a generic (non-)abelian fractional quantum Hall edge, where the particular mapping for the Laughlin states might not work anymore.

Both approaches to the exact curve, arbitrary high order perturbation expansion and a numerical solution, require a substantial amount of additional effort. The perturbative approach seems to be more universal, since it can be applied to any quantum Hall state. A numerical solution might be more specific to a specific FQH state, but should provide a quicker way to the exact solution. Both directions are thus worth investigating further.

Finally, one should ask, what does the exact *mathematical* solution say about the *physical* reality? The physics we are trying to describe is that of the measured tunneling conductance at a quantum point contact in a fractional quantum Hall setting, as introduced in Sec. 1.1. If this problem can be modelled through a mathematical description of tunneling of quasiparticles at a single site, then the exact mathematical solution does have a physical meaning. In the end experiments will be the judge.

7.1.4 Exact interference curve

A spin-off of an exact result for the tunneling current would be an exact result for the interference I-V curve (including temperature dependence as well). To observe a strong interference signal, one would rather not operate in the weak-tunneling regime but rather in a range where the 'transmission' of the point contacts is on the order of 50%. An exact solution would e.g. show how higher harmonics of the Aharonov-Bohm phase enter the interference oscillation pattern.

Additional issue that arises in such a problem is how the Aharonov-Bohm phase fits in.

One cannot change the Aharonov-Bohm phase without changing arm-lengths and/or area of the interferometer as well. Also, one could argue that applying finite bias voltage V moves the location of the physical edges. In other words, even when the exact backscattering current curve can be calculated for a double point contact interferometer setup, there are definitely several subtleties to consider to compare the theoretical prediction to the results of experimentalist turning actual knobs.

7.1.5 Including more than one tunneling quasiparticle

We have ignored the possibility of multiple quasiparticles tunneling so far, under the assumption that the most relevant quasiparticle operator will dominate the tunneling. But it is straightforward to include more than one quasiparticle. Suppose that two quasiparticles, of types a and b, are allowed to tunnel. Then there are two parameters $\theta_a = |\Gamma_a|^2/(2\pi T)^{2-2g_a}$ and $\theta_b = |\Gamma_b|^2/(2\pi T)^{2-2g_b}$ in which the tunneling conductance (current) can be Taylor series expanded.

Depending on the magnitude of Γ_a and Γ_b one of the two quasiparticle may dominate tunneling at a given temperature, or both may contribute about equally. However, upon lowering the temperature the quasiparticle with the smallest exponent g will at some point become dominant, since $\theta_a/\theta_b = |\Gamma_a/\Gamma_b|^2(2\pi T)^{2(g_b-g_a)}$. This is exactly the statement that the quasiparticle with the smallest scaling dimension will dominate tunneling, with the implicit assumption that temperature is low enough to suppress tunneling of other quasiparticle operators.

7.2 Comments on recent other work

We give some brief comments on other people's recent work in relation to the results in this thesis.

7.2.1 Experiment by Goldman group

The results reported by Camino, Zhou, and Goldman (2007) were both promising and somewhat disappointing. This group realized a double contact interferometer setup at filling fraction $\nu = \frac{1}{3}$ (and several integer filling fractions) and observed some oscillating signal in the conductance as a function of magnetic field and back gate. What was promising is that it seems very likely that in their setup the entire system was in the $\nu = \frac{1}{3}$ FQH, both bulk, under the point contacts, and inside the interferometer. In earlier attempts by the same group there seemed to be a large island inside the interferometer with a filling fraction not equal to $\nu = \frac{1}{3}$.

What is promising about their results is that they appear to observe interference in the tunneling conductance at a $\nu = \frac{1}{3}$ interferometer, where the state is indeed $\nu = \frac{1}{3}$ everywhere.

What is disappointing about their reported results is that they failed to provide additional evidence that the signal they observe is due to tunneling fractional quasiparticles:

- They did not publish the relative sign of the periods of oscillation under a change of back gate and magnetic field. A plot of the interference phase as function of both

magnetic field and backgate would already indicate if the interference is more likely to be interference of quasi-particles or rather a Coulomb-blockade like effect.

- Measurements were reported at zero bias only. One of the hallmarks of tunneling fractional quasiparticles is the non-linear I-V curve, both for the average contribution to the conductance and the oscillating part.

- The point contacts could not be studied separately, hence the obvious $|\Gamma_1|$ and $|\Gamma_2|$ dependence could not be checked. Main reason is that the point contacts in this group's sample are etched, which is obviously different from a point contact due to a gate on top of the sample. Etching the point contacts could potentially lead to a sharper edge, because the confining potential would be more two-dimensional, whereas with gates on top of the sample the repulsion would be a three-dimensional effect and more smooth.[1]

Unfortunately, more than one and a half years after Camino *et al.* (2007) first reported their results, these issues have yet to be addressed.

The $\nu = \frac{1}{3}$ state is the obvious candidate state to verify the theoretically predicted tunneling current and noise curves, as well as interference (all as function of bias and temperature). The $\nu = \frac{1}{3}$ state is the most stable fractional quantum Hall state, with the widest plateau in magnetic field, meaning that the state last longer at higher temperature than other FQH states would. Also, if edge reconstruction does not play a role the $\nu = \frac{1}{3}$ consists of a single charge edge branch, and decoherence due to slow edge velocities is not expected to occur. The only thing the $\nu = \frac{1}{3}$ state does not offer is non-abelian statistics.

7.2.2 Experiment by Heiblum group

In the paper by Dolev, Heiblum, Umansky, Stern, and Mahalu (2008) the authors report shot-noise measurements for a single quantum point contact in the $\nu = \frac{5}{2}$ state. They report that their data fits to a curve that predicts a fractional charge $e^* = e/4$.

There are three main differences between their experimental setup and the typical situation we described here in this thesis, e.g. in Fig. 1-1: (i) the bulk and the point contact are *not* at the same quantum Hall filling fraction, (ii) they measure the noise in the forward-scattered current I_F, instead of the tunneling, or back-scattered, current I_B. (iii) they measure as far away from the middle of the plateau as possible, and in a regime where tunneling is relatively strong and the weak-tunneling approximation is probably not valid. This means we cannot directly compare their data with the curves that are calculated in this thesis.

Furthermore, the formula that these authors use to fit their data is dubious to say the least. This formula is supposed to be an extension of electron scattering for given reflection and transmission coefficients; it seems to be *inadequate by default* to describe (noise of) tunneling of quasiparticles, because this is intrinsically non-linear and therefor there are *no* (fixed) reflection and transmission coefficients.

[1] The technique of etching by itself does not give a sharp edge like cleaving the sample would. The edge could be sharper because of the 2D versus 3D effect only.

The same formula was used in the past in a similar experiment to fit a charge $e^* = e/3$ through shot-noise measurements in the $\nu = \frac{1}{3}$ state. It would seem that a comparison between the mystery formula and the exact solution for the Laughlin states could be useful.

Nevertheless the confusion about the fitting formula, the indication that the fractional charge is $e^* = e/4$ is reassuring that the $\nu = \frac{5}{2}$ state could be non-abelian.

7.2.3 Experiment by Kastner group

Radu, Miller, Marcus, Kastner, Pfeiffer, and West (2008) report tunneling conductance measurements for the $\nu = \frac{5}{2}$ state (earlier work Miller, Radu, Zumbuhl, Levenson-Falk, Kastner, Marcus, Pfeiffer, and West, 2007). They use a setup with one drain, as in Fig. 1-3, but most importantly, through a process called 'annealing', they are able to have both the bulk and the QPC at filling fraction $\nu = \frac{5}{2}$.

Their data is directly comparable to the curves calculated in this thesis, and the authors have fitted their data to such curves. In the linear response curves, both the quasiparticle exponent g and fractional charge e^* are allowed to vary continuously. A best fit was found for $e^* = 0.17$ and $g = 0.35$. Comparing with the candidate states, Sec. 5.2, the data is most consistent with a state with $e^* = e/4$ and $g = 0.5$.

For a different device, one where the point contact is longer and more channel like, they report a feature with a peak followed by a strong side-dip for which the position does not scale like V/T. In light of chapter 6 this could be a feature due to a resonance of the neutral mode edge velocity, at a resonance scale comparable to temperature such that the resonance is not very pronounced.

The one drain setup has the disadvantage that for tunneling that is not weak the differential resistance is not directly proportional to the tunneling conductance as explained in section 1.1. An additional measurement of the tunneling noise could provide a more accurate fit of e^* and g.

7.2.4 Theory by Ardonne & Kim

Ardonne and Kim (2008) are the first to calculate the curve for noise in a filling fraction $\nu = \frac{5}{2}$ double point contact interferometer setup. They find that the noise is sensitive to the fusion channel of the tunneling quasiparticles. Their result relies on a careful calculation that keeps track of various branch-cuts and an intuitive argument cannot be given at this point. However, causality (or the lack thereof for noise) seems to play a role.

These findings seem to contradict the perturbative calculations we perform in this thesis for which we do not see any channel dependence in the noise. A detailed, and probably rather technical, analysis would be required to shine some light on these apparently inconsistent results. Perhaps the causality aspect that we refered to in section 7.1.3 is more subtle than one would naively expect. Another option is that considering the two sides of the quantum Hall liquid to be part of a single edge gives a different answer than from two genuinely distinct edges.

7.2.5 Theory by Feldman and co.

In a series of papers, Feldman and Kitaev (2006); Law, Feldman, and Gefen (2006); Feldman, Gefen, Kitaev, Law, and Stern (2007), Feldman and coworkers explore a Mach-Zehnder type of interferometer setup, and study the implications for a filling fraction $\nu = \frac{5}{2}$ FQH state. The Mach-Zehnder interferometer has two drains, with one drain *inside* the interferometer.

The important difference between this setup and the Fabry-Pérot setup (Sec. 1.1) is that after *every* single tunneling event the probability for the next tunneling quasiparticle is changed, in other words this is not a steady-state calculation. The authors consider a time-averaged outcome. Furthermore the calculation is primarily based on tunneling rates (i.e., single tunneling events with a certain probability rate to tunnel).

It would seem that the dynamic chiral Luttinger liquid theory approach (e.g. chapter 2) could be applied as well, as long as the non-steady-state aspect can be taken care of through some simple form of time-averaging. Another issue that would have to be addressed is the presence of an electrode inside the interferometer, and the effect that it has on the quasiparticle propagators.

The use of Klein factors (Law *et al.*, 2006) to warrant causality seems to be questionable.

7.2.6 Theory by Nayak and co.

Nayak and coworkers (Fendley, Fisher, and Nayak, 2006, 2007; Bishara and Nayak, 2008) have introduced and demonstrated in detail the importance of conformal block decomposition for calculations of tunneling current for the $\nu = \frac{5}{2}$ state. They do typically restrict to a setup where all the edges are part of the same outer edge of the quantum Hall fluid. Our discussion of conformal block decomposition in chapter 3 is in that sense more general, and can also describe e.g. a Mach-Zehnder type of setup.

7.2.7 Theory by D'Agosta et al.

D'Agosta, Raimondi, and Vignale (2003) consider a generalization of the single point contact transport measurement, based on the experimental data reported by Roddaro, Pellegrini, Beltram, Biasiol, Sorba, Raimondi, and Vignale (2003); Roddaro, Pellegrini, Beltram, Biasiol, Sorba, D'Agosta, Raimondi, and Vignale (2004). These experiments considered bias dependence of the tunneling current in the $\nu = \frac{1}{3}$ regime for both weak and strong backscattering.

The theoretical model is extended by allowing the quasiparticle exponent g to be renormalized over a finite length L. In other words, the assumption is that through the application of a point contact the edges come close enough that interactions will locally play a role; actual tunneling still occurs at a single site.

The authors (D'Agosta *et al.*, 2003) perform an exact calculation of the scattering problem, using bosonization techniques specialized to the Laughlin states; we have not been able to quantitatively confirm their results. The authors do mention an approximation that fits their results well. For this approximation we can show that it can be generalized to all other fractional quantum Hall states as well, in the weak-scattering regime, including the $\nu = \frac{5}{2}$ candidate states.

7.2.8 Numerical simulations

Numerical simulations provide a valuable tool for the study of quantum Hall states. Especially for the filling fraction $\nu = \frac{5}{2}$ state, results from numerics are a guide for both theory and experiment. Techniques that are used in such numerical studies are exact diagonalization on finite size systems (for geometries both with and without an edge), DMRG, and Monte-Carlo (Wan, Yang, and Rezayi, 2006; Baraban and Simon, 2008; Feiguin, Rezayi, Yang, Nayak, and Das Sarma, 2008; Peterson and Das Sarma, 2008; Peterson, Jolicoeur, and Das Sarma, 2008a; Wan, Hu, Rezayi, and Yang, 2008). Aspects that can especially be probed numerically are the effects of the confining potential near the edge, the influence of the third dimension, as well as the inclusion of other Landau levels. Separation of charged and neutral mode velocities has been observed, and there are signatures of edge-reconstruction for certain systems.

As far as Pfaffian versus anti-Pfaffian, i.e., which of these two candidate states is more favorable to describe the observed filling fraction $\nu = \frac{5}{2}$ state, this is a tough question to answer numerically. In a system with spherical geometry the Pfaffian and anti-Pfaffian cannot directly be compared, since these states have a different 'shift'. Furthermore, the anti-Pfaffian wavefunction is given in terms of a highly dimensional integral, which makes it very time-consuming to evaluate numerically. Alternative direction would be to explore the particle-hole symmetry breaking aspect, for which first results were just reported (Peterson, Park, and Das Sarma, 2008b).

Somewhat separate from the 'main-stream' numerical calculations are efforts to simulate what happens at a quantum point contact. This is a hard problem though, since it is not yet known how to combine electrostatic techniques (e.g. density-functional theory) with the presence of quantum Hall state in a strong magnetic field. A spin-density-functional theory calculation, like Rejec and Meir (2006), might capture some of the relevant physics.

7.3 Conclusions

Let us look back through this thesis to the goals that motivated us, section 1.2, and indicate possible future directions.

We have investigated the phases of matter of a specific non-abelian fractional quantum Hall edge and found a phase transition to a Majorana-gapped phase. Such a transition can probably occur in a generic situation, and has close ties to the apparent opposite transition of edge reconstruction. This can be studied further both theoretically (in other systems, or understanding the Majorana-gapping more rigorously) and numerically (e.g. simulations that vary confining potential).

Furthermore we believe we understand the process of tunneling at a single site between edges of the generic (both abelian and non-abelian) fractional quantum Hall state. The next big step to bring this concept closer to experiment is to construct exact solutions that are valid beyond weak tunneling regime. A systematic (and/or diagrammatic) form of perturbation theory can potentially be developed. Alternatively, a numerical procedure can be sought to construct the exact solution.

A direct comparison with experiment in the case of interference is still somewhat subtle, since the effect of experimental knobs (such as magnetic field and QPC gate voltages) is

not well-understood. More experimental input is required here as well, for instance from interferometers in abelian FQH states such as the $\nu = \frac{1}{3}$ state.

A potential observation of a slow edge velocity, e.g. through the resonance at a long tunneling contact that we proposed, will shed some light on an intrinsic source of decoherence on the quantum Hall edge, as well as the actual interactions between different edge branches.

From the topological quantum computation perspective, the good news is we have learned a lot more about the $\nu = \frac{5}{2}$ state and this state is still a very viable candidate for an observation of non-abelian statistics in the future.

Bibliography

Abramowitz, M., and I. A. Stegun, 1964, *Handbook of Mathematical Functions with Formulas, Graphs, and Mathematical Tables* (Dover, New York).

Ardonne, E., and E.-A. Kim, 2008, "Non-abelian statistics in the interference noise of the Moore–Read quantum Hall state," J. Stat. Mech. **2008**(04), L04001.

Arovas, D., J. R. Schrieffer, and F. Wilczek, 1984, "Fractional Statistics and the Quantum Hall Effect," Phys. Rev. Lett. **53**, 722–723.

Baraban, M., and S. Simon, 2008, in preparation.

Bishara, W., and C. Nayak, 2008, "Edge states and interferometers in the Pfaffian and anti-Pfaffian states of the $\nu = \frac{5}{2}$ quantum Hall system," Phys.Rev. B **77**(16), 165302.

Blok, B., and X.-G. Wen, 1990a, "Effective theories of Fractional Quantum Hall Effect at Generic Filling Fractions," Phys. Rev. B **42**, 8133.

Blok, B., and X.-G. Wen, 1990b, "Effective theories of Fractional Quantum Hall Effect: Hierarchical Construction," Phys. Rev. B **42**, 8145.

Blok, B., and X.-G. Wen, 1992, "Many-body Systems with Non-abelian Statistics," Nucl. Phys. B **374**, 615.

Bonderson, P., A. Kitaev, and K. Shtengel, 2006a, "Detecting Non-Abelian Statistics in the $\nu = \frac{5}{2}$ Fractional Quantum Hall State," Phys. Rev. Lett. **96**(1), 016803.

Bonderson, P., K. Shtengel, and J. K. Slingerland, 2006b, "Probing Non-Abelian Statistics with Quasiparticle Interferometry," Phys. Rev. Lett. **97**(1), 016401.

Bonderson, P., K. Shtengel, and J. K. Slingerland, 2008, "Interferometry of non-Abelian anyons," Ann. Phys. In press.

Camino, F. E., W. Zhou, and V. J. Goldman, 2007, "$e/3$ Laughlin Quasiparticle Primary-Filling $\nu = \frac{1}{3}$ Interferometer," Phys. Rev. Lett. **98**(7), 076805.

Chamon, C., and X.-G. Wen, 1994, "Sharp and smooth edge of quantum Hall states," Phys. Rev. B **49**, 8227.

Chamon, C. de C., D. E. Freed, S. A. Kivelson, S. L. Sondhi, and X. G. Wen, 1997, "Two point-contact interferometer for quantum Hall systems," Phys. Rev. B **55**(4), 2331–2343.

Chamon, C. de C., D. E. Freed, and X. G. Wen, 1995, "Tunneling and quantum noise in one-dimensional Luttinger liquids," Phys. Rev. B **51**(4), 2363–2379.

Chamon, C. de C., D. E. Freed, and X. G. Wen, 1996, "Nonequilibrium quantum noise in chiral Luttinger liquids," Phys. Rev. B **53**(7), 4033–4053.

Chang, A. M., 2003, "Chiral Luttinger liquids at the fractional quantum Hall edge," Rev. Mod. Phys. **75**(4), 1449–1505.

Chung, S. B., and M. Stone, 2006, "Proposal for reading out anyon qubits in non-Abelian $\nu = \frac{12}{5}$ quantum Hall state," Phys. Rev. B **73**(24), 245311.

Das Sarma, S., M. Freedman, and C. Nayak, 2005, "Topologically Protected Qubits from a Possible Non-Abelian Fractional Quantum Hall State," Phys. Rev. Lett. **94**(16), 166802.

Das Sarma, S., and A. Pinczuk (eds.), 1997, *Perspectives in Quantum Hall Effects: Novel Quantum Liquids in Low-Dimensional Semiconductor Structures* (Wiley, New York).

D'Agosta, R., R. Raimondi, and G. Vignale, 2003, "Transport properties of a two-dimensional electron liquid at high magnetic fields," Phys. Rev. B **68**(3), 035314.

Di Francesco, P., P. Mathieu, and D. Sénéchal, 1997, *Conformal Field Theory* (Springer-Verlag, New York).

Dolev, M., M. Heiblum, V. Umansky, A. Stern, and D. Mahalu, 2008, "Observation of a quarter of an electron charge at the $\nu = \frac{5}{2}$ quantum Hall state," Nature **452**, 829–834.

Ezawa, Z. F., 2000, *Quantum Hall Effects: Field Theoretical Approach and Related Topics* (World Scientific, Singapore).

Feiguin, A. E., E. Rezayi, K. Yang, C. Nayak, and S. Das Sarma, 2008, "Spin polarization of the $\nu = \frac{5}{2}$ quantum Hall state," `arXiv:0804.4502`.

Feldman, D. E., Y. Gefen, A. Kitaev, K. T. Law, and A. Stern, 2007, "Shot noise in an anyonic Mach-Zehnder interferometer," Phys. Rev. B **76**(8), 085333.

Feldman, D. E., and A. Kitaev, 2006, "Detecting Non-Abelian Statistics with an Electronic Mach-Zehnder Interferometer," Phys. Rev. Lett. **97**(18), 186803.

Fendley, P., M. P. A. Fisher, and C. Nayak, 2006, "Dynamical Disentanglement across a Point Contact in a Non-Abelian Quantum Hall State," Phys. Rev. Lett. **97**(3), 036801.

Fendley, P., M. P. A. Fisher, and C. Nayak, 2007, "Edge states and tunneling of non-Abelian quasiparticles in the $\nu = \frac{5}{2}$ quantum Hall state and $p + ip$ superconductors," Phys. Rev. B **75**(4), 045317.

Fendley, P., A. W. W. Ludwig, and H. Saleur, 1995, "Exact nonequilibrium transport through point contacts in quantum wires and fractional quantum Hall devices," Phys. Rev. B **52**(12), 8934–8950.

Fidkowski, L., 2007, "Double Point Contact in the $k = 3$ Read-Rezayi State," `arXiv:0704.3291`.

Fradkin, E., C. Nayak, A. Tsvelik, and F. Wilczek, 1998, "A Chern-Simons effective field theory for the Pfaffian quantum Hall state," Nucl. Phys. B **516**(3), 704–718.

Freedman, M., C. Nayak, and K. Walker, 2006, "Towards universal topological quantum computation in the $\nu = \frac{5}{2}$ fractional quantum Hall state," Phys. Rev. B **73**(24), 245307.

Fröhlich, J., and T. Kerler, 1991, "Universality in Quantum Hall Systems," Nucl. Phys. B **354**, 369–417.

Fröhlich, J., B. Pedrini, C. Schweigert, and J. Walcher, 2001, "Universality in Quantum Hall Systems: Coset Construction of Incompressible States," J. Stat. Phys. **103**, 527–567.

Fröhlich, J., and U. M. Studer, 1993, "Gauge invariance and current algebra in nonrelativistic many-body theory," Rev. of Mod. Phys. **65**, 733.

Fröhlich, J., and A. Zee, 1991, "Large scale physics of the quantum Hall fluid," Nucl. Phys. B **364**, 517.

Georgiev, L. S., 2003, "The $\nu = \frac{5}{2}$ quantum Hall state revisited: spontaneous breaking of the chiral fermion parity and phase transition between Abelian and non-Abelian statistics," Nucl. Phys. B **651**, 331–360.

Georgiev, L. S., 2006, "Towards a universal set of topologically protected gates for quantum computation with Pfaffian qubits," `hep-th/0611340`.

Georgiev, L. S., and M. R. Geller, 2006, "Aharonov-Bohm effect in the non-Abelian quantum Hall fluid," Phys. Rev. B **73**(20), 205310.

Greiter, M., X.-G. Wen, and F. Wilczek, 1991, "Pairing in the $\nu = \frac{1}{2}$ FQH state," Phys. Rev. Lett. **66**, 3205.

Haldane, F. D. M., 1995, "Stability of Chiral Luttinger Liquids and Abelian Quantum Hall States," Phys. Rev. Lett. **74**(11), 2090–2093.

Halperin, B. I., 1983, "Theory of the quantized Hall conductance," Helv. Phys. Acta **56**, 75.

Kane, C. L., and M. P. A. Fisher, 1997, "Quantized thermal transport in the fractional quantum Hall effect," Phys. Rev. B **55**(23), 15832–15837.

Kane, C. L., M. P. A. Fisher, and J. Polchinski, 1994, "Randomness at the edge: Theory of quantum Hall transport at filling $\nu = \frac{2}{3}$," Phys. Rev. Lett. **72**(26), 4129–4132.

Kao, H.-c., C.-H. Chang, and X.-G. Wen, 1999, "Binding Transition in Quantum Hall Edge States," Phys. Rev. Lett. **83**, 5563.

Kitaev, A. Y., 2003, "Fault-tolerant quantum computation by anyons," Ann. Phys. **303**, 2–30.

Kitaev, A. Y., 2006, "Anyons in an exactly solved model and beyond," Ann. Phys. **321**, 2–111.

Law, K. T., D. E. Feldman, and Y. Gefen, 2006, "Electronic Mach-Zehnder interferometer as a tool to probe fractional statistics," Phys. Rev. B **74**(4), 045319.

Lee, S.-S., S. Ryu, C. Nayak, and M. P. A. Fisher, 2007, "Particle-Hole Symmetry and the $\nu = \frac{5}{2}$ Quantum Hall State," Phys. Rev. Lett. **99**(23), 236807.

Leinaas, J. M., and J. Myrheim, 1977, "On the theory of identical particles," Il Nuovo Cimento **37B**, 1.

Levin, M., B. I. Halperin, and B. Rosenow, 2007, "Particle-Hole Symmetry and the Pfaffian State," Phys. Rev. Lett. **99**(23), 236806.

Miller, J. B., I. P. Radu, D. M. Zumbuhl, E. M. Levenson-Falk, M. A. Kastner, C. M. Marcus, L. N. Pfeiffer, and K. W. West, 2007, "Fractional quantum Hall effect in a quantum point contact at filling fraction $\frac{5}{2}$," Nat. Phys. **3**, 561–565.

Milovanović, M., and N. Read, 1996, "Edge excitations of paired fractional quantum Hall states," Phys. Rev. B **53**(20), 13559–13582.

Moore, G., and N. Read, 1991, "Nonabelions in the fractional quantum hall effect," Nucl. Phys. B **360**, 362.

Moore, J. E., and X.-G. Wen, 1998, "Classification of disordered phases of quantum Hall edge states," Phys. Rev. B **57**(16), 10138–10156.

Moore, J. E., and X.-G. Wen, 2002, "Critical points in edge tunneling between generic fractional quantum Hall states," Phys. Rev. B **66**, 115305.

Morf, R. H., 1998, "Transition from Quantum Hall to Compressible States in the Second Landau Level: New Light on the $\nu = \frac{5}{2}$ Enigma," Phys. Rev. Lett. **80**(7), 1505–1508.

Nayak, C., S. H. Simon, A. Stern, M. Freedman, and S. Das Sarma, 2007, "Non-abelian anyons and topological quantum computation," `arXiv:0707.1889`.

Nayak, C., and F. Wilczek, 1996, "$2n$ Quasihole States Realize 2^{n-1}-Dimensional Spinor Braiding Statistics in Paired Quantum Hall States," Nucl. Phys. B **479**, 529.

Oshikawa, M., Y. B. Kim, K. Shtengel, C. Nayak, and S. Tewari, 2007, "Topological degeneracy of non-Abelian states for dummies," Ann. Phys. **322**, 1477–1498.

Oshikawa, M., and T. Senthil, 2006, "Fractionalization, Topological Order, and Quasiparticle Statistics," Phys. Rev. Lett. **96**(6), 060601.

Overbosch, B. J., and F. A. Bais, 2001, "Inequivalent classes of interference experiments with non-Abelian anyons," Phys. Rev. A **64**(6), 062107.

Overbosch, B. J., and C. Chamon, 2008, "Probing the neutral velocity in the fractional quantum Hall effect with a long point contact," in preparation.

Overbosch, B. J., and X.-G. Wen, 2007, "Dynamical and scaling properties of $\nu = \frac{5}{2}$ interferometer," submitted to Phys. Rev. B, `arXiv:0706.4339`.

Overbosch, B. J., and X.-G. Wen, 2008, "Phase transitions on the edge of the $\nu = \frac{5}{2}$ Pfaffian and anti-Pfaffian quantum Hall state," `arXiv:0804.2087`.

Pan, W., A. S. Yeh, J. S. Xia, H. L. Störmer, D. C. Tsui, E. D. Adams, L. N. Pfeiffer, K. W. Baldwin, and K. W. West, 2001, "The other even-denominator fractions," Physica E **9**, 9–16.

Peterson, M. R., and S. Das Sarma, 2008, "Orbital Landau level dependence of the fractional quantum Hall effect in quasi-two dimensional electron layers: finite-thickness effects," `arXiv:0801.4819`.

Peterson, M. R., T. Jolicoeur, and S. Das Sarma, 2008a, "Finite-Layer Thickness Stabilizes the Pfaffian State for the $\frac{5}{2}$ Fractional Quantum Hall Effect: Wave Function Overlap and Topological Degeneracy," Phys. Rev. Lett. **101**(1), 016807.

Peterson, M. R., K. Park, and S. Das Sarma, 2008b, "Spontaneous Particle-Hole Symmetry Breaking in the $\nu = \frac{5}{2}$ Fractional Quantum Hall Effect," `arXiv:0807.0638`.

de Picciotto, R., M. Reznikov, M. Heiblum, V. Umansky, G. Bunin, and D. Mahalu, 1997, "Direct observation of a fractional charge," Nature **389**, 162–164; this paper apparently also appeared in Physica B, **249-251**, 395–400 (1998).

Prange, R. E., and S. M. Girvin (eds.), 1987, *The Quantum Hall Effect*, Graduate texts in contemporary physics (Springer-Verlag, New York).

Radu, I. P., J. B. Miller, C. M. Marcus, M. A. Kastner, L. N. Pfeiffer, and K. W. West, 2008, "Quasi-Particle Properties from Tunneling in the $\nu = \frac{5}{2}$ Fractional Quantum Hall State," Science **320**(5878), 899–902.

Read, N., 1990, "Excitation structure of the hierarchy scheme in the fractional quantum Hall effect," Phys. Rev. Lett. **65**, 1502.

Rejec, T., and Y. Meir, 2006, "Magnetic impurity formation in quantum point contacts," Nature **442**, 900–903.

Rezayi, E. H., and F. D. M. Haldane, 2000, "Incompressible Paired Hall State, Stripe Order, and the Composite Fermion Liquid Phase in Half-Filled Landau Levels," Phys. Rev. Lett. **84**(20), 4685–4688.

Roddaro, S., V. Pellegrini, F. Beltram, G. Biasiol, L. Sorba, R. D'Agosta, R. Raimondi, and G. Vignale, 2004, "Quasi-particle tunneling between fractional quantum Hall edges," Physica E **22**, 185–188.

Roddaro, S., V. Pellegrini, F. Beltram, G. Biasiol, L. Sorba, R. Raimondi, and G. Vignale, 2003, "Nonlinear Quasiparticle Tunneling between Fractional Quantum Hall Edges," Phys. Rev. Lett. **90**(4), 046805.

Rosenow, B., and B. I. Halperin, 2008, "Signatures of neutral quantum Hall modes in transport through low-density constrictions," arXiv:0806.0869.

Rosenow, B., B. I. Halperin, S. H. Simon, and A. Stern, 2008, "Bulk-Edge Coupling in the Non-Abelian $\nu = \frac{5}{2}$ Quantum Hall Interferometer," Phys. Rev. Lett. **100**(22), 226803.

Rowell, E., R. Stong, and Z. Wang, 2007, "On classification of modular tensor categories," arXiv.org:0712.1377.

Saminadayar, L., D. C. Glattli, Y. Jin, and B. Etienne, 1997, "Observation of the $e/3$ Fractionally Charged Laughlin Quasiparticle," Phys. Rev. Lett. **79**(13), 2526–2529.

Shankar, R., 1990, "Solvable model of a metal-insulator transition," Int. J. Mod. Phys. B **4**(15/16), 2371–2394.

Stern, A., and B. I. Halperin, 2006, "Proposed Experiments to Probe the Non-Abelian $\nu = \frac{5}{2}$ Quantum Hall State," Phys. Rev. Lett. **96**(1), 016802.

Wan, X., Z.-X. Hu, E. H. Rezayi, and K. Yang, 2008, "Fractional quantum Hall effect at $\nu = \frac{5}{2}$: Ground states, non-Abelian quasiholes, and edge modes in a microscopic model," Phys. Rev. B **77**(16), 165316.

Wan, X., K. Yang, and E. H. Rezayi, 2006, "Edge Excitations and Non-Abelian Statistics in the Moore-Read State: A Numerical Study in the Presence of Coulomb Interaction and Edge Confinement," Phys. Rev. Lett. **97**(25), 256804.

Wen, X.-G., 1991a, "Edge Transport Properties of the FQH States and Impurity Scattering of 1D "CDW" States," Phys. Rev. B **44**, 5708.

Wen, X.-G., 1991b, "Non-Abelian Statistics in the FQH states," Phys. Rev. Lett. **66**, 802.

Wen, X.-G., 1992, "Theory of the Edge Excitations in FQH effects," Int. J. Mod. Phys. B **6**, 1711.

Wen, X.-G., 1993, "Topological order and edge structure of $\nu = \frac{1}{2}$ quantum Hall state," Phys. Rev. Lett. **70**, 355.

Wen, X.-G., 1995, "Topological Orders and Edge Excitations in FQH States," Advances in Physics **44**, 405.

Wen, X.-G., 1999, "Projective Construction of Non-Abelian Quantum Hall Liquids," Phys. Rev. B **60**, 8827.

Wen, X.-G., 2000, "Continuous topological phase transitions between clean quantum Hall states," Phys. Rev. Lett. **84**, 3950.

Wen, X.-G., 2004, *Quantum Field Theory of Many-body Systems* (Oxford University Press, New York).

Wen, X.-G., and Q. Niu, 1990, "Ground State Degeneracy of the FQH States in Presence of Random Potentials and on High Genus Riemann Surfaces," Phys. Rev. B **41**, 9377.

Wen, X.-G., Y.-S. Wu, and Y. Hatsugai, 1994, "Chiral operator product algebra and edge excitations of a FQH droplet," Nucl. Phys. B **422**, 476.

Wen, X.-G., and A. Zee, 1992, "A Classification and Matrix Formulation of the abelian FQH states," Phys. Rev. B **46**, 2290.

Wilczek, F., 1982, "Quantum mechanics of fractional-spin particles," Phys. Rev. Lett. **49**, 957.

Willett, R., J. P. Eisenstein, H. L. Störmer, D. C. Tsui, A. C. Gossard, and J. H. English, 1987, "Observation of an even-denominator quantum number in the fractional quantum Hall effect," Phys. Rev. Lett. **59**, 1776.

Witten, E., 1989, "Quantum field theory and the Jones polynomial," Comm. Math. Phys. **121**, 351–399.

Yang, J., Z. Su, and W. Su, 1992, "A hierarchical approach to the even-denominator quantum Hall states," Mod. Phys. Lett. B **6**, 119–125.

Yoshioka, D., 2002, *The Quantum Hall Effect*, Springer series in solid-state sciences (Springer, Berlin).